

# **Formation of Fluorescent Bio-molecular Assemblies by UV Laser Treatment and Solution Phase Molecular Interactions**

**A thesis submitted to the Savitribai Phule Pune  
University for the degree of Doctor of Philosophy in  
Biotechnology**

**By**

**Pradeep Kumar Singh**

**Dr. (Mrs) Asmita Prabhune (Research Guide)**

**Dr. Satishchandra B. Ogale (Research Co-Guide)**

**Biochemical Science Division, Physical and Materials Chemistry Division,  
National Chemical Laboratory, Pune- 411008, India**

**February 2015**



राष्ट्रीय रासायनिक प्रयोगशाला  
(वैज्ञानिक तथा औद्योगिक अनुसंधान परिषद)  
डॉ. होमी भाभा रोड, पुणे - 411 008. भारत  
**NATIONAL CHEMICAL LABORATORY**  
(Council of Scientific & Industrial Research)  
Dr. Homi Bhabha Road, Pune - 411008. India



## Certificate

This is to certify that the work presented in the thesis titled "*Formation of Fluorescent Biomolecular Assemblies by UV Laser Treatment and Solution Phase Molecular Interactions*" by Pradeep Kumar Singh, submitted for the degree of **Doctor of Philosophy in Biotechnology** was carried out under our supervision at the Biochemical Sciences Division and the Physical and Materials Chemistry Division, National Chemical Laboratory, Dr. Homi Bhabha Road, Pune- 411008, India. All the material obtained from other sources has been duly acknowledged in this thesis.

**Dr. (Mrs) Asmita Prabhune (Guide)**  
Scientist  
National Chemical Laboratory,  
Dr. Homi Bhabha Road,  
Pune – 411008. India

**Dr. Satishchandra B. Ogale (Co-guide)**  
Chief Scientist  
National Chemical Laboratory,  
Dr. Homi Bhabha Road,  
Pune – 411008. India

Communications Channels +91 20 25902000  
+91 20 25893300  
+91 20 25893400


Fax +91 20 25902601 (Director)  
+91 20 25902660 (Admin.)  
+91 20 25902639 (Business Development)

URL : [www.ncl-india.org](http://www.ncl-india.org)

## Declaration

I, Mr. Pradeep Kumar Singh, hereby declare that work incorporated in my thesis titled "*Formation of Fluorescent Bio-molecular Assemblies by UV Laser Treatment and Solution Phase Molecular Interactions*" was carried out by myself, for the degree of **Doctor of Philosophy** in **Biotechnology** under the Guidance of Dr. (Mrs.) Asmita Prabhune and Dr. Satishchandra B Ogale. This work has not been previously submitted to this University or any other University for the degree of PhD, or any other degree. Any material that has been obtained from other sources has been duly acknowledged in this thesis.

Date: February 11, 2015  
Place: NCL, Pune

  
**Pradeep Kumar Singh**  
(Research Student)

*Dedicated to My Beloved Family,  
Teachers and Friends*





# Acknowledgement

---

*I take this opportunity to thank all who have been instrumental in the completion of my PhD research and thesis.*

*Firstly, I wish to express my deep sense of gratitude towards my research supervisor Dr. Asmita A. Prabhune for her continuous support and giving positive direction to my work. I greatly respect her valuable and insightful guidance. I would also like to thank my research co-supervisor Dr. Satishchandra B. Ogale for giving me an opportunity to work under his guidance. His influence on my work, philosophy and life has been phenomenal. He gave me the creative space and freedom which every researcher earnestly desires. Not only has his guidance been tremendously inspiring in our scientific endeavours but his general approach and philosophy towards life and people has also helped us grow as human beings.*

*I am really grateful to both Dr. Ogale and Dr. Prabhune for their critical comments and tremendous efforts in preparing this dissertation. I thank them for their endless support filled with patience and enthusiasm during my whole tenure of Ph.D.*

*I take this opportunity to express my gratitude to Dr. S. Sivaram (former Director, NCL), Dr. Sourav Pal (Director, NCL), Dr. Vidya Gupta (Head of Biochemical Science Division) and Dr. Anil Kumar (Head of Physical and Materials Chemistry Division) for providing the infrastructure and advanced facilities for research and giving me an opportunity to work at CSIR-NCL. I would also like to acknowledge the role of Council of Scientific and Industrial Research (CSIR), Govt. of India for providing me with research fellowships during my PhD study period.*

*I wish to thank our collaborators Reihaneh Haghniaz, Dr. Ruchika Kaul-Ghanekar and Keerti Wani for all the help and support during the course of the research work. I thank all the journal editors, reviewers of our published articles and the editors, authors who have allowed us to reprint their published material in this thesis.*

*I would like to thank my teachers Prof. Sathyanarana Gummadi and Prof. Ligy Philip for inspiring me in the way they did during my M. Tech days and later on as well. The MSc study circle with great friends like Akhil, Bikesh, Amit, Atul, Kandarp, Kamlesh and Sumit is indeed a wonderful academic memory of the time. I would also like to*

*thank my teachers in the Dept. of Bioscience, SP University, Dr. Datta Madamwar, Dr. Rao, and Dr. Kiran for their help and support. I would like to thank Dr. R A Pandey for his help and encouragement during my MSc. Project days at NEERI Nagpur.*

*Words cannot express my indebtedness to my grandparents, Mr. Bhoop Singh and Mrs Sharwati Devi. Their love, encouragement and support have always been a pillar of strength and inspiration in my life. I feel their loss tremendously and only wish they were here to see this. May their souls rest in peace.*

*I wish to thank my family, Father (Lokman Singh), Mother (Premwati Devi), Brother (Rakesh Kumar) and Sister (Seema Kumari) for their constant and unconditional love, support and comfort. My father's constant emphasis on the importance of education, ambition and his scientific curiosity has always been a guiding light for me. I wish to thank my Mother for her unconditional love and support. She has unhesitatingly shared all my joys and pains in equal measure and made them her own.*

*I deeply acknowledge the help and support from my laboratory friends/intern students, Dr. Abhimanyu, Dr. Anup, Dr. Arif, Dr. Parvez, Dr. Antad, Dr. Harish, Dr. Ashish, Dr. Dattakumar, Dr. Prasad, Vishal, Upendra, Satyawar, Rohan, Satish, Yogesh, Wahid, Umesh, Sambhaji, Sumit B, Kush, Sarika, Divya, Meenal, Lily, Mandakini, Reshma, Anil, Anirudh, Shruti, Dipti, Rounak, Pravarthana, Dhanya, Megha, Pooja S, Shraddha, Mukta, Ketaki, Dr. Jaishree, Dr. Kasturi, Aditi B, Vrushali, Pushpa, Parul, Ruchira, Avinash, Priti, Mihir, Pooja G. Special thanks to my seniors/friends, Dr. Vivek Dhas, Dr. Subas, Dr. Mandakini, and Dr. Kasturi for their tremendous help during the laboratory research work. Happy cheers to the gang of friends, Vishal, Abhik, Satish, Dhanya, Pushpa and Avinash for all our memorable discussions, fun and work together.*

*I wish to thank my friends, Harshal, Vijay, Amit, Brij, Vijay, and Ketan for always being there for me. I must also acknowledge the great time I had with my friends Akhil, Bikesh, Atul, Amit, Ravi, Santosh, Sawan, Raju, Meenakshi, Deepti, Archita and others.*

*Finally, I thank the almighty God for making my life so special and being with me all the way.*

**Pradeep Kumar Singh**

# List of Abbreviations

---

<b>Abbreviation</b>	<b>Name</b>
NPs	Nanoparticles
HPLC	High Pressure Liquid Chromatography
NMR	Nuclear Magnetic Resonance
TEM	Transmission electron microscopy
TGA	Thermo gravimetric analysis
UV	Ultraviolet
XPS	X-ray photoelectron Spectroscopy
DLS	Dynamic Light Scattering
FE SEM	Field emission scanning electron microscopy
Maldi-MS	Matrix-assisted laser desorption/ionization
LCMS	Liquid Chromatography–Mass Spectrometry
FTIR	Fourier Transform Infrared Spectroscopy
FL	Fluorescence
Zeta	Zeta-Potential
<i>C. bombicola</i>	<i>Candida bombicola</i>
HR TEM	High resolution transmission electron microscopy
OD	Optical Density
PL	Photoluminescence
SL(A)	Acidic Sophorolipid
SL(L)	Lactonic Sophorolipid
PLD	Pulsed laser deposition
TLC	Thin Layer Chromatography
SEM	Scanning electron microscopy
SL	Sophorolipid
SLIR	Laser irradiated sophorolipid
Cep	Cephalexin
Cep IR	Laser irradiated Cephalexin
<i>E. Coli</i>	<i>Escherichia coli</i>
<i>S. aureus</i>	<i>Staphylococcus aureus</i>
Cur	Curcumin

# Contents

---

## Abstract

<b>Chapter 1- 1.1 Self-assembly in Biological field: Basics and Applications</b> .....	1-37
1.1.1 Self-assembly in biological system.....	4-5
1.1.2 Examples of the use of self-assembled structures in applications.....	5-7
1.1.3 Bio-surfactant mediated self-assembly.....	8-9
<b>1.2 Biosurfactants: an Introduction</b> .....	9-11
<b>1.2.1 Different types of Bio-surfactants</b>	
1.2.1.1 Glycolipids.....	11-12
1.2.1.2 Lipopeptides and lipoproteins .....	12
1.2.1.3 Phospholipids and fatty acids .....	12-13
1.2.1.4 Polymeric biosurfactants.....	14
1.2.1.5 Particulate bio-surfactants .....	14
<b>1.3 Sophorolipid: An Introduction</b> .....	15-16
1.3.1 Applications of Sophorolipid.....	17-20
<b>1.4 Fluorescence: Mechanism, systems and applications</b> .....	20
1.4.1 Mechanism of fluorescence.....	21-22
1.4.2 Fluorescent materials and systems.....	22-23
1.4.3 Self-assembly induced Fluorescence.....	23-24
1.4.4 Applications of fluorescence (Fluorescence sensing).....	24-26

<b>1.5 Drug loaded biosurfactant assemblies</b> .....	26
1.7.1 Drug loaded soft nanostructures.....	26-28
1.5.2 Synthesis of Curcumin.....	28
1.5.3 Derivatives of Curcumin.....	28-31
1.5.4 Curcumin stability and bioavailability.....	31-32
1.5.5 Medicinal activity and molecular targets of Curcumin.....	32
<b>1.6 Scope and Nature of Present Work</b> .....	33-34
<i>References</i> .....	34-37
<b>Chapter 2 - Synthesis and Characterization techniques</b> .....	38-57
2.1 General synthesis techniques.....	39-44
2.2 Characterization techniques.....	44-56
<i>References</i> .....	56-57
<b>Chapter 3 - Fluorescent sophorolipid molecular assembly and its magnetic nanoparticle loading: a pulsed laser process</b> .....	58-80
3.1 Introduction.....	59-61
3.2 Experimental and Characterization.....	62-64
3.3 Results and Discussions.....	64-69
3.4 Mechanism.....	69-75
3.5 Magnetic SL structure by embedding Fe <sub>3</sub> O <sub>4</sub> nanoparticles.....	75-78
3.6 Conclusion.....	78
<i>References</i> .....	78-80

<b>Chapter 4 - From Micron to Nano-Curcumin by sophorolipid co-processing:</b>	
<b>Highly enhanced bioavailability, fluorescence, and anticancer efficacy....</b>	81-99
4.1 Introduction.....	82-83
4.2 Experimental.....	83-84
4.3 Characterization.....	84-87
4.4 Results and Discussions.....	87-97
4.5 Conclusion.....	97
<b>References.....</b>	97-99
<b>Chapter 5 - Pulse laser (UV) drive molecular self-assembly of Cephalexin:</b>	
<b>Aggregation induce fluorescence and its utility as mercury sensor.....</b>	100-114
5.1 Introduction.....	101-102
5.2 Experimental.....	103-103
5.3 Characterization.....	103-105
5.4 Results and Discussion.....	105-111
5.5 Conclusion.....	112
<b>References.....</b>	112-114
<b>Chapter 6 - Research Summary and Future Scope.....</b>	115-119
7.1 Thesis Summary.....	116-118
7.2 Future Work.....	118-119
<b>List of Publications.....</b>	120-121



# Abstract

---

Nanobiotechnology is a new class of technology, where engineered nanomaterials are studied for their huge projected potential in medicinal applications. It includes a synergistic goal-oriented integration of various disciplines such as biology, physics, chemistry, materials science and engineering for the betterment of human life. It offers great advantages towards the construction of bio-macromolecules and biological systems according to modern biomedical needs. From the ancient time, nature has been known to use self assembly of amphiphilic building blocks as a tool for the creation of complex molecules. These natural processes have inspired researchers worldwide to realize the importance of self assembly and investigate its basic principles. Most of the biological systems, including well-known structures; deoxyribonucleic acid (DNA), ribonucleic acid (RNA), cell membranes and virus capsid protein, form by self-assembly processes.

Biosurfactants are amphiphilic compounds which are mainly secreted extra-cellularly by microorganisms or may also be produced on their cell surfaces. They are surface-active compounds capable of lowering surface tension between solids, liquids and gases, thus permitting their dispersion in water as well as in other solvents. Biosurfactants mediate reduction of interfacial surface tension due to the presence of both hydrophilic and hydrophobic moieties in their basic structure. Sophorolipid (SL) consists of a dimeric sugar- sophorose as a carbohydrate head (polar) and a long hydroxy fatty acid chain (nonpolar), made it amphiphilic compound. This amphiphilic nature allows SL to form unique structures such as micelles and bilayers in heterogenous systems. This character enables SL to reduce the surface and interfacial energies leading to formation of emulsions.

Sophorolipid find applications in wide range of fields including Petroleum, food, pharmaceuticals, cosmetics, laundry and bioremediation. The foremost reasons for a high and increasing level of interest in sophorolipid is its biodegradability, low toxicity and unique structures that can facilitate molecular engineering to suit a specific application domain. Sophorolipid is synthesized by employing non pathogenic yeast strains (*Candida bombicola*) and they present several physiological advantages over various forms of chemical surfactants. There are two distinct forms

of sophorolipid produced by the yeast; lactonic and acidic. They are generally present in the form of disaccharide sophoroses (2-O- $\beta$ -D-glucopyranosyl-D-glucopyranose) linked  $\beta$  glycosidically to the hydroxyl group at the penultimate carbon of fatty acids. Different applications are known to be associated with each form.

Fluorescence appears one of the most powerful transduction mechanisms due to its high sensitivity and the number of different analytical parameters. A good understanding about fluorescence could offer great improvements towards the expansion of medicinal therapeutics for various human diseases. Such as fluorescent imaging is a leading technique for monitoring biological reactions by high-quality of its reproducibility, sequential resolution and excellent sensitivity. Currently available fluorescent materials for the inspection of protein peptide interactions are dual-labeled peptides, green fluorescent protein and fluorophores labeled peptide.

Bio-organic compounds are now being widely used in sensing application because of their biodegradability, perfect biocompatibility and non-chemical synthesis procedure over inorganic nanomaterials (Quantum dots and dyes) as fluorescent sensors application. These compounds applied in wide range of field because of unique optical properties and non toxic synthesis source. Researchers from worldwide have significantly expanded their search for aggregation induces emission fluorescence that shows specific applications in materials science.

In this thesis, a new photochemical route towards the synthesis of fluorescent materials has been explored. This process involves a rapid laser irradiated unsaturation in material, as well as aggregation induces emission, subsequent realization of intrinsic fluorescent. The process can take place at room temperature and ambient conditions. This bottom-up method involves the use of small biosynthesized molecule as reaction precursors. It is also shown that this laser irradiation route presents new avenues and possibilities of formation of novel biological structure that have been hitherto unexplored. The medicinal applications of these fluorescent structures have been tested and proved to enhanced biocompatibility in hyperthermia treatment. Furthermore, the use of natural synthesized antibiotics compound like cephalexin has also been investigated in order to introduce for fluorescent material and their use in heavy metal sensor product. A method of improve hydrophobic drug (curcumin) bioavailability with sophorolipid encapsulation

(SL(A)+Cur) has been used. Sophorolipid improve curcumin's bioavailability and enhance cyto-toxic activity in towards human cancer cell line.

In the **first chapter**, introduction to biosurfactant and its various forms, properties, synthesis protocols and applications has been presented. A scope of the present work has also been included.

In the **second chapter**, basics of synthesis protocols and characterization methods used in the thesis have been described.

In the **third chapter**, an application of Pulsed Laser Irradiated fluorescent mesostructures has been presented. The use of UV laser irradiation fluorescent sophorolipid mesostructures has been applied for hyperthermia and bio-imaging on cancer cell lines. A plausible mechanism for the new phenomenon has been studied.

In the **fourth chapter**, we have developed a novel formulation, acidic sophorolipid + curcumin ((SL(A)+Cur) self-assembly, to improve curcumin's aqueous solubility, stability and bioavailability for enhancing its anti-cancer activity. This study suggests a new cost effective nano self-assembled approach for improved curcumin delivery and therapeutic efficacy.

In the **fifth chapter**, we report pulsed UV laser induced formation of novel self-assembled fluorescent nanostructures of cephalixin. Our experiment showed Hg<sup>++</sup> ions conc. dependent fluorescence quenching with these nanostructure application.

The **sixth chapter** summarizes the work presented in the thesis and emphasizes on possible further research in this area.

**Dr. (Mrs) Asmita Prabhune**

(Research Guide)

**Dr. Satishchandra B. Ogale**

(Research Co-Guide)

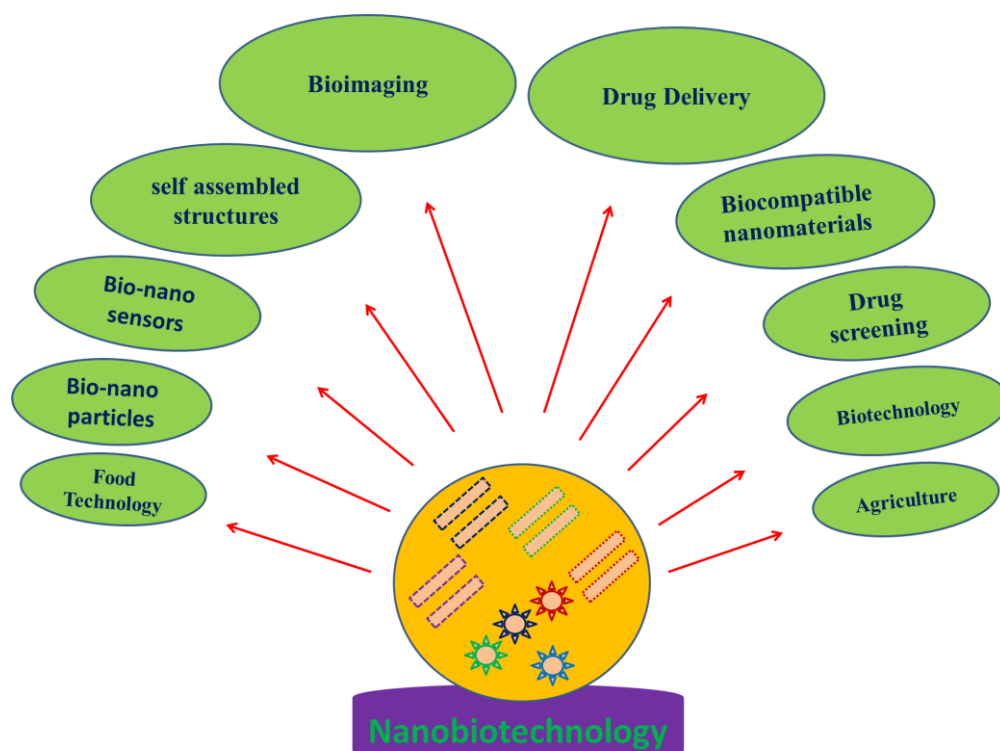
# Chapter 1

---

## Introduction

---

This chapter gives a basic introduction to the premise of the research work described in this thesis. A broad introduction is presented about the basics of nanobiotechnology, self-assembly, fluorescence, bio-surfactants and different types of bio-surfactants, curcumin and fluorescent sensors. This chapter also presents discussion about the possible synthesis protocols and the diverse applications of the materials thus derived. Finally, this chapter lays out a roadmap for the direction of research presented in this thesis.



*Nanobiotechnology application (From Ref. 1)*

## Preamble

Nanobiotechnology includes a synergistic goal-oriented integration of several disciplines such as biology, physics, chemistry, materials science and engineering for the betterment of human life. It is a new class of technology, where engineered nanomaterials are studied for their huge projected potential in medicinal applications. Nanobiotechnology can solve many biological problems by applying the properties of tailor-made nanomaterials. Molecular devices can be constructed by utilizing well known concepts involved in natural molecular machinery. Control of process and system parameters and their optimization for individual problem needs represent the main driving force of Nanobiotechnology. In the context of the construction of bio-macromolecules and biological systems according to modern biomedical needs, nanotechnology offers great advantages. By focusing on biological systems and their capabilities, we can design new emerging methods for the improvement of human life. From the biological standpoint, eventually we have to understand how to apply physical principles to understand how these techniques actually work. Recently, significant work is in progress on the development of new powerful nano substances for controlled drug discovery applications. Based on current research, it is clear that expansion of novel drugs alone is not adequate to ensure progress in drug therapy. In

the context of hydrophobic drug molecules the major obstacles are their water solubility, poor bioavailability, variable plasma concentration and necessity of high doses. Therefore many efforts are in progress for the development of customized drug carriers to overcome inadequate bioavailability of hydrophobic drugs. Ideal drug carriers should have non-toxic nature, controlled release characteristics as well as sufficient drug loading capacity. Another characteristic for drug carriers are their chemical and physical storage stability with efficient drug targeting point with enhanced production at reasonable cost. In recent years biosurfactant materials have gained major attention due to their proficient ability to be efficient drug carriers to fulfil the above mentioned requirements. It will be a great advantage in drug delivery systems, if we could formulate the drug molecule itself as drug delivery carrier for therapeutic application.

## **1.1 Self-assembly in Biological field: Basics and Applications**

---

Self-assembly is a phenomenon where disordered systems of existing components make an ordered structure or outline as a result of precise local communications without any outside interference. Nature has been known to use self-assembly of amphiphilic building blocks as a tool for the creation of complex molecules which has inspired researchers worldwide to realize the importance of self-assembly and investigate its basic principles.<sup>2</sup> Presently, self-assembly protocols used in lab experiments are much more simple in contrast to nature's mechanisms which are highly complex, although the guiding principles are not necessarily as complex. To understand the principles and mechanisms behind each of the nature's processes is important in order develop sophisticated and functional devices for their applicability in non-biological systems. Although remarkable improvements have been attained in this field, it is still a continuous process to completely understand the basics of self-organization of molecules and materials. Therefore self-assembly is a distinguished branch of science and technology that enables individual molecules to be configured at nano-scale level as well as their manipulation to achieve diverse functionality.<sup>3</sup> In recent times, self-assembly of bio-derived molecules has created sizeable interest in biomedical science for the development of advanced complex structures.



### 1.1.1 Self-assembly in biological field

Self-assembled biological materials have been getting extra attention due to their widespread suitability such as cost effectiveness, functional versatility, structural simplicity as well as their structure tunability.<sup>4</sup> Self-assembly in biological system is efficiently organized by non-covalent bond interactions such as of hydrogen bonds, hydrophobic interactions,  $\pi$ - $\pi$  stacking interactions as well as electrostatic interactions.

Most of the biological systems, including well-known structures; deoxyribonucleic acid (DNA), ribonucleic acid (RNA), cell membranes and virus capsid protein, form by self-assembly processes.<sup>5</sup> Self-assembly is not only crucial to elucidate configuration of biomolecular complexes in cells but also gives direct understanding for their practical applications in nanotechnology research (Figure 1.1).<sup>6</sup>

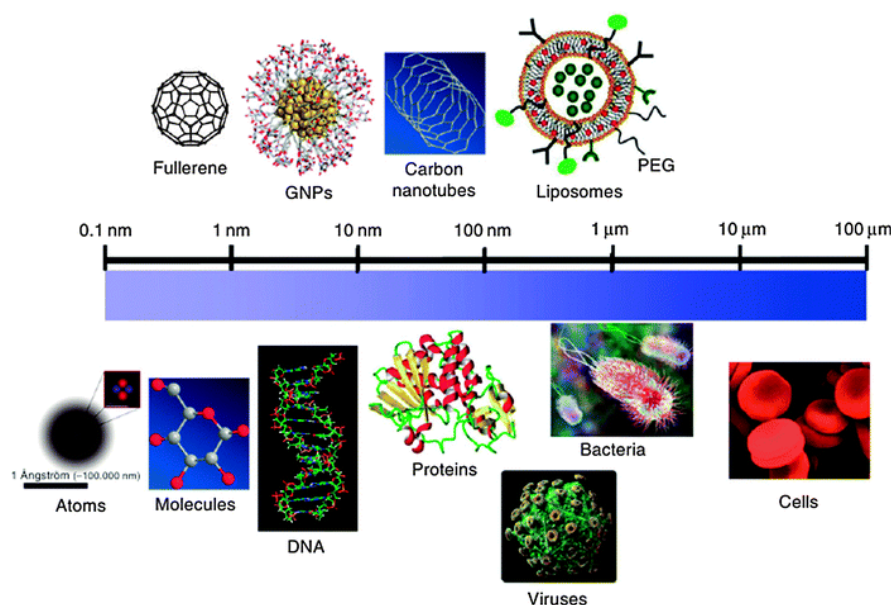


**Figure 1.1** Self-assemblies of compounds in bio-nanotechnology with size dimensions

(From Ref. 5)

There are several examples available for *in vivo* self-assembly formation in biological systems such as thermodynamic phase transition due to the structure-inducing process. This type of *in vitro* self-assembly behaviour could be correctly described by the inspection of the existing theories. There are several examples of highly selective self-assembly systems in biological science that show indistinguishable subunits such

as lipid bilayer membranes, hemocyanin, actin, flagella, viruses as well as microtubules. Some other essential self-assembly combinations within human biological systems are DNA, RNA, globular proteins, polypeptides, and collagen. These contain changing features due to the pairing of chemical phase. Generally these chemical changes are responsible for induced structure stabilization. Occurrence of self-assemblies in biological systems is an exploitable characteristic for the development of new materials in biomedical science. There are some chemically crystalline biological examples of self-assembly systems such as crystal structures of ribosome and peptide-amphiphile nanofibers. Other examples include thin films of a nematic liquid crystals on an isotropic substrate, micrometer-sized metallic polyhedral configurations folded from planar substrates as well as three-dimensional aggregates of micrometer plates assembled by capillary forces (Figure 1.2).<sup>7</sup>

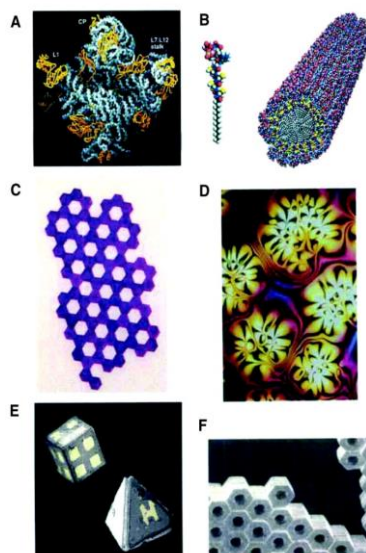


**Figure 1.2** (A) Ribosome. (B) Peptide amphiphile nanofibers. (C) Polymeric plates (D) Nematic liquid crystal (E) Metallic polyhedral folded (F) Aggregate of micrometre plates (From Ref. 7)

### 1.1.2 Examples of the use of self-assembled structures in applications

Self-assembled biological compounds find several interesting applications in biomedical science such as for example the lipid membranes which create selective permeable membrane. Self-assembly of biological materials also prepares molecular machines for various life activities for cell survival such as protein aggregates, folded proteins, and structured nucleic acids (Figure 1.3). Liquid crystals, molecular crystals, phase-separated polymers and crystalline structures with regular forms also result from molecular self-assembly processes. Self-assembly have great possibilities for its

applications in condensed matter and materials science which generally occur by arrangement of mechanisms superior than basic molecules. In recent times, the generation of nanostructures via self-assembly formation has gained importance as a universal strategy for making novel materials with interesting property features.<sup>8</sup>

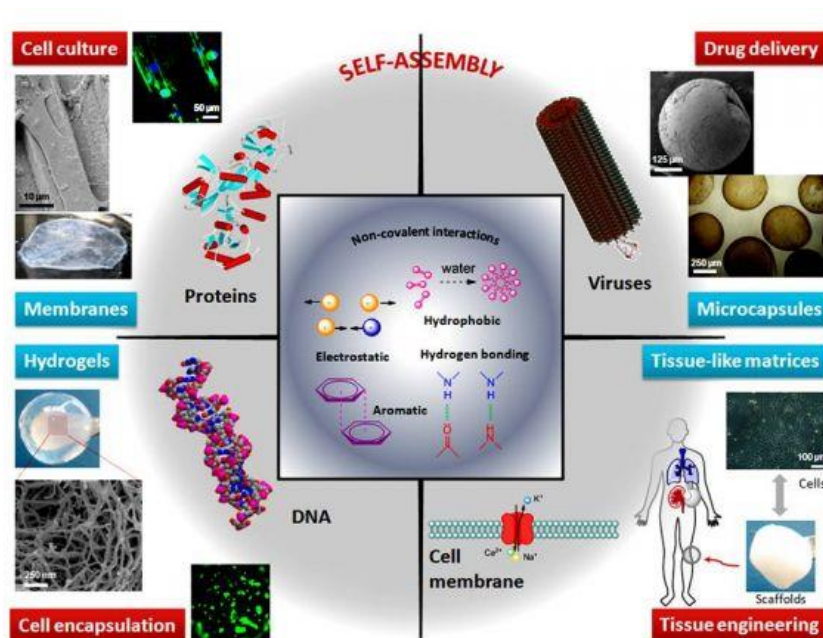


**Figure 1.3** Spontaneously organized molecular self-assembly of molecules into ordered aggregates by non-covalent interactions, this is a revolutionize tissue engineering. (From Ref. 8)

Magnetic nanoparticles self-assembly formed via magneto-tactic bacteria are a chain of nanoparticles arranged in order. This is one of the modern examples for self-assembly in a biological system at the micro and nano metre scale. In this process controlled arrangement of nanoparticle represents genetic level collective size and morphology manipulation and control. Properties of these hierarchical shapes and arrangements impart specific directional magnetic properties to the bacteria.

Liposome-derived nanoparticle assemblies (LNAs) have established their great potential for various diagnostic and therapeutic applications in clinical trials. For better performance and efficient biomedical function, self-assembly forming materials should be biocompatible, stable, and bio-available, with enhanced encapsulation properties. Stimuli-responsive and targeted-delivery of therapeutic and imaging complexes/compounds has been achieved by liposome nanoparticle assemblies' for *in vivo* and *in vitro* cell systems. LNAs have the ability to design and control the size

parameter for bilayer-decoration, surface coupling and encapsulation of a variety of diverse therapeutic drugs (Figure 1.4). The potential of LNAs has been established for future studies such as lipid bilayer interaction and cell membrane penetration through nanoparticle assembly, which is necessary to develop and understand for their clinical trials.

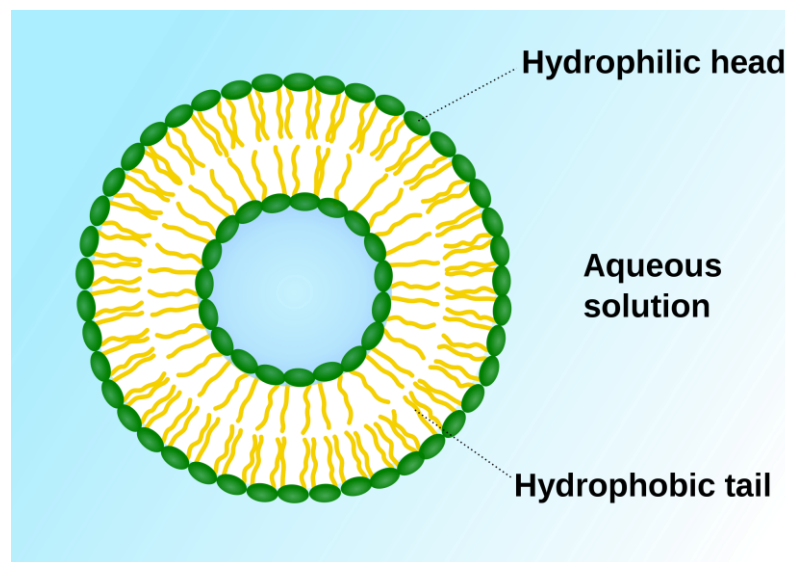


*Figure 1.4 Liposome synthesized by phospholipids in aqueous solution.*

Self-assembled monolayer (SAM) is a technique in which organic molecule monolayer spontaneously forms a controlled network on appropriate substrate surface. To get the desired functionality, SAM can be used for positioning and designing the molecules at proper place on the device. There are several devices prepared by SAM processes such as molecular wires, molecular memories etc.

Colloidal nano crystals have been prepared via different kinds of self-assembly processes. Different types of materials have been constructed for photonic band gap engineering by formation of ordered arrays of metal oxides through self-assembly with various diameters from 100 nm to few microns such as CuO, ZnO, or TiO<sub>2</sub> spheres. Self-assembly of bio-derived compounds and their potential functions rely on their controlling design ability as well as interactions with targeted molecules. In modern molecular science technology, self-assembly is an exceptionally influential technique.

### 1.1.3 Bio-surfactant mediated self-assembly

Being easy to synthesize (and from renewable sources), biosurfactants find significant applications in science and technology, ranging from their straight use as surfactants or as antibacterial to anticancer agents. Effectiveness of biosurfactants is typically determined by their surface tension minimization. Amphiphilic biosurfactant dispersed self-assembled structures are considered to be rather unique materials in the field of nanocarriers and nanobiotechnology. Biosurfactant has the intrinsic ability to form self-assembled structures in various solvent systems due to its amphiphilic nature. Amphiphilic biosurfactant materials generally show evidence of spherical shape such as micelles, vesicles with their diameter size range depending on the hydrophilic-hydrophobic ratio. They can also self-assemble into a variety of nanostructures such as nanowires, nanotubes, and ordered molecular chains. The above mentioned structures are described as supra-molecular assembly of molecular systems.

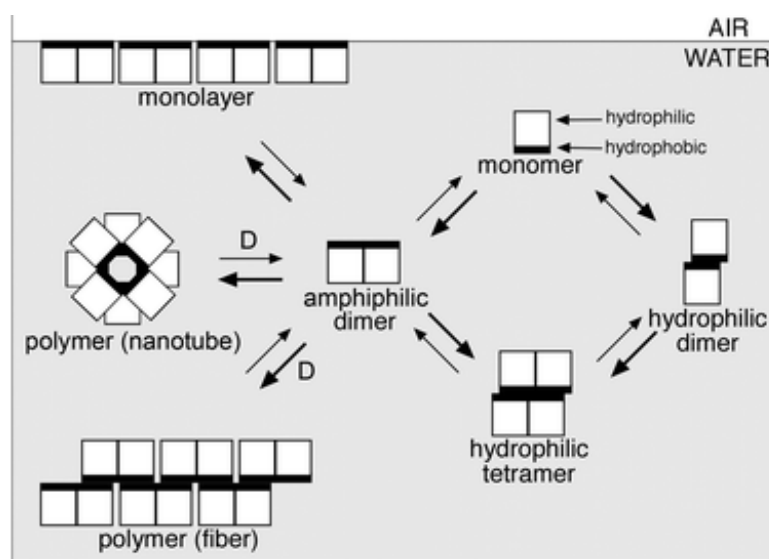


*Figure 1.5 Functional mechanism of amphiphilic biosurfactant based on self-assembly (From Ref. 9)*

These self-assembled biosurfactants have significant roles in several biomedical applications. It is well known that hydrophobic–hydrophobic associations are the driving-energy for amphiphilic molecule based self-assembly formation in aqueous media (Figure 1.5).<sup>9</sup> Several studies have detailed the formation of biosurfactant self-assemblies in aqueous media. Biosurfactants are arbitrarily grafted with lower amounts of hydrophobic moieties which play a significant role in the solubility of the

entire compound. Such differences can organize the morphology of self-assembled structures due to inter and intra-molecular interactions between hydrophobic groups in biosurfactant. The amphiphilic nature of biosurfactant can also be exploited to encapsulate lipophilic materials due to their intrinsic lipophilic core. It also improves hydrophobic drug water solubility in addition to its use as a carrier vehicle for targeted delivery which enhances their bioavailability. This type of drug encapsulation might be due to micro- and nano sized biosurfactant micelles formation.

It is well known that biomaterial compounds can offer exclusive applications in bio imaging field due to their high biocompatibility with minimal interferential absorption. Moreover biomaterial-derived fluorescent compounds have expressed great suitability in bio sensing and bio imaging. Entirely biocompatible and easily available biosurfactants would be the best biomaterials for design and preparation of fluorescent materials with the simplest approach. In our belief, hydrophilic sophorose group moiety in the sophorolipid molecule probably improves its aqueous solubility because of its interactions with water (hydrogen bond formation) while oleic acid moiety is also anticipated to encourage the interaction with any steroid containing compound with highly specific hydrophobic interactions. Therefore sophorolipid with aqueous solubility (sophorose moiety) and phospholipid interaction (Oleic acid moiety) represent the best materials for the development of fluorescent materials for bio-imaging applications. In the present thesis we have developed sophorolipid based nanostructures through UV pulse laser irradiation experiment. Fluorescent sophorolipid nanostructures synthesized by laser irradiation displayed size range around 100 nm which is one of the main acceptability criteria for bio imaging experiments.

## **1.2 Biosurfactant: An Introduction**

---

Biosurfactants are surface-active compounds capable of lowering surface tension between solids, liquids and gases, thus permitting their dispersion in water as well as in other solvents. They are amphiphilic compounds which are mainly secreted extracellularly by microorganisms or may also be produced on their cell surfaces. Biosurfactants mediate reduction of interfacial surface tension due to the presence of both hydrophilic and hydrophobic moieties in their structure. Even though emulsifiers might not reduce surface tension, bio-emulsifiers are frequently considered as



biosurfactants because biosurfactants and bio-emulsifiers both display emulsification properties.<sup>10</sup> Glycolipids, polysaccharide-lipid composite, mycolic acid, phospholipid, and lipoprotein/Lipopeptides are considered as biosurfactants which are produced by microbial synthesis.

Because of the potential utilization of biosurfactants in food-processing, oil industry, and pharmacology science, substantial attention has been given to their synthesis from biological sources as surface-active molecules. Types and quantity of the microbial surfactants mostly depends on their producer organism with other ambient factors such as nitrogen, carbon, temperature, aeration and trace elements. Biosurfactants can be utilized to boost the surface area of hydrophobic component of pesticides in water and soil atmosphere, thus expanding their water solubility (Figure 1.6).

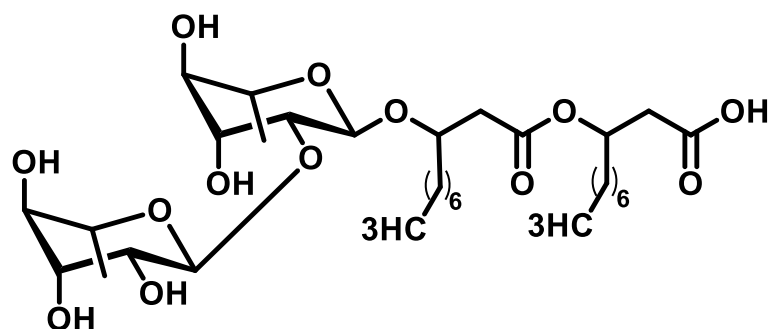


**Figure 1.6** Basic structure of microbial synthesized glycolipid biosurfactant

Therefore the survival of surfactant producing microbes in contaminated environment might enhance the degradation of pollutants. Hydrophobic pollutants close to petroleum hydrocarbons, water and soil environment require solubilization before degradation by microbial cells.<sup>11</sup> The use of biosurfactants for pesticides degradation in water and soil environment has been applied at significant level in recent times.

For the synthesis of biosurfactants, microbes can use a broad range of organic materials as carbon and energy resource. Whilst the energy source is present in its insoluble form, microbes make their availability feasible into the cell membrane by producing a variety of substances, called biosurfactants. Some of the microbes such as bacteria and yeasts excrete ionic surfactants which emulsify the  $C_xH_y$  substance in the growth medium. Three groups of biosurfactant such as rhamnolipids, sophorolipids and trehalose are produced by different *Pseudomonas sp.*, *Torulopsis sp.* and

*Arthrobacter sp.* respectively. There are lipopolysaccharides, such as Emulsan, produced by *Acinetobacter sp.* and lipoproteins such as surfactin and subtilisin, are produced by *Bacillus subtilis*.<sup>12</sup> From the beginning of their invention, due to their excellent biodegradability and easy synthesis procedure, biosurfactants gained attention as alternative surfactants. For the last few decades, exclusive properties of biosurfactants such as biocompatibility, non-toxicity which are lacking in usual chemical surfactants, were apprehended. The molecular structures of biosurfactants have been optimized and refined throughout the synthesis process of microbial production. Moreover, biosurfactant are chiral compounds stereo-selectively synthesized by enzymatic reactions. Therefore at their interfaces, biosurfactants are capable to display excellent packing and orientation properties.<sup>18</sup> Molecular features of biosurfactants allow them to carry out astonishing actions greater than conventional chemical surfactants. Interest in biosurfactants has been continuously increasing in various fields as multifunctional materials are in great demand for the new century.

Several studies have been done for the application of biosurfactants as surface active as well as antimicrobial agents against different types of microbes. Therefore recounting the several types of biosurfactants production and their properties, the present study specifies their new emerging role in the synthesis of fluorescent mesostructures for bio-imaging and hyperthermia potential in cancer study. Fluorescent nanoparticles synthesized by laser irradiation experiment were highly biocompatible.

## **1.2.1 Different types of Biosurfactant**

Some of the important types of biosurfactants discovered so far include Lipopeptides, phospholipids, fatty acids, glycolipids, lipoproteins, particulate surfactants and polymeric surfactants.

### **1.2.1.1 Glycolipids**

Most of the microbial synthesized biosurfactants known are glycolipids. Structural forms of these compounds are made by combination of hydroxyl-aliphatic acids or long-chain aliphatic acids with carbohydrates. Sophorolipids, rhamnolipids, and trehalolipids are known as glycolipids. Sophorolipids, which are mostly produced by yeasts, consist of a combination link between long-chain hydroxy fatty acid and

dimeric carbohydrate sophorose unit. Sophorolipid biosurfactant is a mixture of minimum six to nine different sophoroside hydrophilic moieties.<sup>13</sup> Microbial biosurfactant trehalolipid has been reported in different structural forms. These occur due to the difference in degree of unsaturation, number of carbon atoms and presence of mycolic acid (Figure 1.7).

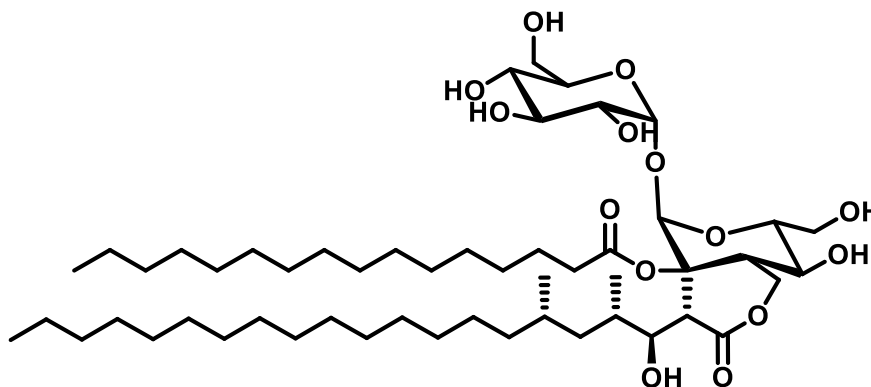


**Figure 1.7** Chemical structures of some common biosurfactants i.e. Trehalose lipid

Production of trehalose dimycolate reported by *Phodococcus erythropolis* has been studied extensively. In the case of rhamnolipid biosurfactant, one or two rhamnose subunits are connected to one or two  $\beta$ -hydroxydecanoic acids side chain. Rhamnose-containing glycolipid production from *P. aeruginosa* was initially studied by Jarvis and Johnson.

### 1.2.1.2 Lipopeptides and lipoproteins

Lipoprotein is a biochemical assembly formed when proteins molecules are covalently or non-covalently bound to the lipids or their derivatives. Several bio-derived molecules have been made by this self-assembly process including structural proteins, lipoproteins, adhesions, enzymes, antigens, transporters, and toxins. This also includes the high density (HDL) lipoproteins and low density lipoprotein (LDL), which primarily work to transport fat globules present in the blood plasma (Figure 1.8). Lipoprotein particles have important function to carry cholesterol and water-insoluble fat globules throughout the body via blood circulation.<sup>14</sup> There are many types of cyclic Lipopeptides that possess remarkable surface-active properties such as lipopeptide and decapeptide antibiotics.<sup>15</sup> *Bacillus subtilis* produces a powerful biosurfactant which is a cyclic lipopeptide called surfactin.<sup>16</sup> It shows excellent

surface tension reduction from 72 - 27.9 mN/m at very low concentrations of 0.5 $\mu$ g/mL. Another example is Viscosin, a potent lipopeptide biosurfactant, which synthesized by the broccoli head rot pathogen *P. fluorescens*. It can bring down the aqueous surface tension from 72 - 27 mN/m at concentration as low as 4 $\mu$ g/mL.



**Figure 1.8** Basic structure of lipoprotein made by phospholipid and triglycerides  
(from Ref. 14)

### 1.2.1.3 Phospholipids and fatty acids

Phospholipid is a compound which is assembled by a glycerol unit, a phosphate group, a polar molecule and two fatty acids. The phosphate group and polar head region of the molecule is hydrophilic, whereas the fatty acid tail is hydrophobic in aqueous medium. Phospholipids orient themselves into a bilayer when they are placed in aqueous medium. A network of bilayers is formed by the polar head section of phospholipids when they are placed in the aqueous environment (Figure 1.9). Animal cell membrane contains phospholipids as a major component which surrounds the cytoplasm as well as other contents present inside the cell.<sup>17</sup> The phospholipids vesicles usually outline the semi-permeable lipid bilayer allowing certain molecules enter or exit across the cell membrane. Many yeast and bacteria, when they grow on n-alkanes produce large amount of phospholipid surfactants and fatty acids throughout their life cycle.

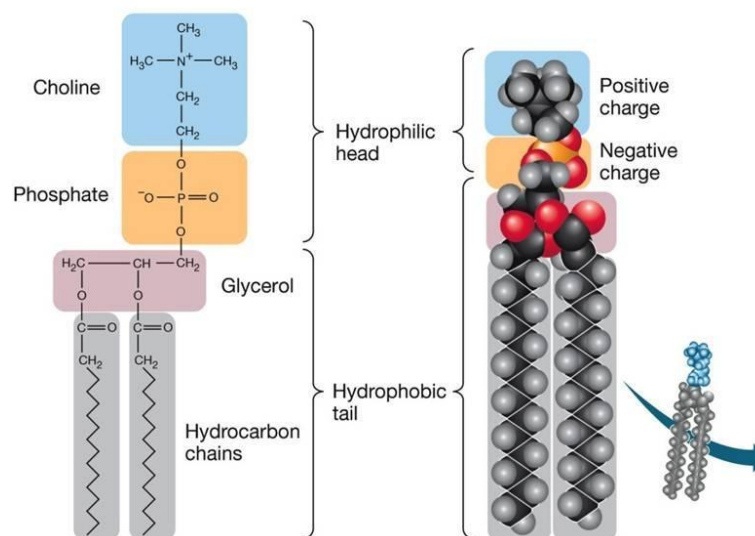


**Figure 1.9** Phosphatidylcholine is the major component of lecithin. It is also a source for choline in the synthesis of acetylcholine in cholinergic neurons. (from Ref. 17)

#### 1.2.1.4 Polymeric biosurfactant

Most recognized polymeric biosurfactants are high molecular weight compounds and generally produced by *Pseudomonas spp.*, *Acinetobacter calcoaceticus*, *Saccharomyces cerevisiae*, *Candida lipolytica*. General examples of polymeric biosurfactants are mannoprotein, oligosaccharide-protein complexes and emulsan. Emulsan, liposan are synthesized by *Acinetobacter calcoaceticus*. Polymeric biosurfactants are very efficient emulsifying compounds at very low concentration 0.001% to 0.01% for hydrocarbons in water. Polymeric biosurfactants are one of the most dominant emulsion stabilizers recognized till date and refuse to accept inversion at a water-to-oil ratio 1:4.<sup>18</sup> Polymeric biosurfactants are produced by *P. fluorescens* throughout their growth on gasoline demonstrated by Desai *et al.* (1988). This bio-emulsifier is comprised of 50% carbohydrate, 10% lipid and 9.6% protein.

#### 1.2.1.5 Particulate biosurfactant

Particulate bio-surfactant which plays a significant task in alkane uptake by microbial cells is an extracellular membrane vesicle. For example, *Acinetobacter sp.* Strain HO1-N produced vesicles with size range 20 to 50 nm with 1.158 g/cm<sup>3</sup> buoyant density are composed of phospholipid and lipopolysaccharide protein. In many hydrocarbon-degrading micro-organisms; surface activity is credited to some cell surface ingredients. These cell surface ingredients contain some formulation such as

M protein, A protein in *Staphylococcus aureus* and lipoteichoic acid in group A *Streptococci*. Some other examples are thin fimbriae in *A. calcoacetiis*, *Bacillus brevis* spores containing gramicidins and prodigiosin in *Serratia spp.*

### 1.3 Sophorolipids

Sophorolipids is a biosurfactant glycolipid material which can be synthesized by selected non-pathogenic species of yeast. When this species (*Candida bombicola*) of yeast cells are challenged with glucose and fatty acids, a glycolipid produced which is known as sophorolipids (SL). Sophorolipids are an amphiphilic compound with hydrophilic sophorose and hydrophobic fatty acid moiety.

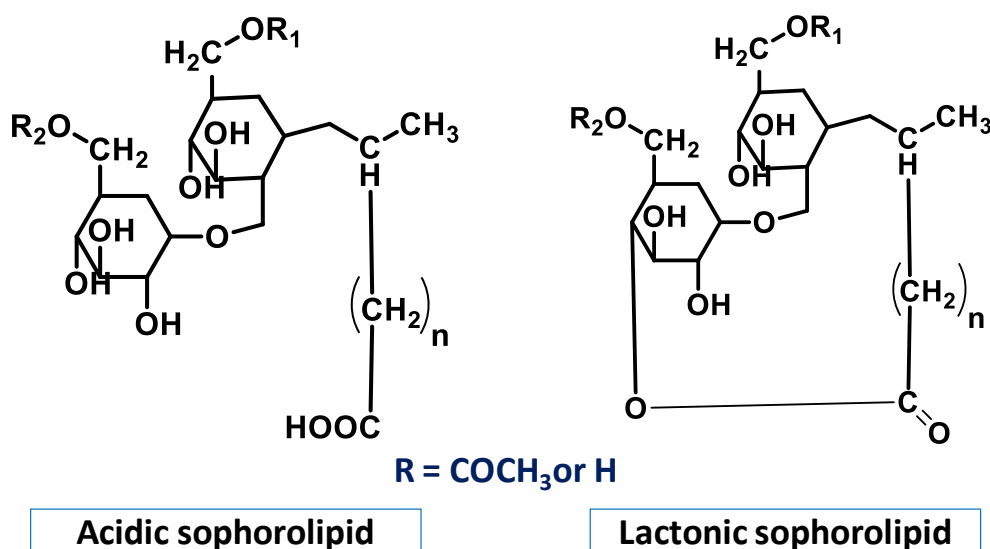


*Figure 1.10 Sophorolipid produced by Candida bombicola*

In sophorolipid, fatty acid carbons have glycoside association with sophorose moiety either at  $\omega$  or  $\omega-1$  position. Sophorolipids are synthesized as a mixture of acidic and lactonic forms (Figure 1.10). Sophorolipid has been synthesized by different *Candida* species, such as *Candida gropengiesseri*, *Candida apicola*, and *Candida bombicola* are common species.<sup>19</sup> *Candida bombicola*, previously identified as *Torulopsis bombicola*, is osmophilic yeast isolated from the honey of bumble-bees. More than eight different structural forms of sophorolipids have been investigated (Figure 1.11). Structural variations in both acidic and lactonic forms are revealed by fatty acid length differences, fatty acid unsaturation, OH group position as well as the degree of acetylation of the sophorose part.<sup>20</sup>



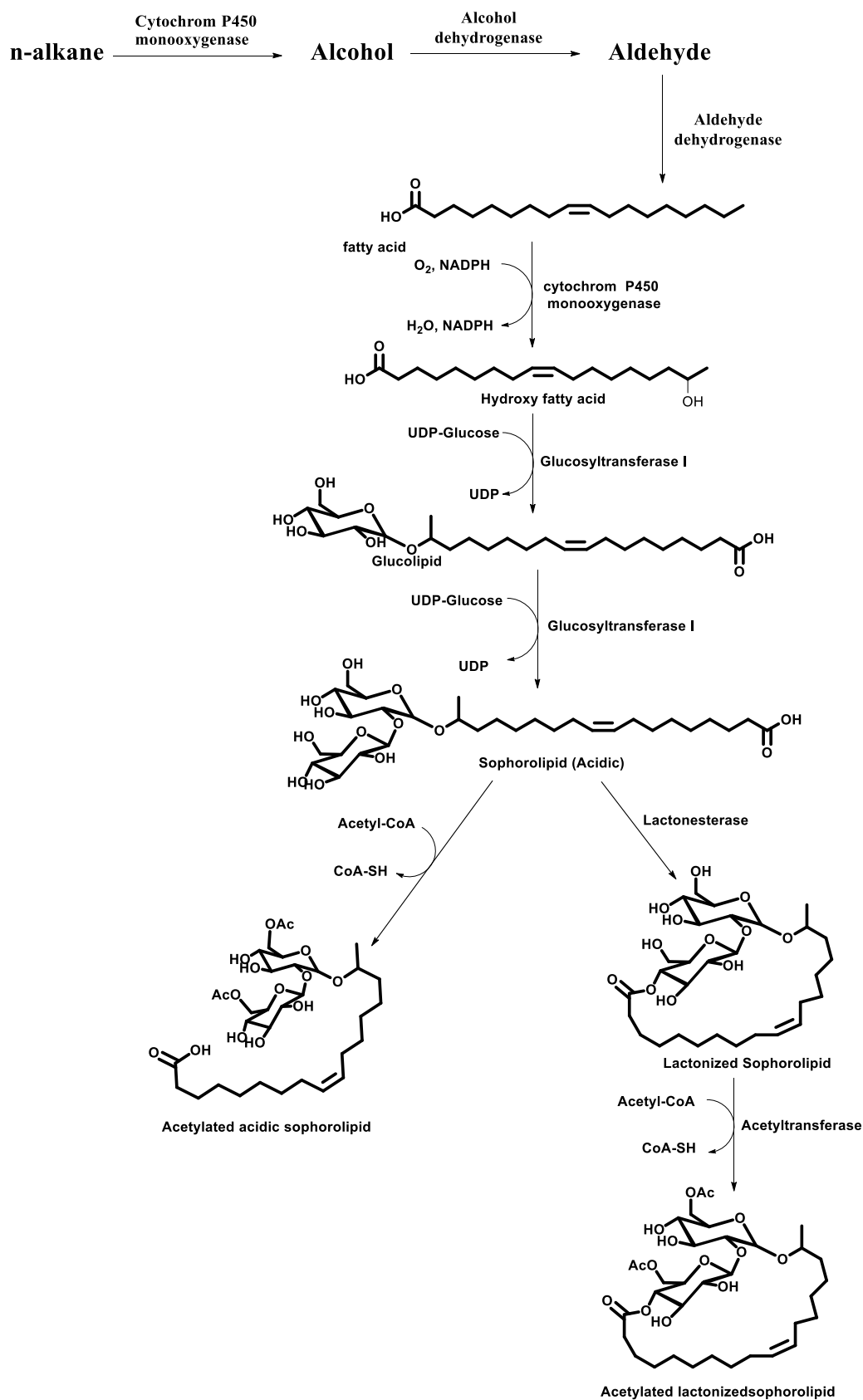


*Figure 1.11 Biosynthetic pathway of sophorolipid production from yeast species candida bombicola proposed by Van Bogaert in 2007*

These crude mixtures are usually viscous brown oils, which are thicker than water. The purpose of sophorolipid synthesis by *Candida bombicola* has been recommended to be associated with alkane uptake.<sup>21</sup> One hypothesis is that the sophorolipids, due to their surface activity, enhance the bioavailability of alkanes which encourage the growth of organism. Because of rising commercial awareness sophorolipids can be simply synthesized in plenty amount from economical raw materials, such as vegetable oils, alkanes and industrial waste products.

### 1.3.1 Application of Sophorolipids

For commercial applications, sophorolipids have to compete with petro chemical origin surfactants in three aspects: production capacity, cost and functionality. Therefore sophorolipid production success relies on the low cost raw materials, and cheaper processes expansion which will reduce its overall cost by 10–30%. Because of their surface tension reducing ability sophorolipids have been used in the manufacture of commercial detergents (Figure 1.12). Sophorolipids also find applications in antibacterial properties, deodorants and cosmetics industries due to their cell membrane perturbation ability. The antimicrobial action is not merely restricted toward bacteria; they also act as antifungal, anti-algal, anti-mycoplasma and antiviral agents.<sup>22</sup> There are many patents available on these applications.

Recently, sophorolipids have also shown promising anti-cancer activity. Sophorolipids could be applied as safe and effective therapeutic agents. Sophorolipids could also be used as probiotics, particularly at a time when drug resistance in many life-threatening diseases organisms is increasing.

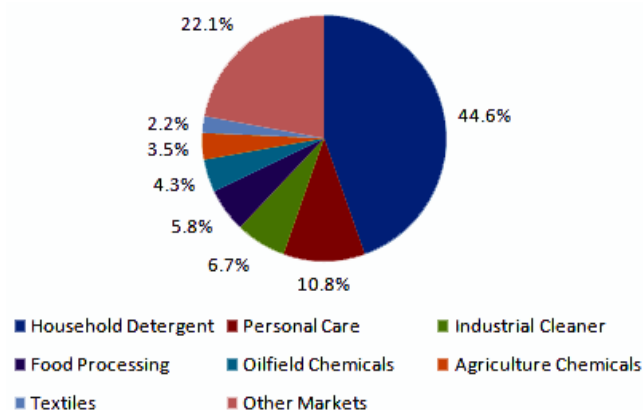


*Figure 1.12 Industrial applications of microbial synthesized biosurfactant*

The anticipated primary action of a sophorolipid is lipid membrane penetration which affects the microorganism's survival in cell environment. Furthermore sophorolipids offer the advantages of biodegradability, low cyto-toxicity and the production based on renewable-resource substrates. Treatment tests with sophorolipid have confirmed that they are not harmful to the skin, do not cause allergic reactions and have an oral safety level which is greater than or equal to 0.05g/kg body-weight. Therefore the US FDA has also approved for the use sophorolipid in food and pharmaceuticals. Cytotoxicity of sophorolipid was evaluated with human epidermal keratinocytes and was proven to be low.

Crude sophorolipid mixture has both acid and lactonic sophorolipids, the lactonic form generally considered the main fraction of the product.<sup>23</sup> It is important to note that lactonic part of the crude sophorolipid is crucial for biomedical applications. Lactonic sophorolipids have revealed superior antimicrobial activity than the acidic sophorolipid. The acetylated form of lactonic sophorolipid has been developed as stimulating agents for cell metabolism of skin dermal fibroblast.

The amphiphilic nature of sophorolipids has widened their scope in nanotechnology. They have been witnessed to play a vital role in synthesis of different types of nanoparticles as size and shape directing agents. Sophorolipids are the governing factors of physiochemical properties of metal nanoparticle synthesis process. Oleic acid, which is an interesting choice as a nanoparticles capping agent, is a frequently used precursors for the synthesis of sophorolipids.

Sophorolipids as well as their tailored analogues have been broadly explored in our lab for different type's nanoparticles synthesis, though their biophysical and biochemical aspects are yet to be explored.<sup>24</sup> Being biosurfactants in nature, sophorolipids have been used for  $\text{Ag}^+$  ions to  $\text{Ag}^0$  reduction, a novel technique without affecting its antibacterial properties reported by Singh *et. al.*

The use of sophorolipids for nanoparticle capping and concurrent reduction has been well established. These results have encouraged the preparation of polymer scaffolds with covalently attached silver nanoparticles. For the synthesis of porous polyethylene scaffolds, sophorolipids were applied to  $\text{N}_2 + \text{H}_2$  plasma treatment, concurrently it was covalently bound to polymer surface by amine groups.<sup>25</sup> To immobilize silver nanoparticles on polymer scaffold a simple amide chemistry was applied, in which

Ag<sup>+</sup> ions were directly exposed to sophorolipid grafted polymer scaffold. The effectiveness of these scaffolds antibacterial activity was tested on *Escherichia coli*, *Pseudomonas aeruginosa*, *Bacillus subtilis*, and *Staphylococcus aureus*. Results of these experiment showed that microorganisms present on silver studded scaffolds do not survive whereas CHO-K1 cells do, therefore making them excellent substrates for tissue engineering bio-implant applications.

Magnetic nanoparticles are well recognized for the various applications in field of mechanical, electrical and biomedical science. In biomedical applications their synthesis in aqueous phase is mandatory. So far, oleic acid as the capping agent has been used for synthesis of cobalt nanoparticles in aqueous medium. However, oleic acid is not a very efficient method for nanoparticle capping due to its poor water solubility.<sup>26</sup> Therefore oleic-acid derived sophorolipid as new water soluble capping agent has been reported in our group for the synthesis of aqueous dispersible cobalt nanoparticles.

Silver nanoparticles with favorable physiochemical properties show excellent toxicity against various microorganisms. Application of aqueous dispersible silver nanoparticles in the biomedical field is well known which is achieved by the use of hydrophilic polymers. Oligo and polysaccharide materials had been used as capping agents, while the reduction process is carried out by sodium boro-hydride and citric acid salts.<sup>27</sup> Production of water dispersible silver nanoparticles by using sophorolipids as capping and reducing agent has been demonstrated by *Singh et al.* Sophorolipid capped silver nanoparticles are considered extremely strong antibacterial agents against both gram-negative and gram positive bacteria. Sophorolipid simultaneously with gellan gum has been used for entirely green synthesis of gold nanoparticles. The gold nanoparticles prepared by using both compounds showed superior killing efficacy against glioma stem cell lines.<sup>28</sup> The anticancer effects of these nanoparticles conjugated with doxorubicin hydrochloride became more prominent. Acidic form of sophorolipids has been reported for the synthesis of magnetic iron oxide nanoparticles by *Baccile et. al.* Characterization of sophorolipid mediated gamma-Fe<sub>2</sub>O<sub>3</sub> nanoparticles showed that iron oxide surface interact with its carboxylic group which confers a large stability to the final material.<sup>33</sup>

Sophorolipid being a natural biosurfactant can travel freely by trans-membrane active transport. Hydrophobic drug could be encapsulated inside hydrophobic core of sophorolipid (amphiphilic material) which will help to transport the drug inside cell membrane by endocytosis movement.<sup>29</sup> Absorption of sophorolipid encapsulated hydrophobic drug inside the cytoplasm might be increased due to sophorose moiety of the molecule which could mimic glucose molecule needed in cancer cell lines. Moreover, when the concentration of sophorolipid increases in cytoplasm, it would bring enough amount of anticancer drug for treatment of the cancer challenge. As an alternative encapsulation material for hydrophobic drug, we have tried to introduce new efficient material at quite lower concentration compared to the earlier described technique. Another advantage of amphiphilic sophorolipid encapsulated drugs is its stability in the gastrointestinal tract and good permeability. Compared to other applications, medicinal purposes require small sized nanoparticles (100nm) which will increase retention time and high improved permeability. Thus in this work we are proposing the synthesis of sophorolipid nanostructure, biophysical and biochemical aspects and their application in targeted drug delivery.

## **1.4 Fluorescence: Mechanism, systems and applications**

---

Fluorescent nanomaterials based on  $\pi$ -conjugated systems have gained considerable attention in biological, optoelectronic devices and chemical sensing applications during last two decades. These  $\pi$ -Conjugated systems provide highly fluorescent materials which are now applied extensively in day to day life. Micro and nanometre scale materials often display diverse physical properties compared to their crystalline solids. Strong fluorescence from these crystalline solids is rather very weak or rare. Aggregation caused by strong intermolecular  $\pi$ - $\pi$  stacking in aggregated or solid states form often enhances fluorescence in feebly fluorescent materials. Some compounds display fluorescence enhancement in the aggregated or solid state called aggregation induced fluorescence.

### **1.4.1 Mechanism of fluorescence**

Fluorescence is a process in which absorption of photons promotes the molecule from singlet ground state to singlet excited state while the spin of the electron still match with ground state electron. When the excited molecule reverses to ground state; it

involves photon emission with higher wavelength and lower energy, than the absorbed one.<sup>30</sup> In luminescence family, the fluorescence process is associated with liable molecule which emits light from electronically excited state either by a physical, chemical or mechanical mechanism. The lifetime of molecules excited states is short-lived ( $<10^{-8}$  seconds). For a molecule, the molecular structure and environment define whether it would be luminescent. Fluorescent molecules usually contain conjugation bond in their molecular structure. Emission and excitation frequency of the compound are completely dependent on the atomic or molecular structure. Luminescence of the molecules through ultraviolet or visible light photon excitation is called photoluminescence.

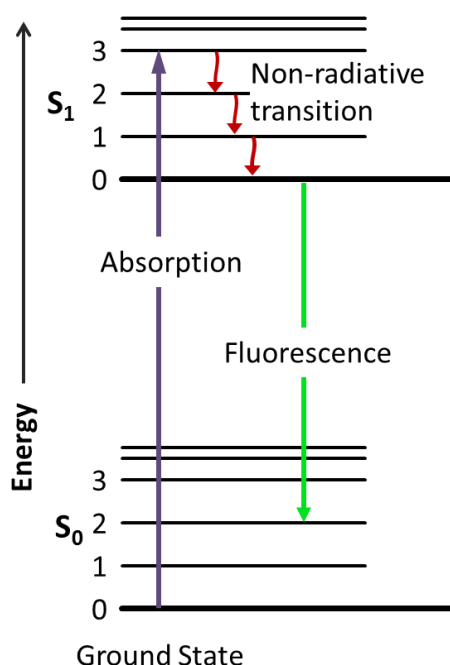


**Figure 1.13** Fluorescence diagram Jablonski diagram (from Ref. 31)

Figure 1.13 depicts the fluorescence energy diagram of Jablonski, absorption of light (purple arrow), fluorescence of the singlet ground state S<sub>1</sub> to S<sub>0</sub>, (green arrow) and non-radiative relaxation where excitation energy is dispersed as heat or vibrations (red arrow). Photoluminescence is usually classified into two modules based on excited and emission state process - fluorescence and phosphorescence.

$$S_0 + h\nu_{\text{ex}} = S_1$$

Where photon energy is  $h\nu$  with Planck's constant  $h$ , the frequency of light is  $\nu$ , the ground state is S<sub>0</sub> of the Fluorophore and its first electronically excited state is S<sub>1</sub>.

## 1.4.2 Fluorescent materials and systems

Phosphorescence of molecules occurs similar to fluorescence, but the lifetime of excited state is much higher. Fluorescent compounds which re-emits light through light excitation is generally called as fluorophores. Cyclic molecules with combined aromatic groups or plane and several  $\pi$  bonds are the general characteristics of fluorophores. Sometimes fluorophores are used as a substrate or probe or indicator in enzymatic reaction, tracer in fluids mechanism or as a dye for staining certain structures.<sup>31</sup>

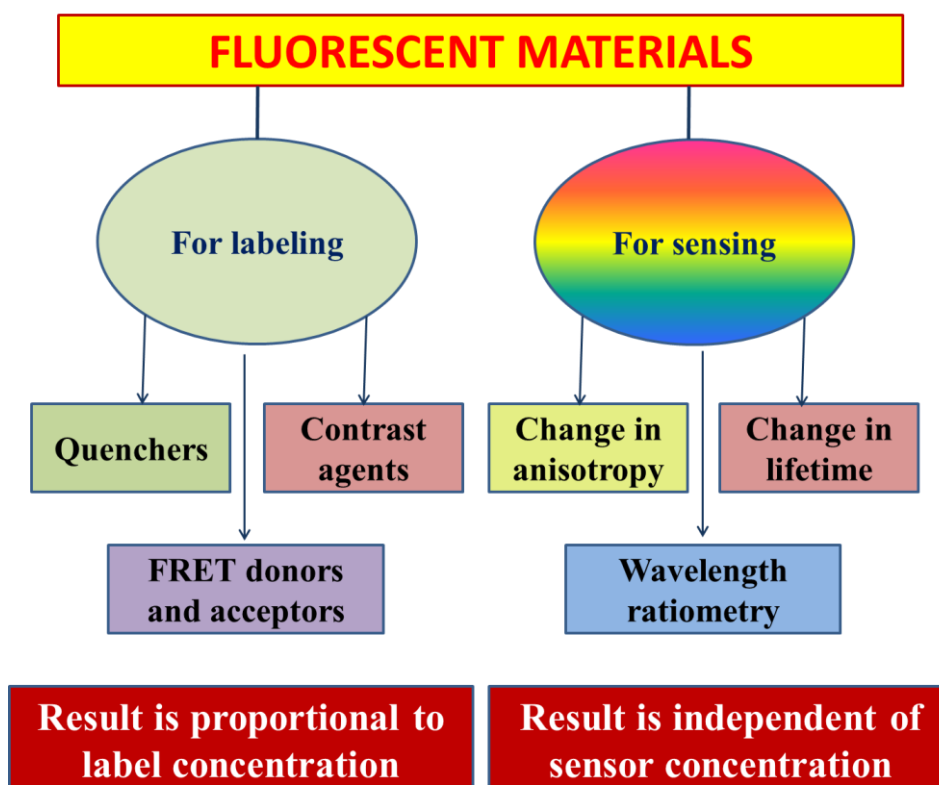


*Figure 1.14 Application of fluorescent materials (from Ref. 32)*

The fluorescence behavior of Fluorophore compounds is affected by conditions such as environment polarity and the presence of ions. Generally the fluorescent molecule is covalently bonded to a reaction substrate, such as a marker (reporter, tag, dye) or bioactive reagents (nucleic acids, peptides, antibodies). Fluorophore materials are normally used in a variety of analytical methods such as detection sensors, cells imaging, tissues staining, i.e., spectroscopy and fluorescent imaging (Figure. 1.14).

### 1.4.3 Self-assembly Induced Fluorescence

In recent time it is realized that self-assembled compounds provide improvement of fluorescence in non-fluorescent or feebly fluorescent materials. This creates avenues for the development of new materials by detecting changes in the fluorescence wavelength, intensity and lifetime of the fluorescent materials. Recently, a straight forward approach for designing fluorescent probes has been developed by captivating improvement of the fluorophore's intrinsic fluorescence activation without any quenching mechanisms. It is well known that the self-assembly of feeble fluorescent material can provide luminescent features by employing the aggregation induced fluorescence process. In the case of some luminous compounds emission was often highly damaged by the aggregated form; this is known as aggregation-caused quenching (ACQ). In 1961 Tang et al. introduced the aggregation induced emission (AIE) process (Figure 1.15). In AIE process molecules that are highly soluble in solvents are non-fluorescent, while they emit fluorescence in aggregated form in contrast to aggregation-caused quenching.

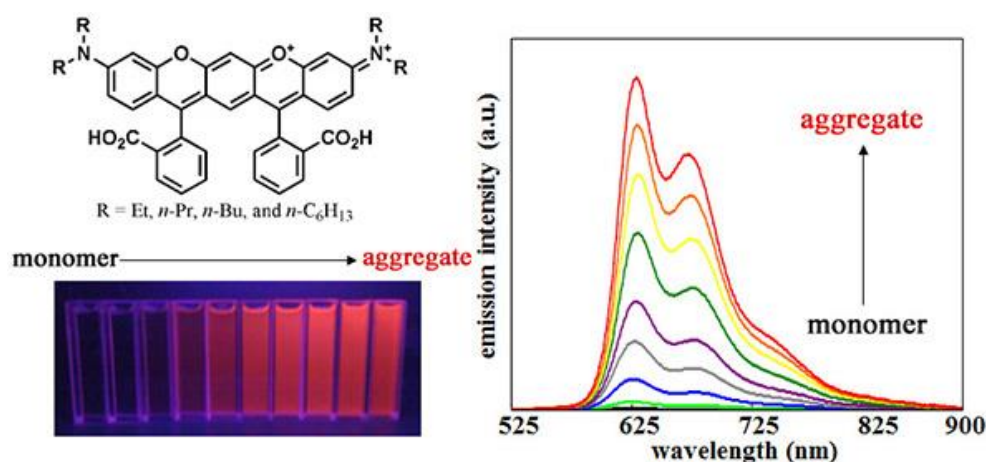


**Figure 1.15** The chemical structure and emission conditions, strong fluorescence is emitted as the monomer turns to aggregate. (From Ref. 33)

The production of self-assembled fluorescent materials is a growing field by employing AIE-effective molecules. Further study for the development of nano/micro scale biomaterials micro-optical self-assembly with AIE process would be the emerging technique in fluorescent sensor field. AIE fluorophores generally require restriction of intra-molecular rotating units such as phenyl rings, which can switch on its fluorescence in aggregate form. In contrast to aggregation-induced emission, the



environment sensitive fluorophores demonstrate feeble fluorescence in polar medium however they are highly fluorescent in hydrophobic medium due to the charge-transfer-induced fluorescence quenching.

#### 1.4.4 Applications of fluorescence (Fluorescence sensing)

A good understanding about fluorescence could offer great improvements into the expansion of medicinal therapeutics for many human diseases. Fluorescent imaging is a leading technique for monitoring biological reactions by high-quality of its reproducibility, sequential resolution and excellent sensitivity. Currently available fluorescent materials for the inspection of protein peptide interactions are dual-labeled peptides, green fluorescent protein and fluorophores labeled peptide.

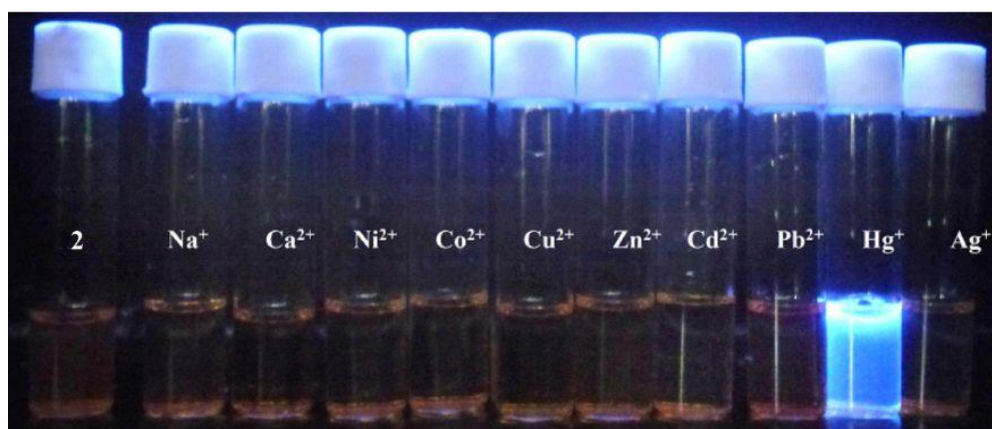


**Figure 1.16** Fluorescent materials application in heavy metal detection (from Ref. 34)

Aggregation induce fluorescent technique would have many applications in controlled drug release and regenerative medicine. For example, some fluorophores are usually weakly fluorescent whereas their fluorescence can be broadly amplified in aggregated form due to aggregation-induced emission (AIE) with probes restrained. The aggregation-induced emission (AIE) technique has unlocked new openings in toxic content detection in biological atmosphere with excellent signal-to-background ratio and great sensitivity.<sup>34</sup> Fluorescence sensors are more-sensitive and elegant, which display signal strength with objective molecule quantity (Figure 1.16). Several self-assembly based materials have been recognized for the sensing purpose with quenching-recovery technique.

Generally, organic synthesis of these complex materials requires efficient and well-designed process despite its wide application in chemical sensing. Chemical sensing is an important aspect of our daily life. Capability towards atmosphere parameter sensing is necessary for tactile stimulation, vision, auditory and olfactory system. Fluorescent sensing is as crucial as chemical sensing for the development of better analysis techniques. Fluorescence sensing is an advanced technique to quantify compounds in any biological and chemical environment. Even though so many techniques have been developed, there are still many notable analytes which couldn't be merely detected. Therefore, new materials for quick and inexpensive testing methods have to be planned for application in biomedical diagnostics, national security and industrial manufacturing. Amongst the diverse types of biosensors, optical and chemical sensors are anticipated on top to develop.

Fluorescence sensors are emerging as one of the most important transduction mechanisms due to their high response as well as many diverse analytical factors that can vary with target analytes. In addition, as compared to electrochemical techniques, fluorescence spectra can travel without a physical waveguide. In the last two decades, several fluorescent sensing materials have been proposed.<sup>35</sup> A crucial part of the development of fluorescent sensing probes is the invention of functional materials with inherent sensing characteristic.

New proposals for the synthesis of self-assembled fluorescent materials for improvement in sensing are an emerging field. Consequently the sensitivity and selectivity of fluorescent materials towards the presence of other factors should be neutral for the better performance of sensor. Nonetheless, sensing is more important due to the fact that majority of analytes are found in aqueous medium, particularly in the environmental and medical applications. Therefore development of fluorescence sensing towards metal ions present in aqueous environment is a key step. The synthesis of new fluorescent materials which would be stable in aqueous environment is clearly preferred; in addition, their sensing abilities towards specific heavy metal ions in aqueous environment should be highly selective. To increase the effectiveness of sensing materials new technique has been applied for the production of nano sized sensors, in the form of nanoparticles. Nano sensors perform better due to their nano sensing probes and small dimensions which would act as individual to resolved intracellular inspection. Photo stability of nano scale fluorescence sensors is still a

problem regardless of improvement sensitivity. We have proposed a new sensing tactic in the field of fluorescence sensing for heavy metal detection. The fast and simple nature of the synthesis process, high-throughput fabrication characteristics and screening of the specific metal properties support this approach.

## **1.5 Drug loaded biosurfactant assemblies**

---

Due to their self-assembly formation characteristics, biosurfactants have been the emerging materials in the field of drug delivery carrier system. Self-assembly of biosurfactant could improve the possibilities to solubilize and protect it from unfavorable external environment. Some other soft materials including microemulsions, biopolymers, emulsions, and bio-membranes have been used in drug delivery carrier system. In order to increase the applicability of these materials in everyday life their atomic scale interactions have to be understood. Therefore it is important to identify the interactions behind self-assembly formation between hydrophobic drug-biosurfactant.<sup>36</sup> Applications of biosurfactant in drug delivery systems are normally favored because of their biocompatibility and tuning flexibility. Therefore biosurfactant tuning flexibility is exploited to improve its surface activity and internal storage for hydrophobic drug delivery.

### **1.5.1 Drug loaded soft nanostructures**

Bioavailability is the most significant limitation to attain the desired drug concentration in the circulatory system of human for the anticipated clinical reaction. Lower aqueous solubility of hydrophobic drugs has been the main setback for their encountered chemical effect. Poor bioavailability is the major challenge to design improved and highly effective drug molecules which can effectively bind with amphiphilic nature of the cell membrane structure. Therefore in recent times, biosurfactants can be used for the preparation of a variety of drug delivery vehicles such as liposomes, vesicles, micelles, dendrimres, exosomes and encapsulated complexes (Figure 1.17). Additionally, to tune their physicochemical properties, specific environments play an important role within the body and allocate the preferred conditions. Phospholipids (phosphatidylcholine and phosphatidylethanolamine) are extensively used natural surfactants in drug delivery systems due to their ability to form various self-assemblies such as liposomes, vesicles and micelles.

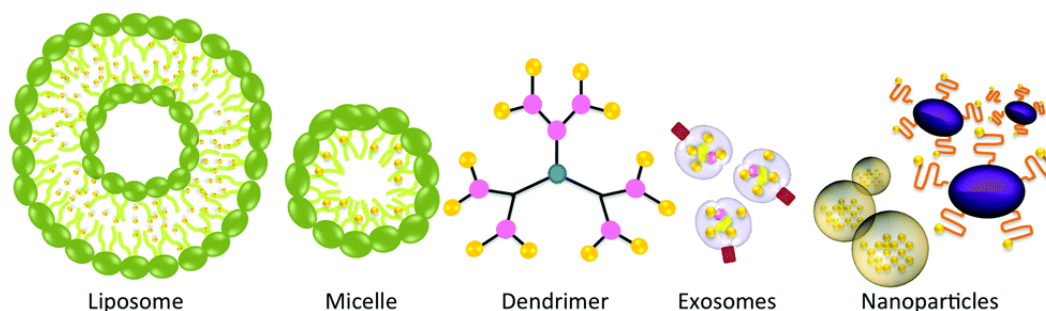


**Figure 1.17** various types of nanostructures assembly have been applied for drug delivery system (from Ref. 37)

Despite their good biocompatibility and low toxicity, phospholipids were not preferred materials for drug delivery as they are expensive.<sup>37</sup> Therefore in the present study we have developed a new class of biosurfactant material (sophorolipid) to increase solubility and enhanced bioavailability of the hydrophobic drug curcumin.

Traditionally turmeric is used as a spice and coloring additive in food preparation. Because of its distinguishing yellow color, turmeric has been used as a coloring agent in food preparation from ancient time (Figure 1.18).<sup>38</sup> Turmeric contains three different types of curcuminoids: curcumin, demethoxycurcumin, and bis-demethoxycurcumin.



**Figure 1.18** Curcumin powder as it is available in market (from Ref. 38)

Due to the endogenous antioxidant properties, curcuminoids encourage defense mechanisms in the human being and have anti-inflammatory efficiency. Therefore curcuminoids influence epigenetic machinery as well as genetic expression of the body. Rhizomes of *curcumina longa* possess curcumin as a main pigment, which express biological properties such as anti-inflammatory, antiangiogenic and antioxidant character. In the last two decades, curcumin has received mounting

attention as a good remedy for various health related problems e.g. neuroprotection, chemo and cancer prevention.

### 1.5.2 Synthesis of Curcumin

Separation of curcumin from crude compounds is lengthy process and various methods have been developed to produce curcumin and its analogues. In 1815, curcumin was first time isolated by Vogel and Pelletier, but its crystallized form was effectively isolated in 1870. Curcumin's structural formula diferuloylmethane and molecular formula  $C_{21}H_{20}O_6$  was hypothesized in 1910 by Milobedzka et al. Later in 1918, Lampe established its five step synthesis procedure starting from ethyl acetoacetate and carbomethoxy feruloyl chloride.<sup>39</sup> Roughley and Whiting (1973) have confirmed the curcumin chemical structure. Occurrence of keto and enol tautomeric form of the curcumin in solution was identified by Payton et al in 2007 using NMR spectroscopy. Pristine curcumin is very rare and costly, and it's always found in the form of curcuminoids (curcumin, demethoxycurcumin, and bisdemethoxycurcumin). However, it could be economically isolated from commercially available curcuminoid mixture by using column chromatography. In a review article in 2010 around 700 healths related medicinal activities of curcumin analogues have been described. In some studies, biological activity of curcumin analogues emerged to be more powerful than curcumin.<sup>40</sup>

### 1.5.3 Derivatives of Curcumin

Depending on the geographical environment, curcumin content in turmeric could change 2 and 9%. Based on the study of different plant species investigated, *Curcuma zedoaria* contain the maximum curcuminoid (>100  $\mu\text{g/g}$ ). Various studies have revealed that biosynthesis of curcuminoid is a very long process, which starts by p-coumaroyl-CoA synthesis from amino acid phenylalanine, with cinnamic acid and p-coumaric acid appearing as intermediates.<sup>41</sup> However, curcumin is specially biosynthesized from cinnamoyl-CoA. Basic molecular formula of curcumin is  $C_{21}H_{20}O_6$ , formula weight 368.39 g/mol and melting point about 170–175 °C.<sup>42</sup> Commercially available curcumin is a mixture of about 77% curcumin, 17% demethoxycurcumin, and 3% bisdemethoxycurcumin (Figure 1.19).<sup>42</sup>

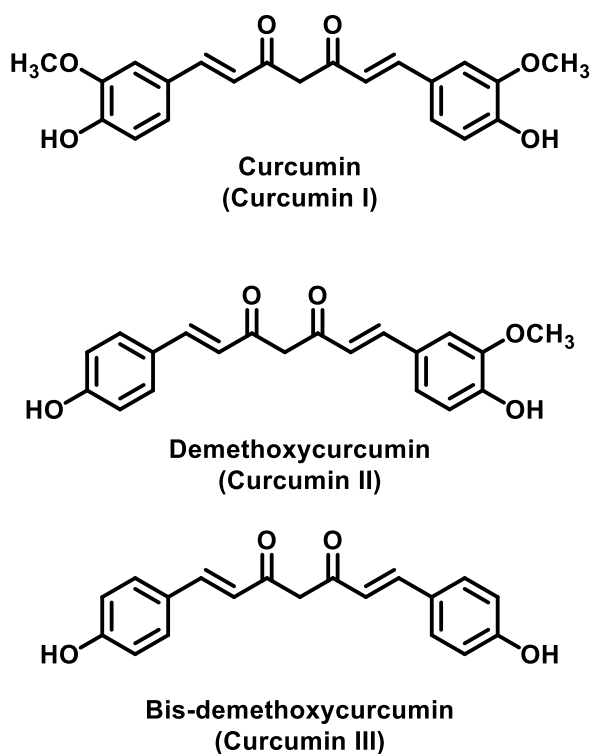


**Figure 1.19** Commercial available curcumin typically contains curcumin I (~77%), curcumin II (~17%) and curcumin III (~3%) as its major components.

Molecular structure of curcumin comprises two ferulic acid units, linked via a methylene group. Curcumin in solution typically represents keto–enol tautomerism state which is stabilized by hydrogen bond. Tautomeric equilibrium of curcumin structure is partially dependent upon solvent pH value and its polarity.<sup>43</sup> Enol form of the curcumin appears in non-polar solvent due its intramolecular hydrogen bond formation while diketo form appears in polar solvent. Enol form of curcumin dominates at more than pH 8 and act as proton donor while diketo form dominates at acidic pH and act as a proton donor (Figure 1.20).

Curcumin is a yellow-orange pigment that is ethanol soluble and exhibits weak green fluorescence.<sup>44</sup> Methanol, chloroform, dichloromethane, dimethyl sulfoxide, acetone and ethyl acetate are also good solvents for curcumin solubility. Water and Diethyl ether are bad solvent for curcumin application. It is light-sensitive and unstable in alkaline solutions. Yellow color of curcumin is due to the presence of conjugated double bond (C=O-C=C) and structurally symmetrical arrangement of two chromophores.

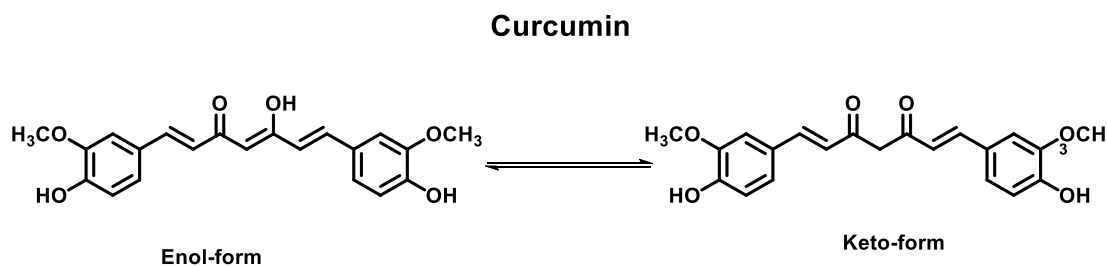


*Figure 1.20 Curcumin as it appears in solution medium*

Curcumin exhibits strong absorption at 420 nm in organic solvents. In aqueous solutions its absorption is significantly decreased.<sup>45</sup> Absorption spectra of curcumin illustrate diverse profile at various pH values and maximum absorption appearing by gradual hypsochromic shift. Curcumin absorption strength reduces with its declining pH value.

#### 1.5.4 Curcumin stability

Curcumin stability is pH dependent in aqueous solution, maximum at pH 1.0–6.0, thereby its degradation is extremely slow in the stomach or small intestine while its solubility is weak. It is most likely stable at this pH range due to the undissociated hydroxy groups. At pH >7.0 curcumin turned out to be unstable and within 30 minutes of in vitro preparation its 90% part is already degraded.<sup>46</sup> Trans-6-(4'-hydroxy-3'-methoxyphenyl)-2, 4-dioxo-5-hexenal and minor extent into feruloylmethane, ferulic acid, and vanillin are curcumin's main degradation components (Figure 1.21).

The curcumin degradation rate is very high at pH>10. Bis-demethoxycurcumin degradation process is considerably long compared to demethoxycurcumin and curcumin. This might be due to the absence of two methoxy groups in its structure. Therefore bis-demethoxycurcumin is used as additive in foods to improve color stability due to its low degradation rate and increased heat stability.<sup>46</sup> Moreover curcumin is able to prevent its degradation at acidic pH value, due to antioxidant nature in presence of glutathione, N-acetyl-L-cysteine and ascorbic acid. In cell culture medium, stability of curcumin is higher due to the presence of 10% fetal calf serum in contrast to alkaline medium. Therefore stability of curcumin might be improved by addition of bovine serum albumin and phospholipid liposomes.



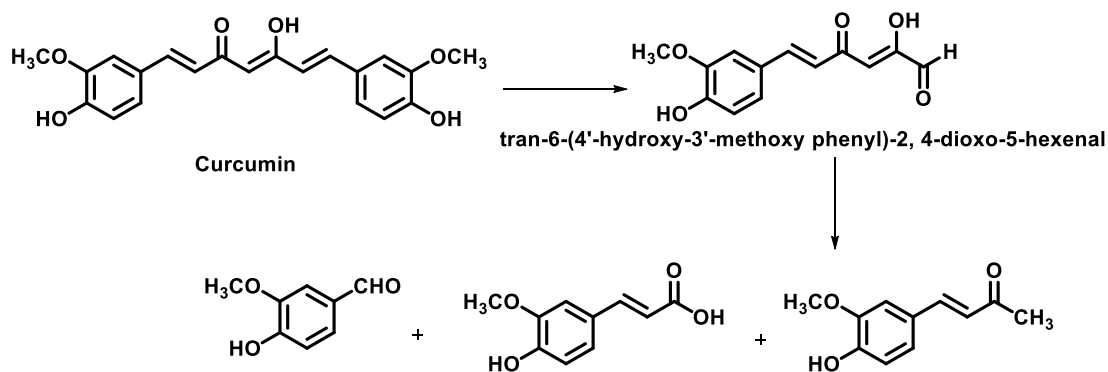


*Figure 1.21* Final product of curcumin degradation

### 1.5.5 Curcumin bioavailability

The most significant negative point about curcumin applications in humans and animals is its low bioavailability which limits its biological efficacy. Bioavailability study elucidates the rate and amount of curcumin that appears in the blood plasma due to absorption and finally reaching to the destination point. Liver and intestine are the two main points for the estimates of curcumin bioavailability. Bioavailability of curcumin has been calculated in many studies on human and rodents under laboratory conditions.<sup>47</sup> Due to the little intestinal absorption and quick degradation in liver, curcumin bioavailability is very low and it is finally discarded via the gall bladder. In an experiment on Sprague Dawley rats it has been revealed that after 1 g/kg body weight curcumin administration, majority of the curcumin is removed unaffected.<sup>48</sup>

Elimination amount of curcumin in urine is negligible; it's mostly excreted by fecal excretion.<sup>49</sup> Therefore detectable amount of curcumin is present in human plasma after gram range dose of its oral administration. Several bioavailability studies show that the plasma levels of curcumin was below 1 mM after its administration. The maximum amount of curcumin was usually detected in plasma after 1–2 h administration.<sup>50</sup> Various techniques have been projected to enhance aqueous solubility of curcumin to improve bioavailability due to its hydrophobic nature. Several studies have been performed to increase curcumin solubility by methods such as complex formation with metal ions, such as  $\text{Cu}^{2+}$ ,  $\text{Mg}^{2+}$ ,  $\text{Se}^{2+}$ , and  $\text{Zn}^{2+}$  as well as with serum albumin.<sup>51</sup> Piperine, nanoparticles, liposomes, and phospholipids are also employed to enhance curcumin bioavailability. Poly lactic-co-glycolic acid (PLGA)



was also applied to enhance curcumin bioavailability through its nano-encapsulation. According to Xie et al, bioavailability of curcumin could be elevated six-fold with PLGA encapsulation nanoparticle (size 200 nm), compared to oral administration in clinical studies.<sup>52</sup> Furthermore, PLGA-curcumin nanoparticles (158 nm) in some other animal studies have shown 20 times more enhanced bioavailability as compared to oral administration.<sup>53</sup> In addition, lecithin liposomes have been used for the encapsulation of curcumin to increase its bioavailability in rats. Cyclodextrin was also used for the encapsulation of curcumin with higher cellular concentrations in vitro. For the encapsulation of curcumin, phospholipid or phosphatidylcholine complexes have also been applied to increase curcumin absorption in rats as compared to its oral administration. Curcumin levels in plasma were found to increase usually five times in liver via curcumin–phospholipid complexes compare to control.<sup>54</sup>

### 1.5.6 Medicinal activity and molecular targets of Curcumin

*Curcuma longa* had been very popular and considered as a therapeutic plant for basic treatment from thousands of years. According to long-established Indian (Ayurveda) and medicine of China, turmeric had been used for healing inflammation.<sup>55</sup>

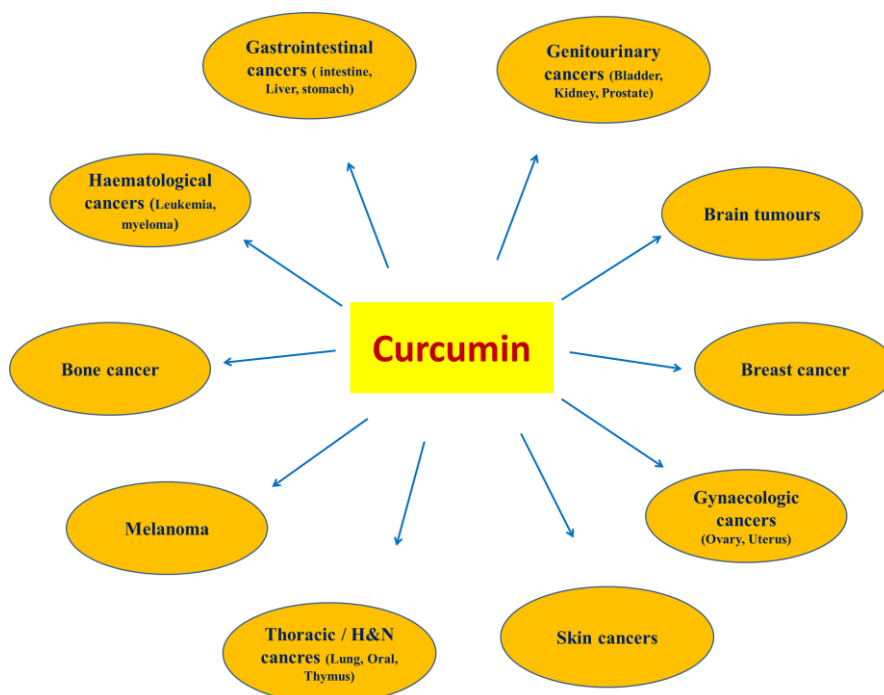


*Figure 1.22 Applications of curcumin in various cancer treatments*

In 1937, first scientific article on turmeric was published for biliary disorders treatment. After that the number of articles on curcumin significantly increased, especially in the last two decade (Figure 1.22). More than 1200 publications can be searched in Pub Med with curcumin search term for the year 2012 alone.<sup>56</sup>

However the number of concluded clinical studies is relatively low. Several health advantages have been credited to curcumin, such as anti-inflammatory, wound healing, antioxidant, analgesic, antibacterial, and eupeptic properties.<sup>57-60</sup> Moreover, anti-carcinogenic and neuroprotective properties of curcumin were also being explored. Presence of the  $\beta$ -diketone, phenolic, and its methoxy groups in curcumin contributed towards scavenging and free-radical activity. Several authors have claimed that radical-scavenging properties of curcumin are mostly obtained by its phenolic structure, and presence of two methoxy groups, at the ortho positions.

## 1.6 Scope and Nature of Present Work

---

During the course of this PhD work, work is performed on the development of novel/atypical routes to the synthesis of sophorolipid self-assembled structures and their use for important biomedical applications like bio-imaging and drug delivery. The different problems undertaken are briefly described below.

**1.** A novel photochemical route employing UV laser pulses (KrF Excimer, 248 nm) is introduced for the synthesis of fluorescent mesostructures of biologically derived sophorolipid. The procedure differs completely from any previously discussed strategies wherein the biologically derived compound has been used for fluorescent nano scale materials synthesis. It is confirmed that this pulsed laser-induced procedure when applied to sophorolipid, gives beautiful nanoscale fluorescent self-assembled structures. This technique is flexible and obviously applicable to the other specific bio-derived compounds for making fluorescent nanomaterials without additions of any metals ions or harmful solvent. The stated method has also been applied for the encapsulation of  $\text{Fe}_3\text{O}_4$  nanoparticles to making them biocompatible for cellular environment.  $\text{Fe}_3\text{O}_4$  nanoparticle loaded fluorescent sophorolipid mesostructures were completely non-toxic for human cell lines.

2. Sophorolipid is used to realize an increase in the solubility and bioavailability of curcumin by co-processing. This technique allowed holding curcumin in its native form in the aqueous environment for a very long time (four month). The process involves sonication of sophorolipid with curcumin in aqueous environment. During the sonication process, curcumin became nano-sized and gets encapsulated by sophorolipid self-assembled structure. Cyto-toxicity of this encapsulated curcumin increases towards human cancer cell line. Enhanced cyto-toxicity of encapsulated curcumin is increase probably due to the presence glucose moiety in sophorolipid molecule.

3. Development of a fluorescent sensor for heavy metal ion sensing which is highly selective is essential for robust and cost-effective analysis of aqueous environments. In the present work this was accomplished by UV laser irradiation of antibiotics cephalixin. The process involves couple of minutes of UV laser irradiation of cephalixin antibiotics dissolved in water. UV irradiation induced aggregation is noted to cause the fluorescence in cephalixin molecular system through self-assembly. This aggregation induced fluorescence is also seen to be specifically quenched by the mercury metal ions in water. Therefore this biocompatible fluorescent sensor holds promise in the context of the environmental toxic metal problem.

## References

1. <http://vtu.ac.in/nano-technology>
2. G. M. Whitesides, M. Boncheva, PNAS, 2002, 99, 4769–4774, <http://pubs.rsc.org/en/content/articlepdf/2013/cs/c2cs35427f>
3. CarstenTschierske, Angew. Chem. Int. Ed. 2013, 52, 8828 – 8878, <http://www.sems.qmul.ac.uk/staff/research/?h.azevedo>
4. M. Grzelczak, L. M. Liz-Marzán, ACS nano, 2010VOL. 4, NO. 7, 3591–3605, <http://en.wikipedia.org/wiki/Liposome>
5. J. Zheng, G. Zhu, Weihong Tan, ACS nano, 2013, VOL. 7, NO. 8, 6545–6554, <http://pubs.rsc.org/en/content/articlehtml/2011/cc/c1cc13139g>
6. N. C. Reichardt, M. Martí n-Lomas, S. Penade´s, *Chem. Soc. Rev.*, 2013, 42, 4358–4376

7. Y. Mochida, H. Cabral, K. Kataoka, *ACS Nano*, 2014, 8 (7), pp 6724–6738
8. L LLocka, M LaCombb, Honggang Cui, *Faraday Discuss.* 2013, 166, 285–301
9. M A. Cohen stuart W T S huck, S Minko, *nature materials*, VOL 9, FEBRUARY 2010
10. Rodrigues, I.M. Banat, J. Teixeira, R. Oliveira, *Journal of Antimicrobial Chemotherapy*2006, 57, 609.
11. J.H. Fuhrhop, T. Wang, *Chem. Rev.* 2004, 104, 2901.
12. P. Singh, S.S. Cameotra, *TRENDS in Biotechnology*, 2004, 22, 142.
13. A. Daverey, K. Pakshirajan, P. Sangeetha, *World Academy of Science, Engineering and Technology*2009, 51, 497
14. I.N.A. Van Bogaert, K. Saerens, C. De Muynck, D. Develter, W. Soetaert, J.E.Vandamme, *Appl Microbiol Biotechnol.* 2007, 76, 23.
15. Z. Ma, A. Haddadi, O. Molavi, J. Samuel, *J of Biomedical Materials Research A*,2007, 300-310
16. L. Zhang, P. Somasundaran, S.K. Singh, A.B. Felse, R. Gross, *Physicochem. Eng. Aspects*2004, 240, 75.
17. N. Baccile, N. Nassif, L. Malfatti, *Green Chem.*2010,12, 1564.
18. T.T. Nguyen, D.A.Sabatini, *Int. J. Mol. Sci.* 2011, 12, 1232.
19. M.B. Kasture, P. Patel, A. A. Prabhune, B. L. V. Prasad, *J. Chem. Sci.*2008, 120, 515.
20. H. Isoda, H. Shinmoto, D. Kitamoto, M. Matsumura, T. Nakahara, *Lipids*1997, 32, 263.
21. A. Furstner, K. Radkowski, J. Grabowski, C. Wirtz, R. Mynott, *J. Org. Chem.* 2000,65, 8758.
22. D. Kitamoto, T. Morita, T. Fukuoka, M. Konishi, T. Imura, *Current Opinion in Colloid & Interface Science* 2009, 14, 315.
23. J. Chen, X. Song, H. Zhang, Y.B. Qu, J.Y. Miao, *Appl Microbiol Biotechnol.* 2006, 72, 52.
24. S.L. Fu, S.R. Wallner, W.B. Bowne, M. D. Hagler, M.E. Zenilman, R. Gross, M.H. Bluth, *Journal of surgical research*2008, 148, 77.
25. M. Kasture, S. Singh, A. Prabhune, B.L.V. Prasad, *Langmuir* 2007, 23, 11409.

26. V. Shah, G. F. Doncel, T. Seyoum, K. M. Eaton, I. Zalenskaya, R. Hagver, A. Azim, R. Gross *Antimicrobial agents and chemotherapy* 2005, 49, 4093
27. V. Shah, G. F. Doncel, T. Seyoum, K. M. Eaton, I. Zalenskaya, R. Hagver, A. Azim, R. Gross *Antimicrobial agents and chemotherapy* 2005, 49, 4093
28. E. Zini, M. Gazzano, M. Scandola, *Macromolecules* 2008, 41, 7463.
29. K. Joshi-Navare, A. Shiras, A. Prabhune, *Biotechnol J*, 2011, 6, 509.
30. Z Chang, Y Jiang, H Qiu, Ben Zhong Tang, *Chem. Commun.*, 2013, 49, 594
31. H Shi, J Dai, Li-wen Shi, Mei-hua, Chuan Dong, *Chem. Commun.*, 2012, 48, 8586–8588
32. <http://en.wikipedia.org/wiki/Fluorescence>
33. B An, S Kwon, S Jung, S Y Park, *J. AM. CHEM. SOC.* 2002, 124, 14410-14415
34. Han Yu and Limin Qi, *Langmuir* 2009, 25(12), 6781–6786
35. A. P Demchenko, *Methods Appl. Fluoresc.* 1, 2013, 022001
36. X Zhang, X Lu, Y Zhen, Jie Liu, W Hu, *J. Mater. Chem. C*, 2014, 2, 5083
37. H. Yu, Q. Huang, *J. Agric. Food Chem.* 2012, 60, 5373–5379
38. P. Anand, Ajaikumar B., B B. Aggarwal, *Molecular Pharmaceuticals*, 2007, 4, 807–818
39. Kuo-Yi Yang, Lei-Chwen Lin, Ting-Yu Tseng, Shau-Chun Wang, Tung-Hu Tsai, *J. Chromatogr. B*, 2007, 853, , 183–189
40. Reason W, Mysore S, M B Wang, Eri S Srivatsan, *Molecular Cancer*, 2007, 10, 12
41. A. Shehzad, J. Lee, Y. S. Lee, *International Union of Biochemistry and Molecular Biology*. 2013, 26, Pages 56–68
42. B. B. Aggarwal, K. B. Harikumar, *The International J of Biochemistry & Cell Biology*, 2009, 41, 40–59
43. B. B. Aggarawal, A. Kumar, A. C. Bharti, *Anticancer Research*, 2003, 23, 363-398
44. A. Barik, K. I. Priyadarsini, H. Mohan, *Photochemistry and Photobiology*, 2003, 77(6), 597–603

45. Albena T. Dinkova-Kostova, Paul Talalay<sup>1</sup>, *Carcinogenesis*, 1999,20(5), 911–914
46. Y. M. Sun, H.Y. Zhang, D. Z. Chen,C. B. Liu, *Org. Lett.*, 2002, 4(17), 2909-2911
47. G. Began, E. Sudharshan, A. G. AppuRao, *J. Agric. Food Chem.* 1999, 47, 4992-4997
48. J. Barry, M. Fritz, A. Ramamoorthy, *J. Am. Chem. Soc.* 2009, 131, 4490–4498
49. P. Basnet, H. Hussain, N Skalko-Basnet, *J of Pharmaceuticals Sciences*, 2012, 101, 598-609
50. T. Ha Ho, T. P. T. Dao, M. C. Dang, *Adv. Nat. Sci.: Nanosci. Nanotechnol.*, 2013, 4, 045008
51. P.R. Krishna Mohan, G. Sreelakshmi, Roy Joseph, *Vibrational Spectroscopy*, 2012, 62, 77– 84
52. Z. Ma, A. Haddadi, O. Molavi, J. Samuel, *J of Biomedical Materials Research A*,2007, 300-310
53. Bhawana, R. K. Basniwal, H. S. Buttar, N. Jain, *J. Agric. Food Chem.*, 2011, 59, 2056–2061
54. B. B. Aggarwal, W. Yuan, S. Li, S. C. Gupta,*Mol. Nutr. Food Res.* 2013, 57, 1529–1542
55. H. HjorthTønnesen, *Pharmazie*, 2006, 8, 696-700
56. E. Gülçür M. Thaqi, F. Khaja, H. Önyüksel, *Drug Deliv. and Transl. Res.*, 2013
57. Z Chang, Y Jiang, H Qiu, Ben Zhong Tang, *Chem. Commun.*, 2013, 49, 594
58. H Shi, J Dai, Li-wen Shi, Mei-hua, Chuan Dong, *Chem. Commun.*, 2012, 48, 8586–8588
59. B An, S Kwon, S Jung, S Y Park, *J. AM. CHEM. SOC.* 2002, 124, 14410-14415
60. Han Yu and Limin Qi, *Langmuir* 2009, 25(12), 6781–6786
61. X Zhang, X Lu, Y Zhen, Jie Liu, W Hu, *J. Mater. Chem. C*, 2014, 2,5083

## Chapter 2

---

# Synthesis and Characterization technique

---

**This chapter briefly describes the experimental procedures for the synthesis of sophorolipid, isolation, purification and the characterization equipment's used in the research that is represented in the thesis. Basic concepts and principles have been discussed herein.**

## 2.1 Sophorolipid biosynthesis

### 2.1.1 Materials

Media composition for the synthesis of sophorolipid such as malt extract, glucose, yeast extract and peptone used in this study were purchased from Hi-media, India; Oleic acid was purchased from Sigma-Aldrich (USA). Sodium sulphate was purchased from Merck, India. Organic solvents such as ethyl acetate and n-hexane used were of analytical grade and were purchased from Rankem India.<sup>1</sup>

### 2.1.2 Microorganism and maintenance

Micro-organism, a yeast *Candida bombicola* (ATCC 22214) was used for synthesis of sophorolipid (SL). It was obtained from American type culture collection, USA. *Candida bombicola* was grown for 48 h at 28 °C on agar slants containing: malt extract, 0.3 %; glucose, 2.0 %; yeast extract, 0.3 %; peptone, 0.5 % and agar, 2.0 %. *C. bombicola* was sub-cultured monthly and maintained at 4 °C in a refrigerator.<sup>2</sup>

### 2.1.3 Inoculum development

Before the production of sophorolipid, inoculum was developed by transferring a loop-ful *C. bombicola* cells from slants to MGYB (malt extract, 0.3%; glucose, 2.0%; yeast extract, 0.3%; peptone, 0.5%) broth medium and incubated for 24 h at 28 °C with 180 rpm orbital shaking (Figure 2.1).



*Figure 2.1 Incubator shakers for sophorolipid synthesis (Image from Ref. 2)*



### 2.1.4 Synthesis of Sophorolipid

Production of sophorolipid was performed in 1000 ml Erlenmeyer flasks containing 200 ml MGYP medium. The fermentative production of SLs was initiated by transferring the inoculum (10%, v/v) into 200 ml of medium followed by incubation at 28 °C with 180 rpm orbital shaking. MGYP medium was supplemented with 1 ml Oleic acid dispersed in equal volume of ethanol. The fermented broths were examined for the production of SL at regular intervals (12, 24, 48, 72 and 96).<sup>3</sup>

Sophorolipid of oleic acid was prepared by resting cell method. In the first step adequate cell mass was harvested by growing the *Candida bombicola* (ATCC 22214) in MGYP medium. Then the cells were redispersed in production medium containing 10% glucose. This production medium is supplemented with hydrophobic secondary carbon source i.e. oleic acid in absolute alcohol. Incubation of yeast biomass with glucose and fatty acid at 28 °C and 180 rpm on shaker for 96 to 120 hrs, a brown and viscous crude SL could be seen at the flask bottom (Figure 2.2).

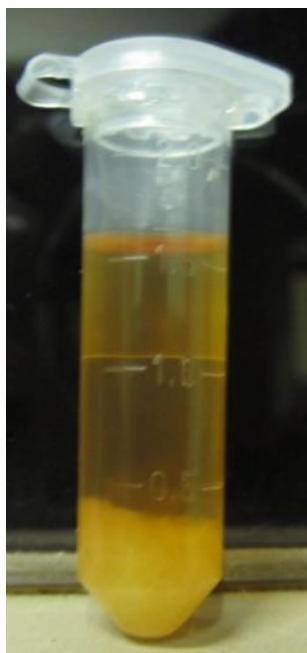


**Figure 2.2** Typical oily crude sophorolipid from *Candida bombicola*.

After incubation period, cells were separated from the broth by centrifugation at 5000 rpm, 10 °C for 20 min. Extracted of SL from supernatant was done with ethyl acetate. To the ethyl acetate phase, anhydrous sodium sulphate was added for removal of residual water, filtered and then ethyl acetate was removed under vacuum. The unconverted fatty acid was removed by washing with n-hexane.

Extraction of the sophorolipids was only possible with solvent extraction. Sophorolipid can be synthesized by other lipophilic carbon materials substrates with carbon chain length C 14-18. Increased interest in lactonic sophorolipid lies in its structure which is single structural form the diacetylated lactone. This form of the sophorolipids has biological importance because of high potential application in cancer treatment.

### **2.1.5 Isolation of sophorolipid**

After incubation of 72 hrs it was observed that SL brownish viscous layer production begin at the bottom of the culture broth which was continuously increased till 96 hrs. After 99 hrs, culture medium was centrifuged at 5000 rpm for 10 min. The supernatant was separated and extracted twice with equal volumes of ethyl acetate. To make sure the isolation of SLs, the cells were also washed with ethyl acetate to remove the glycolipids and fatty acid stick to cells. Then ethyl acetate layer obtained from both the supernatant extraction and washing of cells were collected and dried over anhydrous sodium sulphate and solvent was removed by rotary-evaporation at 45°C. The brownish viscous product was obtained, which was washed thrice with n-hexane to remove the un-reacted fatty acid and was dried under vacuum. The final compound was stored at 4 °C till further use.<sup>4</sup>

### **2.1.6 Qualitative analysis by thin layer chromatography (TLC)**

Thin layer chromatography (TLC) is the simplest, quickest and cheapest then various analytical techniques extensively used for the qualitative analysis of compounds. Commercially available standard silica gel coated on aluminum plates (Kiesel-gel 60F254, Merck, Darmstadt, Germany, silica layer thickness 2 mm) were used for the analysis of SL mixture. Glass micro-capillary is used for the spot application of samples. Many solvent combinations were tried for the separation of compounds. Ultra-visible absorbing compounds can be visualized under detection at 254 nm of UV light. The ethyl acetate extract of SL mixture was used for the determination of number of components present in the mixture by means of thin layer chromatography. Developing system used was  $\text{CHCl}_3:\text{CH}_3\text{OH}$  in the ratio of 95:5, v/v. Poly molybdic acid (PMA) solution was used as charring agent for detection of SL components at TLC plates. Spots were visualized by charring with Poly molybdic acid (PMA) solution.

## 2.1.7 Purification of sophorolipid

### 2.1.7.1 High performance liquid chromatography (HPLC)

Chromatography involves the column resolution of a small batch of flowing, multi-component fluid into separate fluid volumes of (practically) pure solute solutions. There are different types of chromatography, based on the column and method used, such as molecular-sieve (or gel-filtration or gel-permeation) chromatography, ion-exchange chromatography and affinity chromatography. For example, in analyzing mixtures of sugars such as maltose and glucose, the different affinities of these sugars for the primary amino groups on the surface of the support material in a commercially prepared carbohydrate column is used to separate the sugars in an HPLC (High Performance Liquid Chromatography) apparatus (Figure 2.3). The different sugars emerge from the column at different times, and they are then detected and quantified separately using a refractive index detector. Separations based on HPLC are useful in resolving mixtures of related components before their individual quantification. The data was collected on the HPLC system- Delta 600 series from Waters Corporation and 425 nm wavelengths was used for detection. The elution was carried out with gradient solvent systems with a flow rate of 1.0 mL/min at ambient temperature. The compounds were analyzed using HP Chem-Station software.<sup>5</sup>

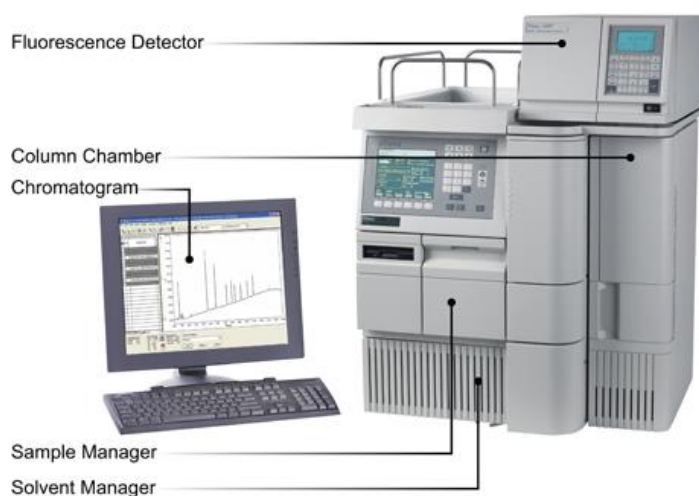


*Figure 2.3 High Pressure Liquid Chromatography (Image from Ref. 5)*

Sophorolipid mixture obtained from fermentative production was dissolved in acetonitrile and analyzed by reversed-phase high performance liquid chromatography (HPLC) with a Waters 2487 separation module (Waters Co. Milford, Massachusetts) using analytical symmetry C18, 5  $\mu\text{m}$  column (250  $\times$  4.6 mm<sup>2</sup>). The gradient solvent elution profile used was as follows: water: acetonitrile (95:5, v/v) holding for 10 min; to a final composition of water: acetonitrile (5:95, v/v) with a linear gradient over 50 min and holding for 10 min. The flow rate was 0.5 ml/ min. The peaks were detected at 220 nm wavelength by absorbance detector. Fractions from different peaks were collected and mixed separately in many runs.

### 2.1.8 Pulsed Laser Synthesis Method

Laser irradiation is a novel and unique technique to synthesize nanostructures from liquid/solid precursors. In this method high energy laser pulses are allowed to interact with the precursor samples present either in solid or liquid medium for certain time period. It is a very unique method for the synthesis of nanoparticles because of heat or photochemical mechanisms which result in molecular level changes. Several transient reactions can be manipulated with the laser irradiation by adding some external reagents which can construct totally new compounds after initial photochemical mechanism.<sup>6</sup>

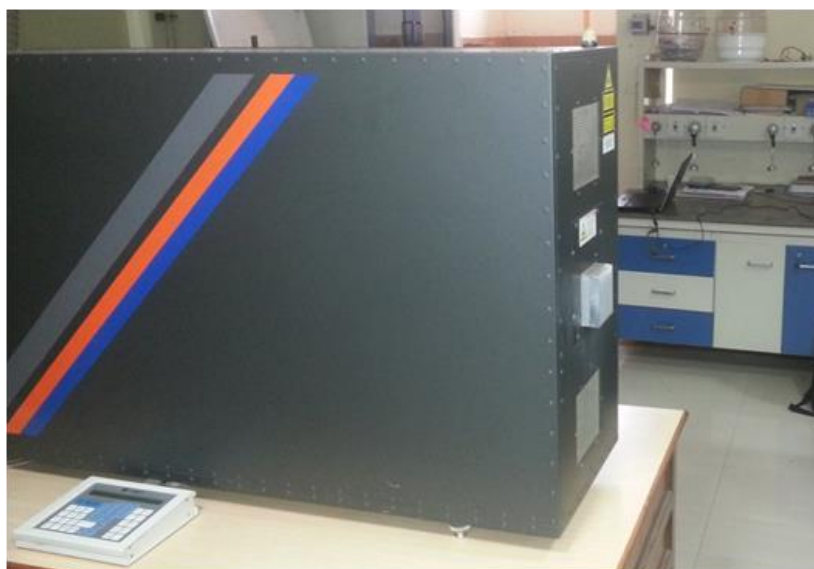


*Figure 2.4 Pulsed UV Laser (KrF excimer)*

Laser irradiation is a similar technique like molecular beam epitaxy (MBE), sputter deposition (CVD) and chemical vapor deposition (CVD). Basic setup of laser irradiation is quite simple compare to other deposition techniques while physical phenomena of target and laser are quite complex (Figure 2.4). All three different types of sophorolipids crude, acidic and lactonic form of sophorolipid were dispersed in water and pulse laser irradiated at different energy intensity. Various concentration of sophorolipid has been applied for laser irradiation experiment for the synthesis of fluorescent mesostructures. Samples were collected at different time interval for complete process time. At various concentration of sophorolipid we have found some undefined morphology but the final parameter for fluorescent mesostructures from sophorolipid were 1; sophorolipid concentration 3.5 mg/ml and 2; laser pulsed excimer laser with  $\lambda=248$  nm, pulse width 20 ns, energy density $\sim 166$  mJ/cm<sup>2</sup>.

## 2.2 General Characterization technique

### 2.2.1 Mass spectra analysis

Matrix assisted laser desorption/ionisation (MALDI) is applicable to analyse soft bio-derived materials such as biopolymers, DNA, protein, peptides and carbohydrate. It could also use for large molecules analysis such as polymers, dendrimres and other macromolecules (Figure 2.5).



*Figure 2.5 Matrix-assisted laser desorption/ionization (Image from Ref. 7)*

These molecules tend to be fragile and fragment when ionized by usual ionization process. It resembles to electrospray ionization technique which used for soft materials analysis. Mass spectrometry techniques have vast application in the field of structural determination of biomolecules. Positive and negative ESI mass spectra were obtained with an API QSTAR PULSAR hybrid MS/MS quadrupole TOF system (Applied bio-systems).<sup>7</sup>

MALDI is a three step technique; sample mix with matrix and drop on metal plate. Then laser irradiation of the sample which trigger ablation and desorption of sample and matrix. Finally the sample is ionized by being deprotonated or protonated in ablated hot plum of gases which accelerated into mass spectrometer to analyze it. The matrix molecules are crystalline in nature. There are three generally used matrix are 2, 5-dihydroxybenzoic acid (DHB),  $\alpha$ -cyano-4-hydroxycinnamic acid (CHCA) and 3,5-dimethoxy-4-hydroxycinnamic acid (sinapinic acid). Preparation of matrix is done by mixed it in purified water and a solvent usually acetonitrile (ACN) or trifluoroacetic acid (TFA).

Acidic and lactonic form of sophorolipid were analyzed by ESI-MS analysis and for this 10  $\mu$ l of SL (stock solution of 2-3 mg dissolved in acetonitrile) was injected into the mass spectrometer for analysis.

### **2.2.2 NMR (nuclear magnetic resonance) analysis**

NMR spectroscopy is study of differences in the magnetic properties of the various magnetic nuclei present in a molecule and to deduce in large measure what is the positions of these nuclei within the molecule. The different kinds of environment and the different kinds of atoms present in a molecule could be deduced as well as the number of atoms present can be known.

The nucleus of the hydrogen atom (the proton) possesses both electric charge and mechanical spin; thus, it generates a magnetic field (Figure 2.6). Upon the effect of an external magnetic field, the proton aligns either with the field (lower energy state) or opposed to the field (higher energy state), in accordance with the quantum restrictions. The spinning proton acting like a spinning magnet precesses around the axis of the applied external magnetic field. The spinning frequency of the nucleus does not change but the speed of the precession does.<sup>8</sup>

The precessional frequency,  $\nu$ , is directly proportional to the strength of the external magnetic field ( $B_0$ ).

$$\nu \propto B_0$$

The exact frequency is given by

$$\nu = (\gamma B_0) \div (2\pi)$$

Where,  $\gamma$  is the magnetic-gyric ratio, being the ratio between the nuclear magnetic moment  $\mu$ , and the nuclear angular momentum,  $I$ ;  $\gamma$  is also called the gyro magnetic ratio.



**Figure 2.6** Nuclear Magnetic Resonance Spectroscopy (Image from Ref. 8)

If the precessing nuclei are irradiated with a beam of radiofrequency, the low-energy nuclei may absorb this energy and move to a higher state. The precessing proton will only absorb energy from the radiofrequency source. If the precessing frequency is identical with frequency of the radiofrequency beam; the nucleus and the radiofrequency are then in resonance, hence the term nuclear magnetic resonance. The only nucleus that exhibit the NMR phenomenon are those for which the spin quantum number  $I$  is greater than 0. The precessional frequency of all protons in the same external applied field is not same and the precise value for any one proton depends on a number of factors. Because these shifts in the frequency depend on the chemical environment, it is called the chemical shift. The factors influencing the chemical shifts



in a NMR spectrum are: van der Waals deshielding, electro negativity (shielding and deshielding), and anisotropic effects. Structural confirmation of purified form of SL was done using NMR technique.  $^1\text{H}$  and  $^{13}\text{C}$  NMR spectra were recorded using Avance Bruker-200 MHz spectrometer. Chemical shifts are given in parts per million downfield from 0.00 ppm using tetra-methyl silane (TMS) as the internal reference. The  $^1\text{H}$  NMR spectra of SL(A) was taken in  $\text{CD}_3\text{OD}$  (deuterated methanol) and SL(L) and curcumin in  $\text{CDCl}_3$  (deuterated chloroform). The following abbreviations are used to present the spectral data: **s** = singlet, **m** = multiplet, **d** = doublet.

### 2.2.3 UV Visible Absorption Spectroscopy

UV-Vis spectroscopy is a form of electronic spectroscopy. Reflected and transmitted light from the sample is measured and information about the electronic transitions is possible through the interpretation of the absorption signals.<sup>9</sup> The perceived colour of the chemicals involved is affected by the absorption or reflectance in the visible region. In this region of the electromagnetic spectrum, molecules undergo electronic transitions. This spectroscopy is complementary to fluorescence spectroscopy. Fluorescence deals with transitions from the excited state to the ground state and absorption measures the reverse transitions. When the incident photon energy exceeds the band gap energy of the material in semiconductors, absorption occurs and signal is recorded by the spectrometer whereas in metals resonant absorption takes place as the surface free electrons vibrate coherently with the incident frequency.

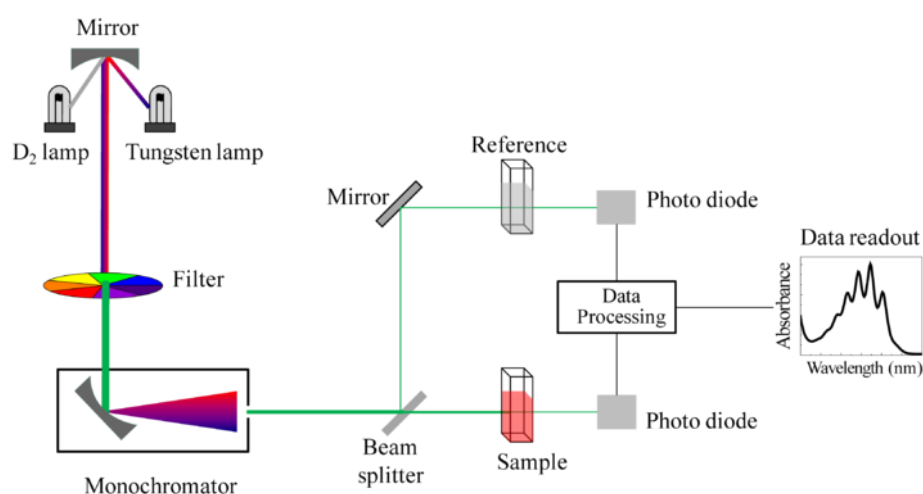


*Figure 2.7 UV Visible spectrophotometer (Ref: en.wikipedia.org)*



This spectrometer can operate in two modes (i) reflection mode and (ii) transmission. In reflectance mode, opaque thin films and NPs which are not dispersible in solvents are analysed. While in transmission mode usually thin films and colloidal NPs, well-dispersed in solvent are used. In UV-Visible absorption spectroscopy, light from a source is transmitted through a monochromator to obtain the light of desired wavelength. The emerging light is then passed through the sample under study and then into a detector (Figure 2.7). Typically, a chopper splits the light from the source to two equivalent beams; one beam passes through the sample and the other through the reference. The photodiode detector alternates between measuring the sample beam and the reference beam.

In many cases the double beam instruments have two detectors, where the sample and reference beams are measured at the same time. Sometimes though in some instruments, the two beams are recombined in a single optical path via the use chopper which blocks one beam at a time.

#### **2.2.4 Photoluminescence**

Spontaneous emission of light on optical excitation of a material is called photoluminescence (PL). In order to probe the sample's discrete electronic states accurately, it is required to scan the required excitation energy and intensity appropriately. When a light of sufficient energy is incident on a material, electronic transitions arise due to absorption of photons within the allowed energy states of the material. Eventually, these excitations relax and the electrons return to the ground state. If radiative relaxation occurs, the emitted light is called PL. This light can be collected and analysed to yield a wealth of information about the photo-excited material. The PL spectrum provides information on transition energies, which can be further used to determine electronic energy levels, defects and impurity states in the sample. The PL intensity also gives a measure of the relative rates of radiative and non-radiative recombination.<sup>10</sup> PL can be categorized into two: fluorescence and phosphorescence, depending upon the electronic configuration of the excited state and the emission pathway. Fluorescence is the property of some atoms and molecules to absorb light at a particular wavelength and to subsequently emit light of longer wavelength after a brief interval, which is characterized as the fluorescence lifetime. The process of phosphorescence occurs in a manner similar to fluorescence, but with

a much longer excited state lifetime. Hence Phosphorescence is a delayed emission process. Figure 2.8 shows of photograph of the photoluminescence set-up.

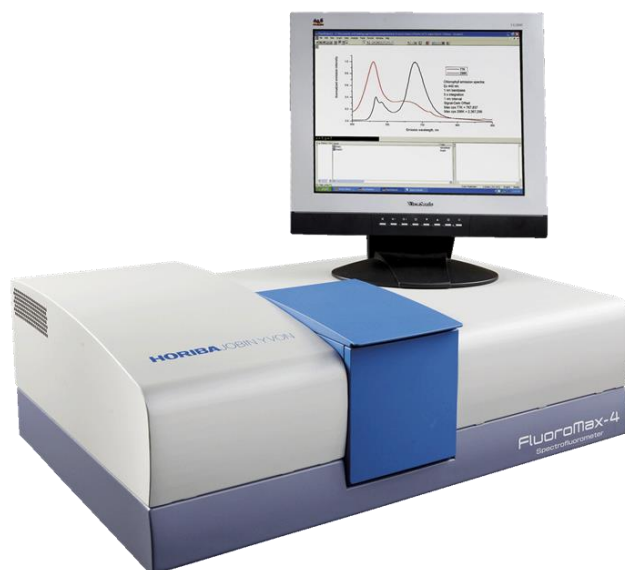


*Figure 2.8 PL spectrophotometer (Ref: [www.fi.tartu.ee](http://www.fi.tartu.ee))*

PL is a simple, versatile, and non-destructive measurement technique. Two essential features describe the PL signal: peak energy and intensity. The excitation energy and optical intensity can be carefully selected in order to yield additional accurate information on the energy levels available to electrons in the material. The PL signal often depends on the density of photo-excited electrons and the intensity of the incident beam. The intensity of the PL signal depends on the rate of radiative and non-radiative events, which depends in turn on the density of non-radiative interface.

### **2.2.5 Fourier Transform Infrared Spectroscopy**

Every compound having covalent bonds absorbs various frequencies of electromagnetic radiation in the infrared region of electromagnetic spectrum. The region lies in between visible (longer and microwaves wavelengths. Similar to other spectroscopy techniques, on absorption of the radiation, molecules are excited to a higher energy state. This absorption process occurs corresponds to energy changes in the order of 8 to 40 kilo J/mol. As there is a very essential requirement for a molecule to show IR spectrum, all the bonds in the molecule are not IR active.<sup>11</sup> Only those bonds, which have a dipole moment that changes as a function of time, are capable of absorbing IR radiation. Symmetric/Homo-nuclear diatomic molecules such as H<sub>2</sub>, O<sub>2</sub>,

Cl<sub>2</sub> etc., do not absorb IR radiation as do not have permanent dipole moment. On the other hand hetero-nuclear diatomic molecules such as CO, HCl, NO do possess permanent dipole moment and hence are IR active. IR spectra occur in the frequency range of 500 - 4000 cm<sup>-1</sup>.

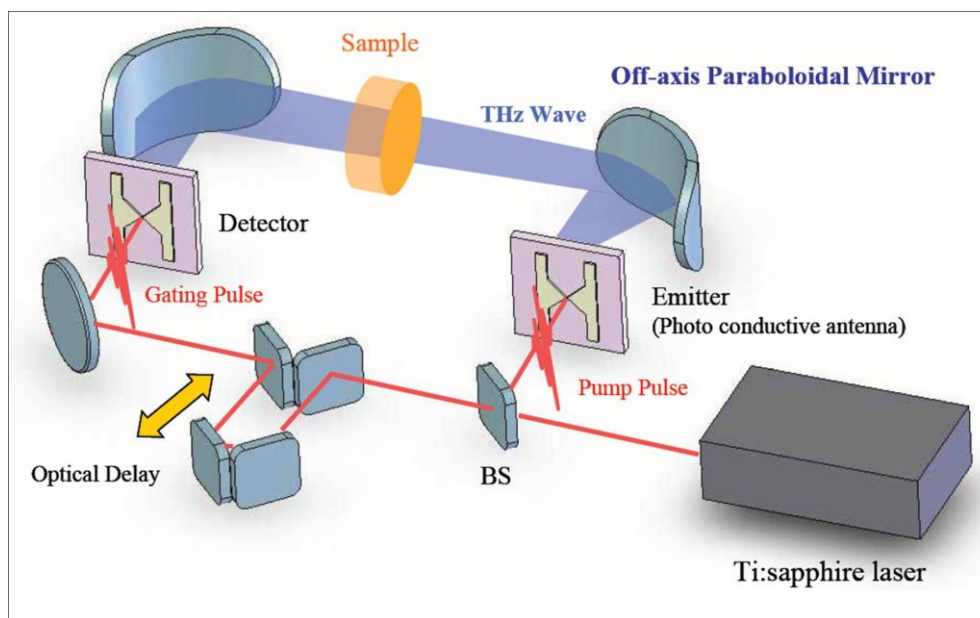


*Figure 2.9 FTIR spectrophotometer schematic (Ref: www.riken.jp)*

Two types of IR spectrometers are in common use (i) Dispersive and (ii) Fourier transform (FT) infrared spectrometer. These instruments give nearly similar spectra for a sample under study of 4000 - 400 cm<sup>-1</sup>. Only the FTIR spectrometers provide the spectrum much more quickly than the dispersive IR spectrometer. Schematic of FTIR spectrometer is shown in Figure 2.9.

### 2.2.6 X-ray Diffraction

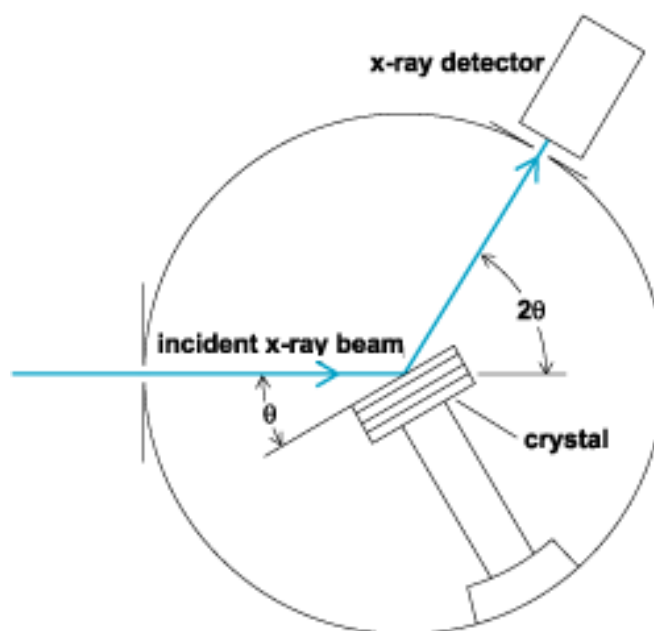
X-ray diffraction (XRD) is a widely used, quick, non-destructive technique helpful in determination and identification of structure in crystalline materials. The technique has been conventionally applied for phase identification and study. A large variety of materials such as metals, minerals, catalyst and inorganic compounds can be characterized by XRD. It is one of the most applicable and efficient general techniques of science.<sup>12-13</sup>

Figure 2.10 shows the schematics of X-ray diffractometer. Diffraction in general occurs only when the wave motion wavelength is of the same order of magnitude as

the repeat distance between scattering centres. This condition of diffraction is nothing but Bragg's law and is given as,

$$n\lambda = 2d\sin\Theta$$

Where,  $d$  = inter-planer spacing,  $\Theta$  = diffraction angle,  $\lambda$  = wavelength of X-ray,  $n$  = order of diffraction



*Figure 2.10 XRD machine schematic (Ref: [www.ehs.columbia.edu](http://www.ehs.columbia.edu))*

In powder XRD method the crystal to be examined is reduced to a fine powder and placed in a beam of a monochromatic X-rays. Each particle of the powder is the tiny crystal, or assemblage of smaller crystals, oriented at random with respect to incident beam. Some of the crystals will be correctly oriented so that their (100) planes, for example, can reflect the incident beam. Other crystals will be correctly oriented for (110) reflections and so on. The result is that every set of lattice planes will be capable of reflection. This is the principle of a powder diffractometer. Ideally, according to Bragg's law, for the particular  $d$  value, the constructive interference of X-rays should occur only at particular  $\Theta$  value i.e. Bragg's angle and for all other angles there should be destructive interference and intensity of diffracted beam will be minimum there.

**Identification of Phases:** From the  $d$ -spacings, phases can be identified in a film using the standard JCPDS powder diffraction file and the reflections can be indexed

with Miller indices. However, if the size of the diffracting tiny crystal is small, there is no complete destructive interference at  $\Theta \pm d\Theta$ , which broadens the peak corresponding to diffracted beam in proportion to the size of the tiny crystal. This can be used to calculate the particle size.

The relation for the same is given by Debye Scherrer formula as,

$$t = \frac{0.9\lambda}{\beta \cos\Theta}$$

Where,  $t$  = particle size,  $\Theta$  = diffraction angle,  $\lambda$  = wavelength of X-rays and  $\beta$  line broadening at Full Width at Half Maxima (FWHM). Further, the powder diffractometer can also be used for X-ray diffraction from thin films. Epitaxial or polycrystalline (may or may not be oriented) thin films can be considered as single crystal or powder (crystals or assembly of crystals spread on substrate) respectively. Hence, a typical epitaxial or oriented film may not show all corresponding reflections and show only few reflections for example say, a c-axis oriented film will show only (hkl) for which h and k indices are zero and l is non-zero. However, these hidden peaks can be detected by small angle X-ray diffraction technique.

### 2.2.6 Scanning Electron Microscopy

It uses a beam of electrons focused to a diameter spot of approximately 1nm in diameter on the surface of the specimen and scanned back and forth across the surface. The surface topography of a specimen is revealed either by the reflected (backscattered) electrons generated or by electrons ejected from the specimen as the incident electrons decelerate secondary electrons.

A visual image, corresponding to the signal produced by the interaction between the beam spot and the specimen at each point along each scan line, is simultaneously built up on the face of a cathode ray tube similar to the way that a television picture is generated. The best spatial resolution currently achieved is of the order of 1nm. The scanning electron microscope (SEM) is a very useful instrument to get information about topography, morphology and composition information of materials.<sup>14</sup> A typical schematic of a SEM is shown in Fig. 2.11. It is a type of electron microscope capable of producing high resolution images of a sample surface. Due to the manner in which

the image is created, SEM images have a characteristic three-dimensional appearance and are useful for judging the surface morphology of the sample.

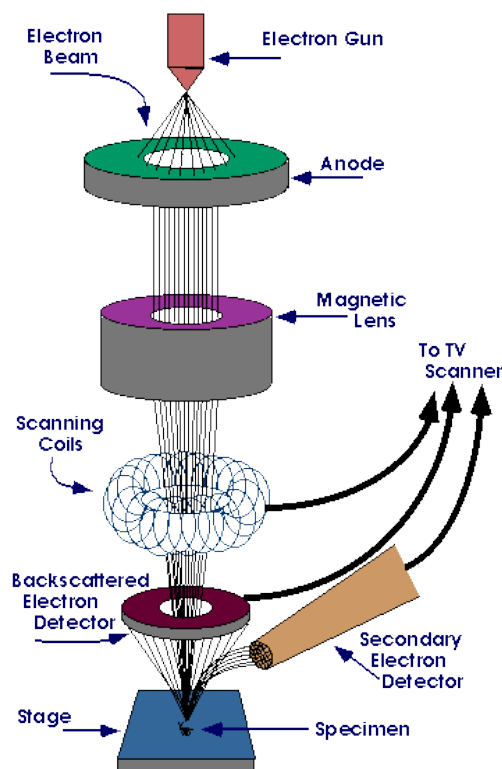


*Figure 2.11 Schematic of Scanning Electron Microscopy (Ref: [www.purdue.edu](http://www.purdue.edu))*

The SEM has an ability to image a comparatively large area of a specimen and also to image bulk materials. Topology of the powder samples in the present study was carried out using a Leica Stereoscan – 440 Scanning Electron Microscope.

### **2.2.7 Transmission Electron Microscopy (TEM)**

Transmission electron microscopy (TEM) is an imaging technique whereby a beam of electrons is focused onto a specimen causing an enlarged version to appear on a fluorescent screen or a layer of photographic film, or to be detected by a CCD camera. TEM operates on the same basic principles as the light microscope but uses electrons instead of light. The line diagram of a typical TEM column is shown in Figure 2.12. The column consists of a source of electrons, electrodes for electron acceleration, electromagnetic focusing and deflecting lenses and the electron detection system such as a CCD array. By using electron energy of several hundred kilovolts the de Broglie wavelength associated with the electron can be reduced to a small fraction of

nanometer and hence atomic resolution imaging becomes feasible.<sup>15</sup> Virtually, TEM is useful for determining size, shape and arrangement of the particles which make up the specimen.

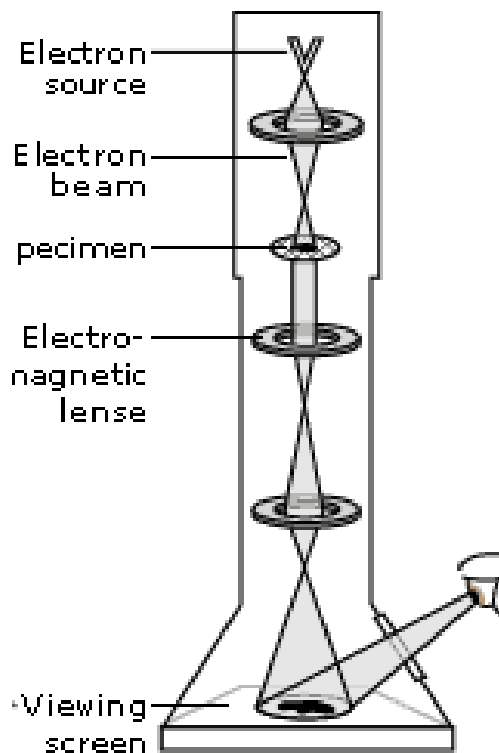


*Figure 2.12 Schematic of Transmission Electron Microscopy (Ref: [www.nobelprize.org](http://www.nobelprize.org))*

Moreover, it is highly useful for the determination of the lattice planes and the detection of atomic-scale defects localized in areas of few nano-meters in diameter with the help of selected area electron diffraction (SAED) technique. The d- spacing between lattice planes of crystalline materials can be calculated from a SAED pattern using the relationship:

$$dr = \lambda L$$

Where, L is the distance between the specimen and the photographic plate,  $\lambda L$  is known as the camera constant and r is the radius of diffracted rings. It is easy to measure r directly from the photographic plate, and  $\lambda L$  can be established from the instrument by calibrating it with a standard material (usually Ag), and hence one can easily get d values. Since, each d value corresponds to a specific lattice plane for a specific crystal structure; description of the crystal structure of a crystalline specimen



can be obtained from SAED pattern. In some cases SAED pattern is more helpful as compared to XRD, due to the limited detection limit of XRD instrument. Also, the XRD generally gives global information.

### 2.2.8 X-ray Photoelectron Spectroscopy

X-ray photoelectron Spectroscopy (XPS) probes the binding energies of core electrons in an atom. Although such electrons play little part in chemical bonding, different chemical environments can induce small changes in their binding energies; this is because the formation of bonds changes the distribution of electrons in the system and hence by modifying the nuclear shielding, produces changes in the effective nuclear charge of the bound atoms.

XPS is also rarely called as electron spectroscopy for chemical analysis (ESCA). Since only the photoelectrons from the atoms near the surface escape the information obtained is typically from the surface layer of 2-5 nm with a typical sampling area of  $1 \text{ cm}^2$ . The actual depth varies with the materials and electron energy. This technique mainly gives information about the elemental composition of the surface of the materials and the information about the chemical state of elements. Usually Al and Mg source is used for producing X-rays to excite photoelectrons from the core levels of atoms in a specimen (Figure 2.13). When an atom or molecule is subjected to higher energy radiations, photons in the radiations collide with and eject electrons from atoms, leaving behind ions. .

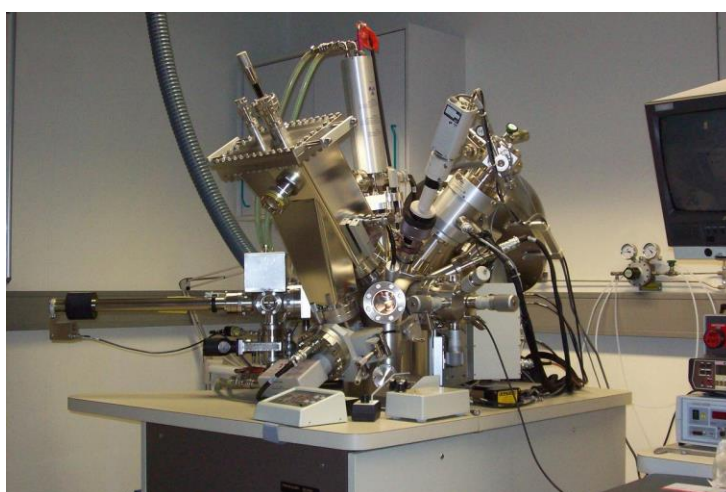


*Figure 2.13 XPS instrument (Ref: [www.ine.kit.edu](http://www.ine.kit.edu))*



Ejected electrons depart with different velocities and photoelectron spectroscopy measures the velocity distribution of the released electrons. Each electron is held in place by nucleus with a characteristic binding energy. The energy of the photon is imparted to the electron and, if this energy is greater than the B.E., the electron will leave the atom and carry with it an excess energy – thus it will have certain K.E. (and velocity). Clearly the total energy must conserve:

$$h\nu = \text{binding energy} + \text{Work Function} + \text{kinetic energy}$$

$$\text{Binding Energy} = h\nu - \text{Kinetic Energy}$$

Since the excitation energy is known and the kinetic energy is measured, the binding energies of electrons in the atom under examination can be determined. Main components of XPS are (i) X-ray source, (ii) Sample holder, (iii) electron energy analyser. The (ii) and (iii) component must be in UHV. The X-ray source is a simple X-ray tube with double anodes (typically Al and Mg) incident radiation energy can be switched from one to the other. In both, XPS, the kinetic energy of the ejected electrons is measured using a hemispherical analyser.

Monochromatic X-ray or UV radiation falls on the sample and ejected electrons pass between a pair of electrically charged hemispherical plates which act as an energy filter, allowing electrons of only a particular kinetic energy to pass through – the pass energy,  $E_{\text{pass}}$ . The resulting electron current, measured by an electron multiplier, indicates the number of electrons ejected from the surface with that kinetic energy.  $E_{\text{pass}}$  can be systematically varied by changing the retarding voltage (VR) applied to the analyser. XPS measurements of different samples were carried out on a VG MicroTech ESCA 3000 instrument at Center for Materials Characterizations (CMC), National Chemical Laboratory Pune. The core level binding energies (BE) were corrected with the carbon binding energy of 285 eV.

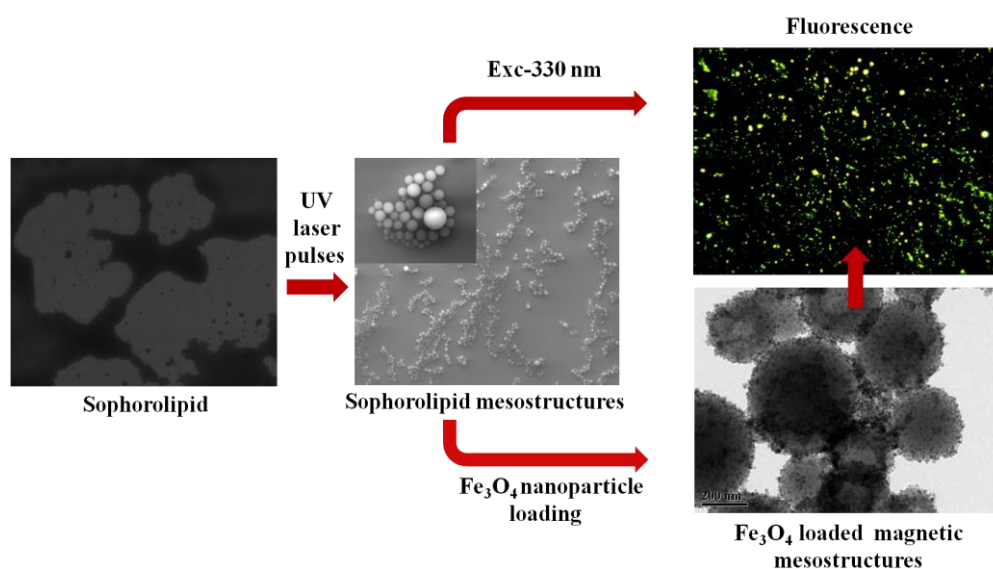
## References

1. Gorin, P.A. J., Spencer, J.F.T., Tulloch, A.P., Hydroxy fatty acid glycosides of sophorose from *Torulopsis magnolia*. *Can. J. Chem.* 1961, 39, 846–855.

2. Van Bogaert, I.N. A., Saerens, K., Muynck, C. D., Develter, D. et al., Microbial production and application of sophorolipids. *Appl. Microbiol. Biotechnol.* 2007, 76, 23–34.
3. Rau, U., Mazke, C., Wagner, F., Influence of substrate supply on the production of sophorose lipids by *Candida bombicola* ATCC 22214. *Biotechnol. Lett.* 1996, 18, 2, 149–154.
4. Hu, Y., Ju, L., Sophorolipid production from lipid precursors observed with LC-MS. *Enzyme Microb. Technol.* 2001, 29, 593–601.
5. Hu, Y., Ju, L., Sophorolipid production from lipid precursors observed with LC-MS. *Enzyme Microb. Technol.* 2001, 29, 593–601.
6. [http://en.wikipedia.org/wiki/Mass\\_spectral\\_interpretation](http://en.wikipedia.org/wiki/Mass_spectral_interpretation)
7. [http://en.wikipedia.org/wiki/Nuclear\\_magnetic\\_resonance\\_spectroscopy](http://en.wikipedia.org/wiki/Nuclear_magnetic_resonance_spectroscopy)
8. C. N. Banwell, E. M. McCash, A Book: *Fundamentals of Molecular Spectroscopy*, 4<sup>th</sup> Edition.
9. M. J. Buerger, “*X-ray Crystallography*”, Wiley, New York, (1942)
10. H. P. Klug and L. E. Alexander, “*X-ray Diffraction Procedures*”, Wiley, New York, (1954).
11. B. D. Cullity, “*Elements of X-ray Diffraction*”, Addison Wesley, Massachusetts (1956)
13. D. A. Long, *Raman Scattering*, McGraw Hill Book Company, New York, 1977, A. C. Ferrari and J. Robertson, *Phys. Rev. B*, 2000, 61, 14095.
14. J. Morgan, L. J. Allen, A. Hashimoto, M. Takeguchi, K. Mitsuishi, M. Shimojo, *Ultramicroscopy*, 2011, 111, 877. 10
15. Y. Hernandez, V. Nicolosi, M. Lotya, F. M. Blighe, Z. Sun, S. De, I. T. McGovern, B. Holland M. Byrne Y. K. Gun'Ko J. J. Boland P. Niraj G. Duesberg S. Krishnamurthy, R. Goodhue, J. Hutchison, V. Scardaci, A. C. Ferrari and J. N. Coleman, *Nat. Nanotechnol.*, 2008, 3, 563.
16. Williams, D.B., Carter, C.B., 2009. *Transmission Electron Microscopy- A Textbook for Materials Science*. Springer.

## Chapter 3

# Fluorescent sophorolipid molecular assembly and its magnetic nanoparticle loading: a pulsed laser process



A novel route employing UV laser pulses (KrF Excimer, 248 nm) to irradiated bio-derived sophorolipid molecules is introduced. We report realization of strong green fluorescence in fully biocompatible highly spherical mesoscale molecular assembly of sophorolipid created by pulsed UV laser processing of a water-based dispersion of sophorolipid. We have separately examined the consequences of laser irradiation of glucose and oleic acid components which form the sophorolipid. This fluorescence character appears to be driven by the oleic component while the assembly process is assisted by the glucose component. Importantly the laser synthesized mesostructures can be easily redispersed in aqueous medium after being dried and can also be loaded with magnetic nanoparticles (magnetite) for inducing hyperthermia effect.

### 3.1 Introduction

Bio-imaging vehicles which can absorb light and facilitate fluorescent or colorimetric detection are of fundamental significance to various medical applications such as photo-thermal or photo-dynamic therapy.<sup>1-2</sup> Inorganic nanoparticles, especially semiconductor quantum dots (e.g. CdSe), absorb light strongly and possess good luminescence properties, making them suitable vehicles for such applications domains.<sup>3-7</sup> Yet one does not witness their widespread use in medical applications possibly because of their limited drug loading capability restricted only to the nanoparticles surface and inherent high level of toxicity.<sup>8</sup>

Another serious problem faced when using such inorganic nanomaterials (e.g. iodine, gadolinium, and radioisotopes) as contrasting agents in magnetic imaging is their unduly long residence time in the body long after the delivery procedure and higher noise to target signal ratio. To overcome these disadvantages, bio-organic nanoparticles are now being extensively used in therapeutics and for diagnostic imaging because of their much higher drug loading capacity, perfect biocompatibility and controlled activation under specific conditions such as pH, temperature etc.<sup>9</sup> Biosurfactants derived from microbes are an interesting category of bio-organic systems with potential for applicability in biomedicine.<sup>10-12</sup>

They can be produced from renewable feedstock or waste material by a natural fermentation.<sup>13-19</sup> Such micro-organism derived biosurfactants are also structurally very diverse. Moreover, they are readily degradable and display low toxicity.<sup>20-22</sup> These properties are clearly desirable over those of traditional surfactants which can be eco-toxic, susceptible to bio-accumulation and generally averse to biodegradability. Some traditional surfactants with improved environmental performance such as alkyl polyglucosides, alkyl polyglucamides and fatty ester methyl ester ethoxylates are in use. However they are not necessarily made from renewable resources and may involve partial chemical processing.

A number of biosurfactants such as rhamnolipids (*Pseudomonas aeruginosa*), sophorolipids (*Candida bombicola*), trehalose lipids, cellobiose lipids, mannosylerythritol lipids, surfactin (*Bacillus subtilis*) and emulsan (*Acinetobacter calcoaceticus*) have been subjected to different scientific studies. Apart from surfactin

and emulsan, all others are glycolipids which represent easily available important class of biosurfactants. Our work involves the use of sophorolipids because they are easily synthesized by non-pathogenic yeast using very cost effective resources. Sophorolipids (SL) are amphiphilic molecules which contain both hydrophobic (nonpolar) and hydrophilic (polar) groups. This character enables them to reduce the surface and interfacial energies leading to formation of emulsions. The foremost reasons for a high and increasing level of interest in Sophorolipid is due to their biodegradability and low toxicity as well as their unique structures that can facilitate their engineering to suit a specific application domain.<sup>23-26</sup>

When dissolved in water Sophorolipid molecules can form micelles-like structures. Some literature reports also discuss supramolecular assemblies<sup>27-30</sup> of sophorolipid monolayer in the form of vesicles, helical fibers/ribbons/tubules, and even rigid rods. Herein we report pulsed UV laser induced formation of novel self-assembled vesicular mesostructures of biosynthesized Sophorolipid without the addition of any stabilizing agent, or other organic or inorganic additives. Most interestingly these Sophorolipid based mesostructures are highly fluorescent as well, in contrast to the non-fluorescent property of the parent molecules. We have performed several experiments to elucidate the possible origin of such fluorescence.

We also show that such mesostructures can be easily loaded with magnetic (magnetite) nanoparticles for easy recovery and potential applicability as RF hyperthermia<sup>31</sup> agents. Indeed, iron oxide nanoparticles ( $\text{Fe}_3\text{O}_4$ ) based magnetic hyperthermia has been extensively investigated in the field of biomedical and pharmaceuticals science. A major problem has been to achieve a sufficiently high concentration of magnetic nanoparticles for bulk solution heating inside the cells. We demonstrate that the Sophorolipid mesostructures can be easily loaded with high density magnetite nanoparticles conferring on them the capability to easily fuse with the cell membrane. Such mesostructures can permeate cells very effectively at high concentration enabling effective delivery of the load.

Concurrent fluorescence and magnetism further enhances the value to these systems in the context of both bio-imaging, targeted drug delivery and controlled drug release. We would like to further emphasize on the green aspect of this work. Herein no synthetic chemical steps are used for production of sophorolipid mesostructures. The

product formed is completely biodegradable and the end products fatty acid and glucose are non-toxic. Sophorolipid used for nano/meso-assemblies is FDA approved and allowable limit for human uptake is as high as 5 ml/kg wt. For nano/meso assemblies we require only few mgs. Moreover there is no stress on the body system if taken in by any route.

The details of experiments performed and related procedures are given in a later section. Briefly, in our experiments, three different types of sophorolipids crude, acidic and lactonic, dispersed in water were laser irradiated with pulsed excimer laser ( $\lambda=248$  nm, pulse width 20 ns, energy density~166 mJ/cm<sup>2</sup>). Microscopy studies and other physical characterizations were performed for all the three types of samples under different conditions. When the crude Sophorolipid was processed with laser irradiation, mixed population of some spherical microstructures with cloudy tube-like structures were obtained. Lactonic sophorolipid formed undefined hazy. However, in the case of the acidic form of sophorolipid, which is diacetate in nature, extremely well-defined and fairly uniform spherical microstructures were seen to form (Figure 3.1). The size range of such sophorolipid mesostructure was 0.5 - 2.5 $\mu$ m which could be reduced to less than 100 nm by optimizing process parameters such as laser irradiation time, energy and stirring solution. Indeed, a ~100 nm size represents an ideal size range for bio-imaging experiment in medical science. Noting that the basic structure of sophorolipid molecule comprises of oleic acid and glucose forms, we also examined the effects of pulsed excimer laser irradiation on these two molecules to elucidate the contributions of these molecular components in assembly and related fluorescence. The reference to Sophorolipid in the following sections implies its acidic form unless specifically stated otherwise.

## 3.2 Experimental

### 3.2.1 Materials & Equipment's

#### Production of Sophorolipid

Sophorolipid was prepared by the resting cell method. In the first step adequate cell mass was harvested by growing the *Candida bombicola* (ATCC 22214) in MGYP

medium.<sup>[15]</sup> Then the cells were re-dispersed in production medium containing 10% glucose. This production medium was supplemented with hydrophobic secondary carbon source i.e. oleic acid in absolute alcohol. Oleic acid Sophorolipid was formed as a brown and viscous liquid which was found to settle at the bottom of the flask after 96 to 120 hrs of incubation. After incubation period the cells were separated from the broth by centrifugation at 5000 rpm, 10°C for 20 min. The SL formed was extracted from the supernatant with ethyl acetate. To the ethyl acetate phase, anhydrous sodium sulphate was added for removal of residual water, filtered and then ethyl acetate was removed under vacuum. The unconverted fatty acid was removed by washing with n-hexane. Crude sophorolipid was purified by column chromatography which has been given four different type sophorolipid forms. Different forms of sophorolipid were analyzed by LCMS, MALDI TOF, NMR and HPLC.

### **3.2.2 The Process**

#### **Synthesis of Sophorolipid mesostructures by Laser Irradiation**

For synthesis of mesostructures, different concentrations range of Sophorolipid (1.0-10 mg/ml) were mixed in distilled water and then sonicated for 3 hours. Sophorolipid water emulsion looked visibly turbid (Figure 3.2) after sonication because of amphiphilic nature of SL which was then irradiated by Laser pulses (wavelength 248 nm, energy density 166 mJ and frequency 10 Hz). Similar experiment was also performed on oleic acid and glucose.

#### **Polyol synthesis of Fe<sub>3</sub>O<sub>4</sub> Nanoparticles**

For the synthesis of super paramagnetic Fe<sub>3</sub>O<sub>4</sub> nanoparticles, 1 mM of iron acetylacetonate was mixed in 30 ml triethylene glycol and sonicated for 5 minutes in the presence of argon gas. A round bottom flask was kept in silicon oil bath and the temperature was raised (2°C/min) to 278°C. After 30 minutes at constant temp (278°C) the product was cooled to room temperature and then thoroughly washed with ethyl acetate and separated by magnet. It was dried overnight in an oven at 50°C.

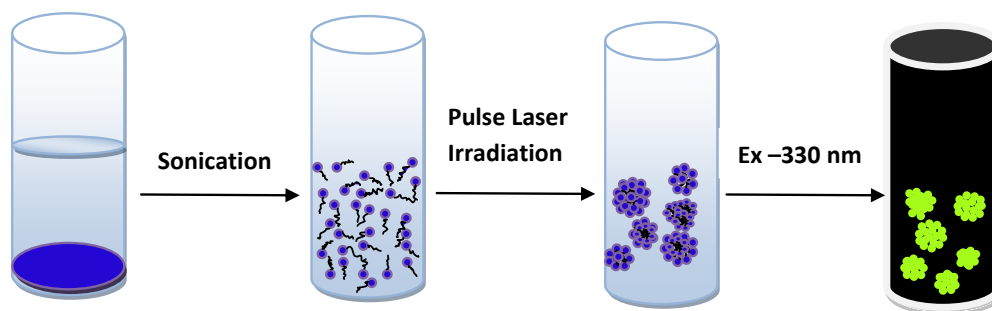


*Figure 3.1* Figurative depiction of the experimental process



*Figure 3.2* Actual image of Appearance of (A) water (B) unirradiated sophorolipid (C) irradiated sophorolipid (D) magnetic sophorolipid mesostructure

### Synthesis of Fe<sub>3</sub>O<sub>4</sub> impregnated Sophorolipid mesostructures

For synthesis Fe<sub>3</sub>O<sub>4</sub> encapsulated Sophorolipid mesostructures, different concentrations of Sophorolipid (1-10 mg/ml) and Fe<sub>3</sub>O<sub>4</sub> (10-100  $\mu$ l, 20 mg/ml) nanoparticles were mixed in double distilled water and sonicated for 3 hours. After sonication Sophorolipid and Fe<sub>3</sub>O<sub>4</sub> solution appeared light brown and turbid, which was then irradiated by UV laser pulses (wavelength 248 nm, energy 150 mJ and frequency 10 Hz). It was found that 5:1 ratio of Sophorolipid to Fe<sub>3</sub>O<sub>4</sub> nanoparticles



gave highly reproducible result. Sample were collected after different time intervals and analyzed by different techniques stated above.

### 3.3 Characterization

Scanning electron microscopy with Energy-dispersive X-ray spectroscopy (EDX) (FEI Quanta 200 3D) was used for the determination of morphology and elemental composition. X-ray photoelectron spectroscopy (XPS) (ESCA-3000, VG Scientific Ltd. UK, with a 9 channeltron CLAM4 analyser under vacuum better than  $1 \times 10^{-8}$  Torr, Al Ka radiation (1486.6 eV) and a constant pass energy of 50 eV) was employed to study the chemical state of carbon in the materials respectively. X-ray Diffraction (XRD, Philips X'Pert PRO) and Raman spectroscopy (a confocal micro-Raman spectrometer LabRAM ARAMIS Horiba JobinYvon, with laser excitation wavelength of 532 nm) were also used to examine the characteristics of the carbonaceous compounds. Thermo gravimetric analysis (TGA) was performed to determine the thermal stability. We also obtained images of the graphitic CNSs by techniques of Field Emission Scanning Electron Microscopy (FESEM, Hitachi S-4200) and High Resolution-Transmission Electron Microscopy (HR-TEM, FEI Tecnai 300). Conductivity measurement was carried out on a pellet by a two probe method.

### 3.4 Results and Discussion

Three different types of sophorolipids crude, acidic and lactonic, dispersed in water were laser irradiated with pulsed excimer laser ( $\lambda=248$  nm, pulse width 20 ns, energy density  $\sim 166$  mJ/cm<sup>2</sup>). Microscopy studies and other physical characterizations were done for all the three types of samples under different conditions. When the crude Sophorolipid was processed with laser irradiation, mixed population of some spherical microstructures with cloudy tube-like structures were obtained. Lactonic sophorolipid formed undefined hazy structure, where only undefined structures were seen to form. However in the case of acidic form of sophorolipid, which is diacetate in nature, extremely well-defined and fairly uniform spherical microstructures were formed (Figure 3.3).

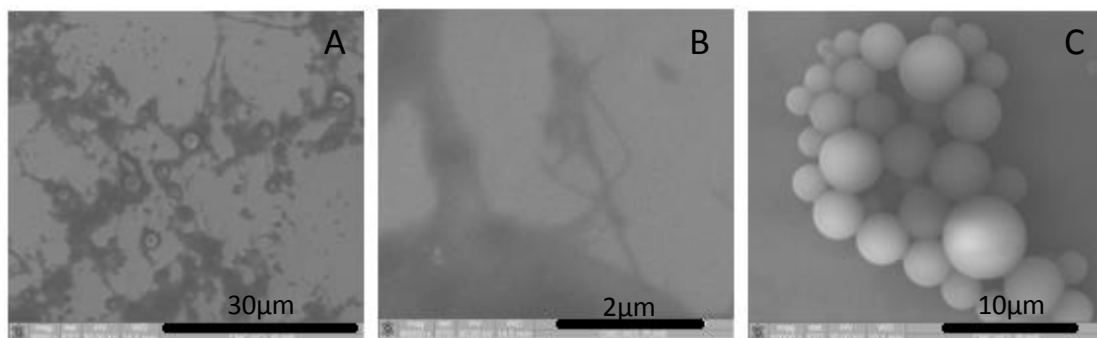


**Figure 3.3** Scanning electron microscope image of laser irradiated Sophorolipid (A) crude sophorolipid (B) lactonic sophorolipid (C) Acidic sophorolipid

Size range of sophorolipid microstructure was 0.5 - 2.5 μm which could be reduced to less than 100 nm by optimizing process parameters such as laser irradiation time, energy and stirring solution. 100 nm sizes represent ideal size range for bio-imaging experiment in medical science. Noting that the basic structure of sophorolipid molecule comprises of oleic acid and glucose forms, we examined the effects of pulsed excimer laser irradiation on these two molecules as well to elucidate the contributions of these molecular components in assembly and related fluorescence.

### 3.4.1 Optical properties

The unirradiated Sophorolipid (SL) and the laser irradiated Sophorolipid (SLIR) show a marked difference in their appearance to the naked eye (Figure 3.2). While the unirradiated SL appears milky, the irradiated one appears transparent and yellowish. The unirradiated Sophorolipid solution shows UV absorption peak at 228 nm, while after laser irradiation the peak exhibits a 50 nm red shift to 278 nm, as clearly seen in Figure 3.4. We will return to this observation later in the discussion. For the study of photoluminescence of the unirradiated and irradiated sophorolipid; these samples were excited at the same wavelength of 330 nm. In the case of the unirradiated sophorolipid sample a very weak excitonic emission is observed in UV at 370 nm, while in the case of the irradiated sample a strong emission is seen to occur in the visible at 510 nm (Figure 3.4 1B) Further study by fluorescence microscopy analyses also confirm the appearance of strong green fluorescence in SLIR, while no fluorescence is observed in unirradiated SL (Figure 3.4 1C, D). Polarized microscopy study was performed to explore the morphologies of vesicular mesostructures formed by the laser processing of the acidic form of sophorolipid.

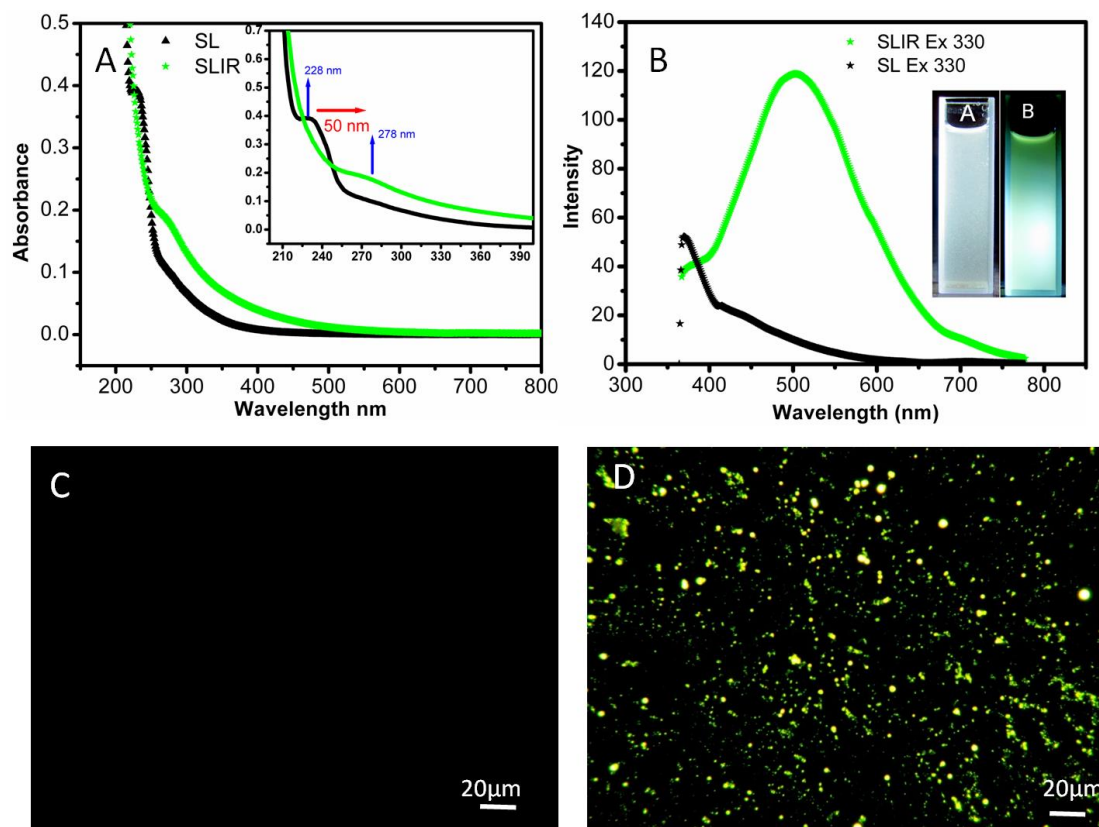


**Figure 3.4** (A) UV–Visible spectra measurement of unirradiated and irradiated Sophorolipid solution. Unirradiated SL solution shows absorbance at  $\lambda=228$  nm while laser irradiation shifts absorption toward visible region  $\lambda=278$  nm. (B) Photoluminescence study of laser irradiated Sophorolipid mesostructures. (C) Fluorescence image of unirradiated SL and (D) laser irradiated SL.

According to Yapei Wang, Xi Zhang <sup>[11]</sup> UV light can help vesicles formation from micelles structure. In their work, they have mentioned that upon UV irradiation, the weak interaction between  $\alpha$ -Cyclodextrin ( $\alpha$ -CD) and cis azobenzene may drive some of the  $\alpha$ -CD to slide onto the alkyl chain, and thus the self-organization of AzoC10 complexes with  $\alpha$ -CD could form different vesicle-like aggregates. In our case non-thermal photochemical process seems to be responsible for the formation of mesoscopic spherical structures since no ambient heating of the solution takes place under laser exposure.

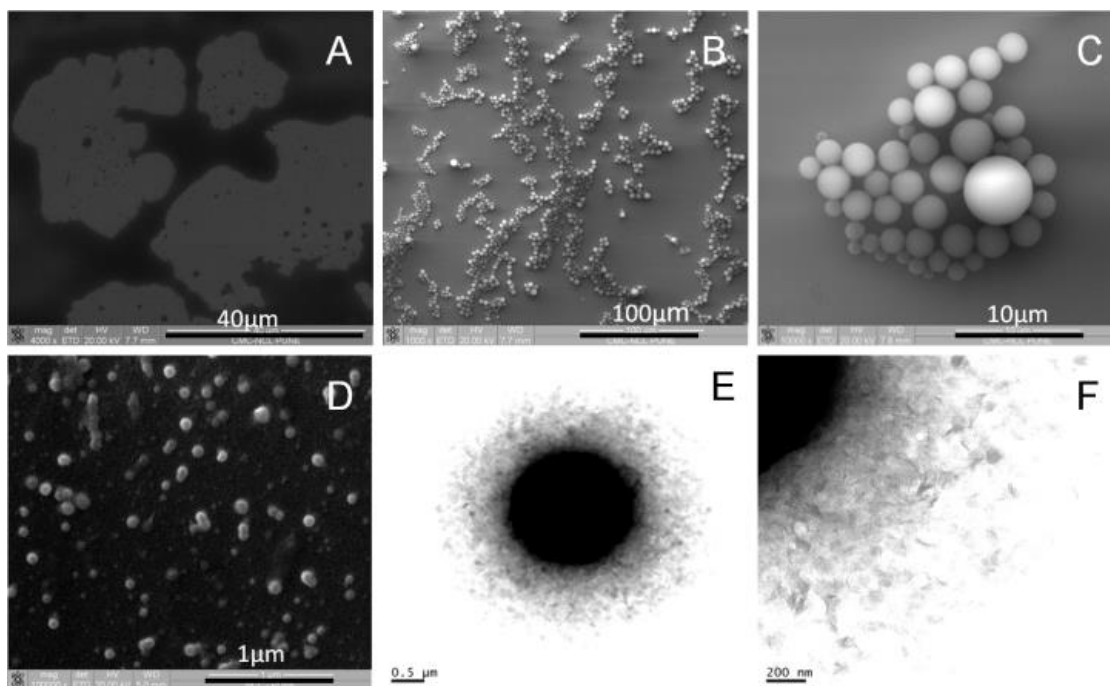


**Figure 3.4** Scanning electron microscopy images of Sophorolipid mesostructures: (A) sophorolipid acidic form as it appears without irradiation; (B-D) after laser irradiation; (E-F) HRTEM images show the mesoporous surface morphology of SL mesostructures which could be very useful for drug loading experiment in drug delivery system.

### 3.4.2 Time evolution of morphology

To study the process of pulsed UV laser induced self-assembly of sophorolipid, time evolution study was performed. Samples were collected at every 10 minutes interval to check for the changes happening due to pulsed laser irradiation (Figure 3.5 A-F). After initial 10 minutes sheet-like structure of sophorolipid could be seen by local shrinking and formation of some defined globule like structures which are seen to be prominent over the hazy mass present. Antonietti and Forster<sup>33</sup> have explained the energy conservation in vesicles formation stating that when lipid sheet spreads, it forms vesicle-like structure to minimize its bending energy. We hypothesize that our mesostructure formation follows similar reaction mechanism. The Reaction mechanism kinetics in our study reveals that during the initial 10 minutes of laser irradiation sophorolipid forms sheet-like structure because of laser energy input (equation 1) which further increases during the next 20 minutes.

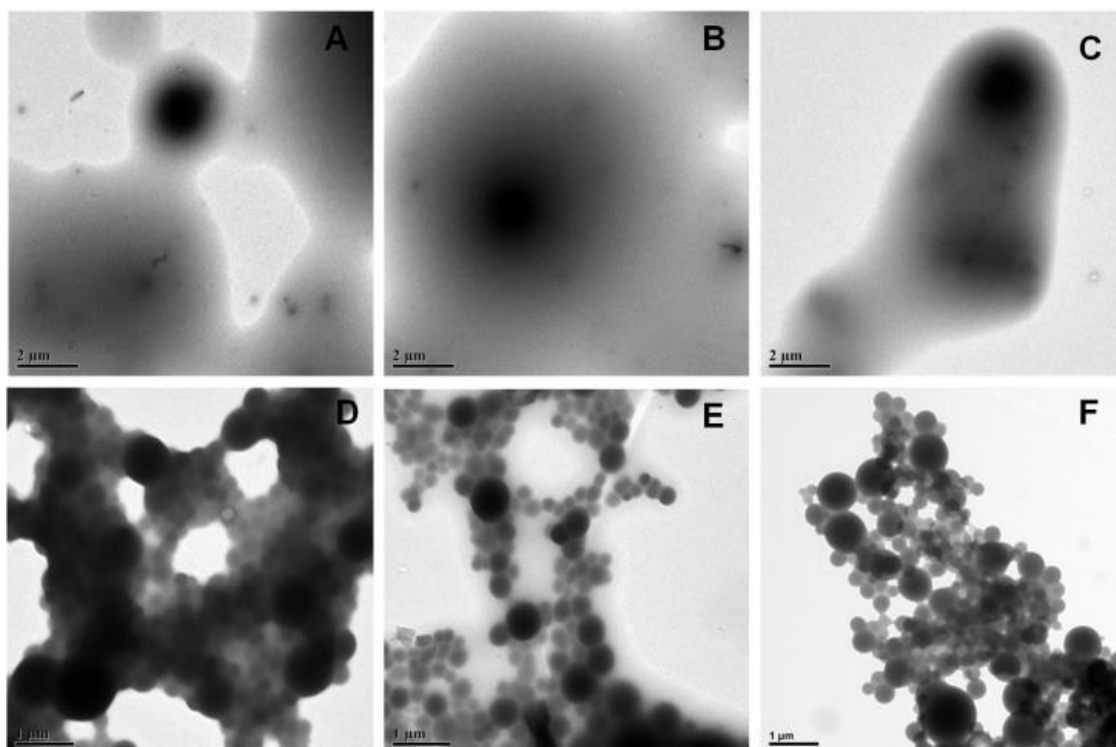


**Figure 3.5** TEM images of Sophorolipid mesostructures evolution with laser irradiation time: (A) sample collected after 10 minutes of laser irradiation; (B) 20 minutes laser irradiation; (C) 30 minutes laser irradiation, sheet like structure begin to form; (D) 40 minutes laser irradiation, sheets start transforming into well-defined structures; (E) 50 minutes laser irradiation, spherical structures begin to form; (F) 60 minutes, complete mesostructures get formed (Scale Bar A -C: 2 $\mu$ m; D-F: 1 $\mu$ m)

After 40 minutes the lipid sheet starts to form some defined structures and these gets converted into spherical mesostructures in the 50 minutes of laser irradiation. Mesostructures start forming when sheet like structures are so large and energy loss due to surface tension is excessive. Laser irradiation for one hour provides the conditions required (equation 2) for the SL mixture to form fully developed spherical mesostructures.

$$(\text{linear energy } E_{\text{disk}} = 2\pi R_D \gamma) \quad (\text{Equation 1})$$

$$(\text{bending energy } E_{\text{bend}} = 8\pi k) \quad (\text{Equation 2})$$

Also it is seen that these structures do not form by providing heat energy from any other source and that laser energy is crucial for the formation of these sophorolipid mesostructures. By fine tuning the laser energy, time and proportion of Sophorolipid, nanoparticles in size domain of ~100 nm could be obtained.

### 3.4.3 Mechanism

#### Understanding the origin of fluorescence of the laser induced molecular assembly

In order to understand the origin of the observed intriguing green fluorescence property and its possible connection with the laser induced reorganization, stitching and assembly of sophorolipid molecules, we performed additional experiments. Noting that the basic structure of sophorolipid molecule comprises of oleic acid and glucose forms (Figure 3.6), we examined the effects of pulsed excimer laser irradiation on these two molecules as well.

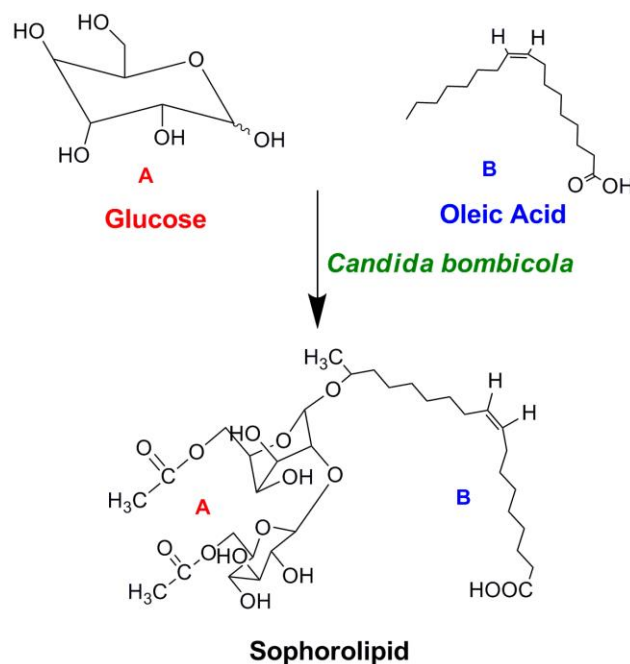


**Figure 3.6** Basic structure of SL produced by yeast *C. bombicola*

Interestingly the corresponding data also bring forth the fact that oleic acid molecules upon laser treatment show similar fluorescence property as the sophorolipid molecules (Figure 3.7 A); however the glucose molecules do not. The fluorescence of laser treated oleic acid induced system is weaker and it does not show a well-defined assembly (Figure 3.7 B) as with laser treated sophorolipid molecules.

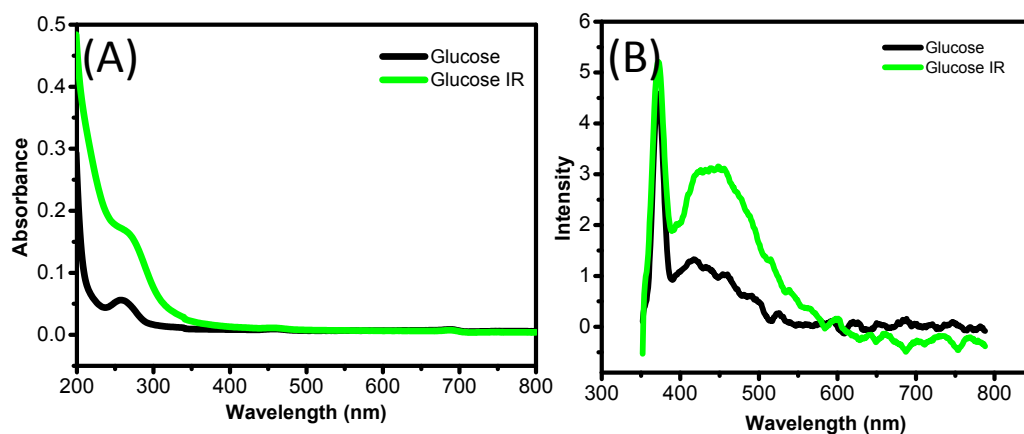


**Figure 3.7** (A) UV–Visible spectra of unirradiated and laser irradiated glucose solution; (B) Photoluminescence of unirradiated and irradiated glucose solution.

Thus the broad conclusion is that the glucose part in sophorolipid serves to develop proper molecular assembly in the form of mesosphere, but the main fluorescence features emanate from transformations occurring in the oleic acid type molecular component in the lipid (Figure 3.8 A).

Solution based spectroscopic characterization of self-assembled organic molecules are quite difficult because of highly insoluble aggregates. The assembly formed by SL after continuous 1 hr. irradiation of laser was insoluble in most the organic solvents. This could be the reason that we are not able to take NMR spectra after complete assembly formation.

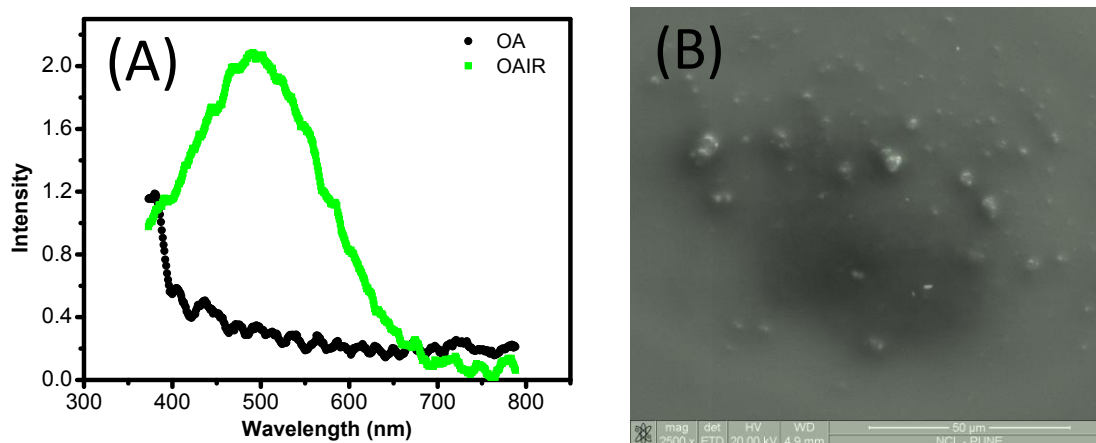


**Figure 3.8** (A) Photoluminescence spectra of oleic acid before and after laser irradiation; (B) SEM image of laser irradiated oleic acid.

In order to at least understand and elucidate the initial stages of formation of the sophorolipid mesostructures upon laser treatment, we examined the consequences of



laser irradiation in the product obtained up to 20 minutes by techniques of Nuclear Magnetic Resonance (NMR) and MALDI (Matrix Assisted Laser Desorption /Ionization). The detailed NMR data for various cases of interest are presented in electronic supplementary information (Figure 3.9).

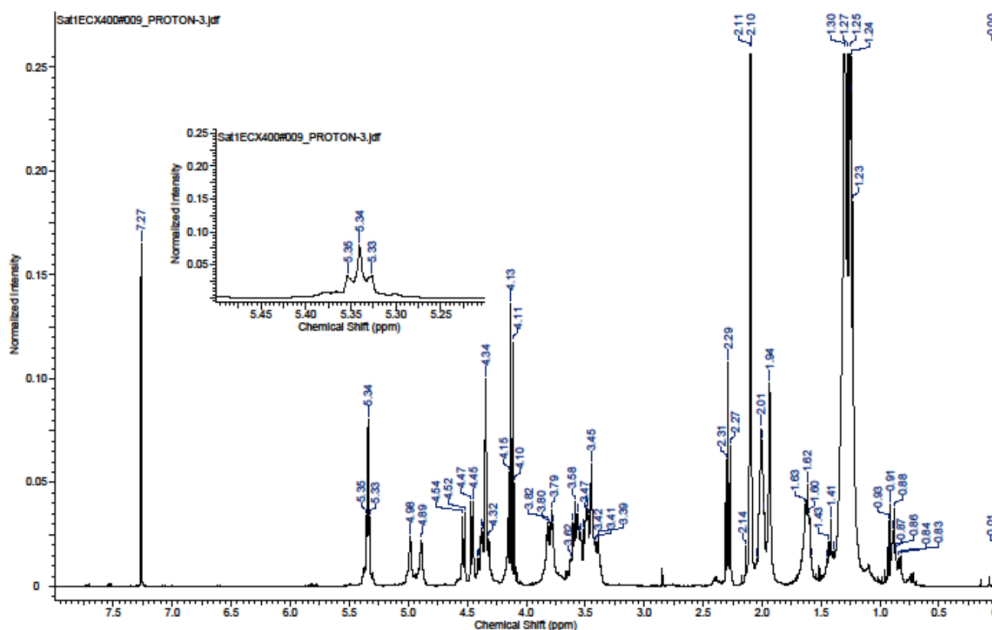


*Figure 3.9*  $^1\text{H}$  NMR spectrum of the sophorolipid, confirming the presence of one olefin group in its structure at 5.34 ppm

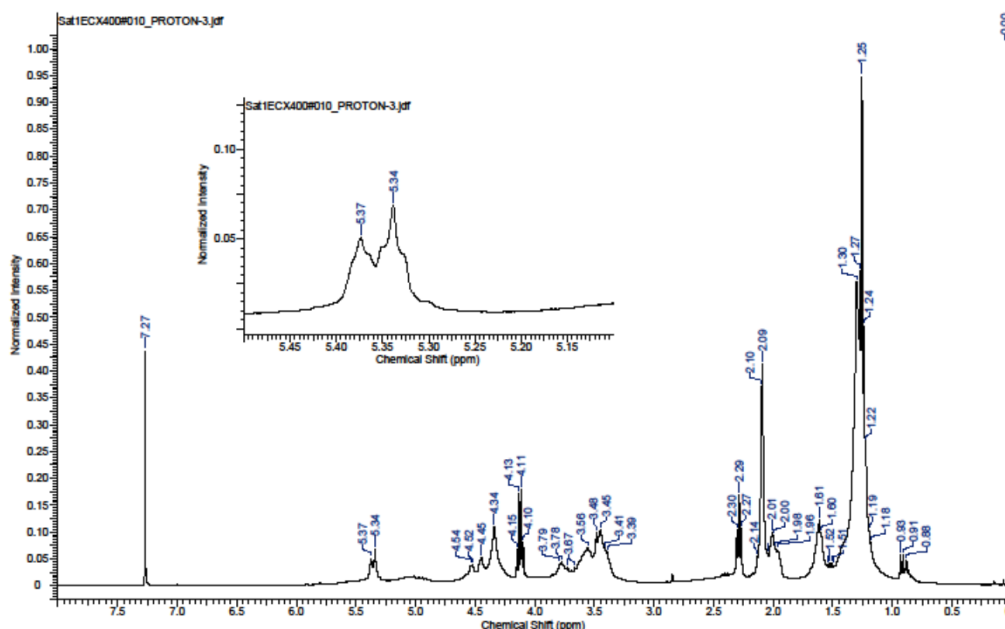


*Figure 3.10*  $^1\text{H}$  NMR spectrum of the sophorolipids, confirming the appearance of one extra olefinic group at 5.37 ppm



In Figure 3.9 we present  $^1\text{H}$  NMR spectra for the unirradiated samples, which form the focus of the following discussion. The NMR spectrum for SL sample matches with the reported data.<sup>34</sup> The triplet signature ( $\text{CDCl}_3$ , TMS, 400 Hz,  $\delta$  (ppm); 5.34) marked in Figure 3.9 corresponds to olefinic C=C bond. In the laser irradiated case (Figure 3.10) an extra triplet state is noted ( $\text{CDCl}_3$ , TMS, 400 Hz,  $\delta$ (ppm); 5.37) and its position implies that it represents downfield C=C bond. Moreover, since we do not see a doublet of doublet, this C=C bond is not conjugated with the bond already present in SL.

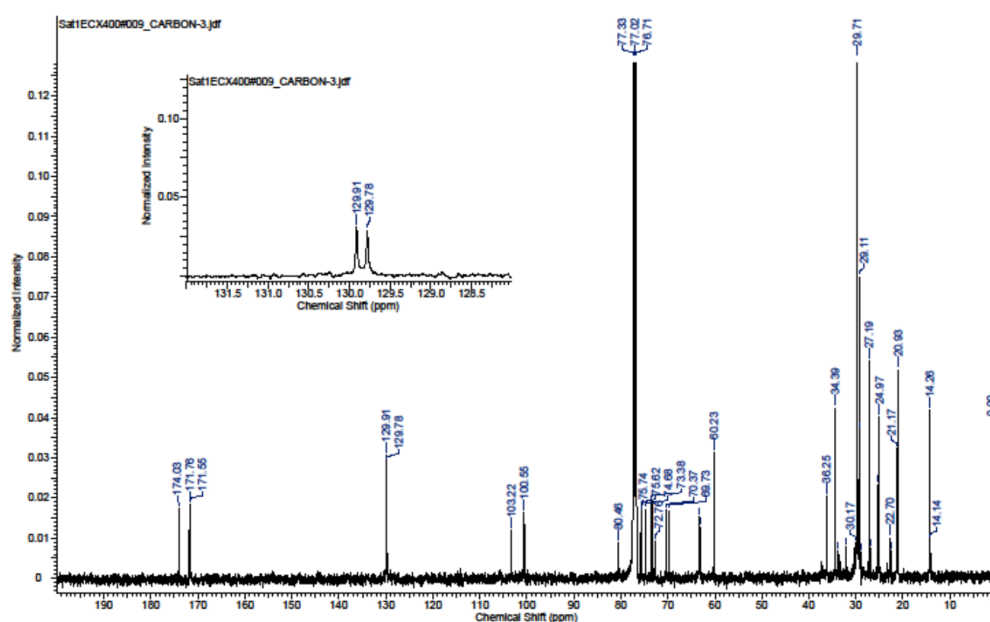


**Figure 3.11**  $^{13}\text{C}$  NMR spectrum of the sophorolipids, confirming the presence of one olefin group in its structure at 129.78, 129.91 ppm.

The downfield shift implies the location of the bond close to the carboxylic group. In Figure 3.11 we present  $^{13}\text{C}$  NMR spectra for the unirradiated samples. Laser irradiated SL  $^{13}\text{C}$  NMR spectroscopy data (Figure 3.12) also show emergence of new peaks at 130.24 and 130.36 ppm which are characteristic of this second C=C bond. This extra C=C clearly enhances the  $\pi$ - character in SL.

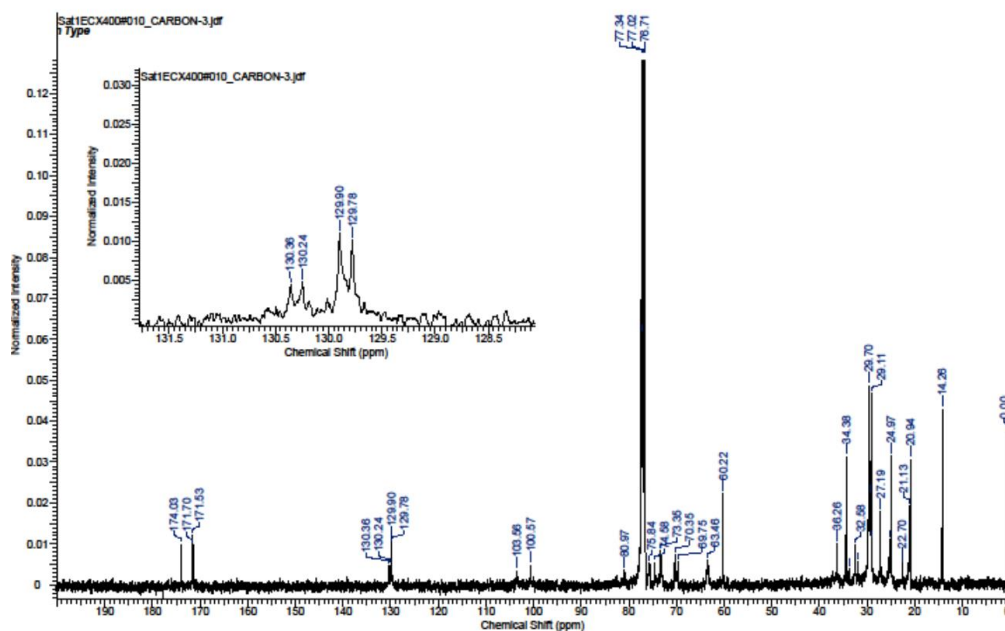


**Figure 3.12**  $^{13}\text{C}$  NMR spectrum of the sophorolipids after laser irradiation, confirming the appearance of one extra olefin group at 130.24, 130.36 ppm

The MALDI data<sup>35</sup> shown in Figure 3.13 also confirm the loss of two hydrogen consistent with the formation of an extra C=C bond.

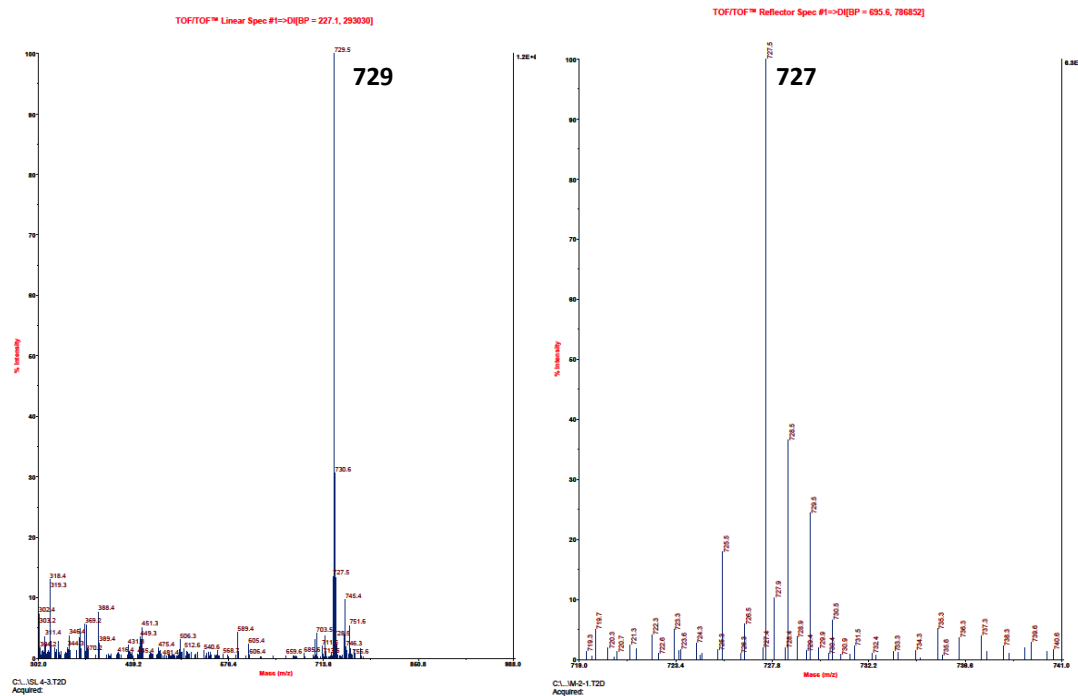


**Figure 3.13** MALDI-TOFMS mass spectra of the acidic sophorolipids. (A) sample collected at 0 min. (B) sample collected at 20 min. Assignments for the  $[M+\text{Na}]^+$  molecular adduct ions

Figure 3.14 A shows the FTIR spectra of the sophorolipid prior to and after laser irradiation for 1 Hr. The ‘before irradiation’ case reveals a broad band at  $3350\text{ cm}^{-1}$  corresponding to the O–H stretch frequency in the glucose moiety of the molecule. The asymmetrical and symmetrical stretch modes of methylene ( $\text{CH}_2$ ) groups occur at  $2928$  and  $2854\text{ cm}^{-1}$ , respectively. Sophorolipid has two strong absorption bands arising from C–O and C–O stretching; the C–O absorption band at  $1,744\text{ cm}^{-1}$  includes contributions from these groups. Moreover, sugar C–O stretch of C–O–H groups is found at  $1,048\text{ cm}^{-1}$  and the band at  $1,452\text{ cm}^{-1}$  corresponds to the C–O–H in-plane bending of carboxylic acid ( $-\text{COOH}$ ) in the structure of the product. All these structural details are in conformity with the literature reports<sup>36</sup>. The laser irradiated sophorolipid brings out some interesting aspects. Most of the peaks that occur in FTIR for this case are similar to the ‘before irradiation’ case demonstrating the fact that the general molecular structure of the sophorolipid is retained after the photochemical process as well. However a specific significant difference arises post-irradiation. FTIR analysis clearly shows appearance of an intense peak at  $1630\text{ cm}^{-1}$  which can be attributed to an increase in the C=C bond ( $\pi$ - character).<sup>37</sup> The 20 minutes treated sample also shows this signature. Intriguingly similar to the sophorolipid case a new peak at  $1630\text{ cm}^{-1}$  is also seen to emerge in the case of laser irradiated Oleic acid (Figure 3.14 B), which also exhibits fluorescence, as stated earlier.

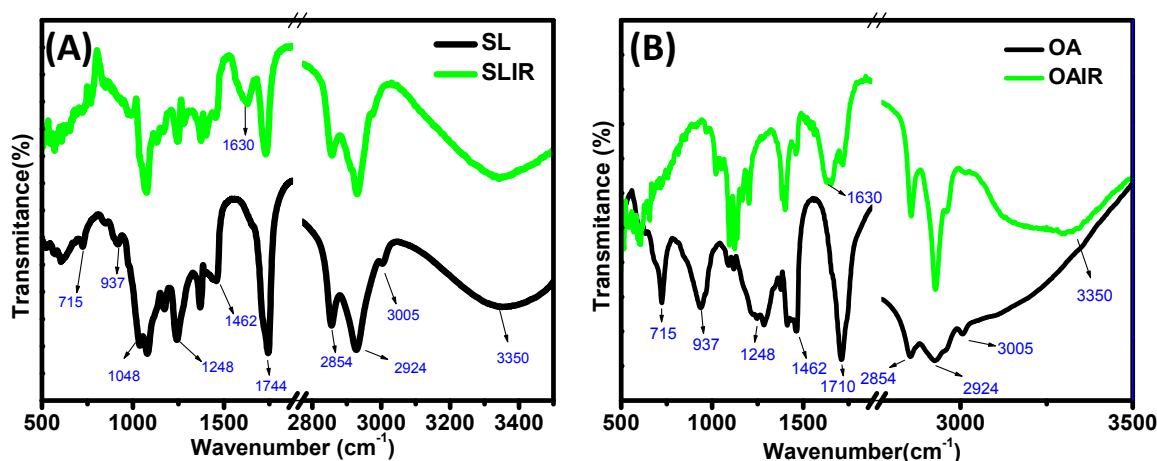


**Figure 3.13 (A, B)** FTIR data of unirradiated and laser irradiated SL and oleic acid respectively. An extra peak at  $1630\text{ cm}^{-1}$  in both SL and oleic acid corresponds to increase alkene ( $-\text{C}=\text{C}-$ ) in oleic acid and SL molecular structure.

Clearly the fluorescence character is tied to the appearance of this extra C=C bond in these structures post-irradiation. It may be remembered that the discussion pertaining to the appearance and the downfield location of the C=C bond from NMR and MALDI refers to the 20 minutes irradiated sample. Further irradiation leading to fully evolved spherical assemblies could have additional modifications which cannot be ascertained easily. The emergent assembly and interactions of the  $\pi$  -  $\pi$  structures induced by laser treatment could explain the strong fluorescence observed in SL case. It may be further noted that Oleic acid does not show equally strong fluorescence (although exhibits the same basic weak fluorescence and molecular changes) because it does not lead to the complex assembly. Thus, our analyses suggest that the elements of fluorescence are induced in the system via laser induced extra C=C bond character, however enhancement of fluorescence originates from the assembly character.

### 3.5 Magnetic SL structure by embedding Fe<sub>3</sub>O<sub>4</sub> nanoparticles

Iron oxide (Magnetite, Fe<sub>3</sub>O<sub>4</sub> or Maghemite, gamma-Fe<sub>2</sub>O<sub>3</sub>) nanoparticles have long been known to be useful in drug delivery and nano-medicinal applications. However their intrinsic surface area is not that high. We therefore undertook the task of exploring the possibility of loading them on the highly spherical laser synthesized sophorolipid mesostructures. Needless to mention that this can render them even more biocompatible, especially in so far as their interaction with cells is concerned. Indeed sophorolipids could help facilitate the entry of the iron oxide nanoparticles inside cells since lipids can easily fuse with the cell membrane. Moreover iron oxide impregnated SL particles can be directed easily to a specific site under the influence of an external magnetic field favoring the applicability of this bio-inorganic composite system to cancer hyperthermia. Super-paramagnetic Fe<sub>3</sub>O<sub>4</sub> nanoparticles were synthesized by polyol method.<sup>38</sup> These monodispersed nanoparticles were then mixed with Sophorolipid solution and irradiated with UV laser pulses. Complex structures embedded with Iron oxide nanoparticles in SL were thus obtained which could be easily separable using a magnet. Studies were also performed by adding Fe<sub>3</sub>O<sub>4</sub> nanoparticles during synthesis of spherical mesostructures at intervals.

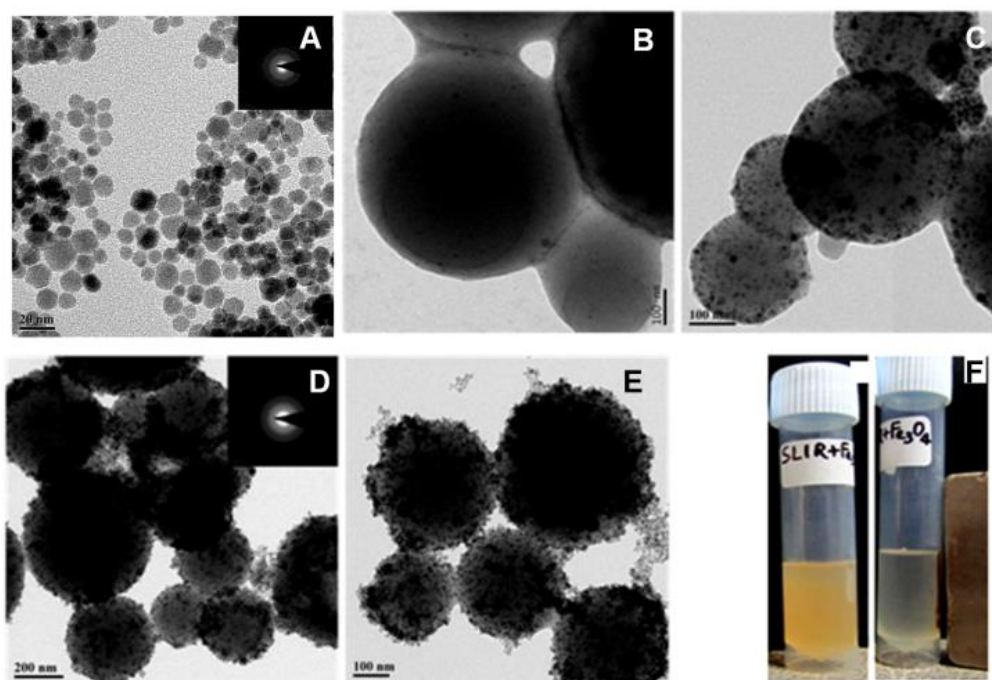


**Figure 3.14** TEM images of (A)  $Fe_3O_4$  Nanoparticles (NP), and (B-E)  $Fe_3O_4$  NP loaded SL assemblies formed by laser irradiation. The images B, C, D and E are for cases when the NPs were added to the SL solution after initial laser irradiation for 0, 20, 30 and 40 mins, respectively. The  $Fe_3O_4$  content and the total irradiation time of 60 minutes were the same in all cases. The picture in (F) shows the appearance of magnetic NP loaded SL mesostructures dispersion for case (B) without (left) and with (right) magnetic field. It is seen that the entire dispersion is pulled by the magnet.

It was observed that when  $Fe_3O_4$  nanoparticles were added during synthesis at the beginning itself, almost all of the particles got embedded in the core of these mesostructures.  $Fe_3O_4$  nanoparticles which were added after 20 and 40 minutes during the synthesis of the SL mesostructures were more peripheral in their location. These embedded SL structures were smaller and compact in nature when compared to pure SL vesicular mesostructures. EDAX analysis of laser irradiated sophorolipid wherein  $Fe_3O_4$  was added right at the beginning is shown in Table 1. It brings out the percentage of iron oxide nanoparticles in the sophorolipid mesostructures. It is important to point out that depending upon the time of addition of  $Fe_3O_4$  nanoparticles; we can define the location of these nanoparticles in Sophorolipid assemblies.

**Table 1 EDAX Analysis of Laser Irradiated magnetic SL mesostructures with Fe<sub>3</sub>O<sub>4</sub> embedded nanoparticles (Figure 3.14 B-E)**

Element	wt	%At	%K-ratio	Z	A	F
C K	79.15	86.32	0.5136	1.009	0.6425	1.0001
O K	15.05	12.32	0.0210	0.9945	0.1402	1.0002
Fe L	5.80	1.36	0.0171	0.8617	0.3415	1.0000

To get a particular location of Fe<sub>3</sub>O<sub>4</sub> nanoparticles (center, periphery and outer surface in sophorolipid mesostructures requisite amounts of Fe<sub>3</sub>O<sub>4</sub> in Sophorolipid solution with various combinations were tried as described in materials in methods.

### Cyto-toxicity and hyperthermia experiment

Cyto-toxicity analysis of the laser-synthesized sophorolipid mesostructures was done using MTT assay. For this a HeLa derived cell line was used. Spherical sophorolipid sample, which had been dried to powder form, was resuspended in sterile distilled water before the assay. Then appropriate concentration of the sample was added to the wells of a 96 well plate and the plate was incubated for 2 days.

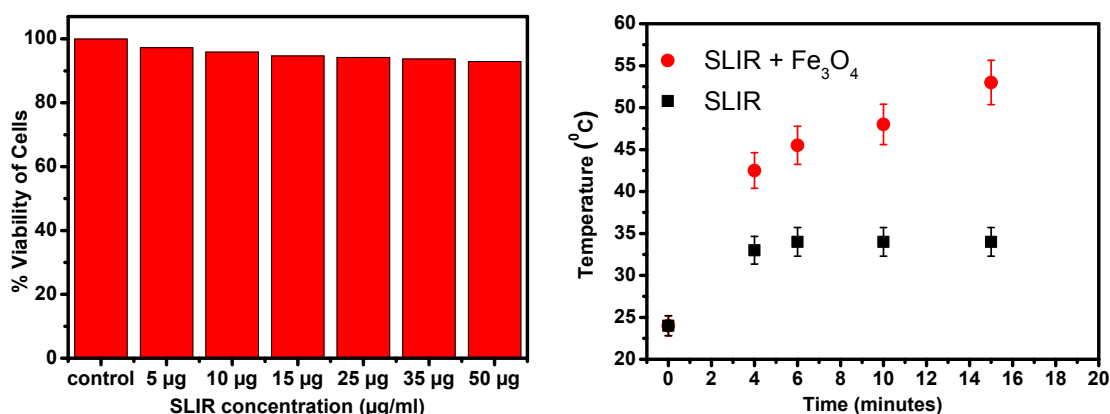


**Figure 3.15 (A)** Cytotoxicity of Sophorolipid mesostructures performed on HeLa derived cell line on 96 well plates; the plate was incubated for 2 days and optical density was measured at 540 nm; **(B)** Temperature rise of water dispersions of SL and magnetic NP loaded SL mesostructures under RF excitation as a function of time

The viability of cells was then checked by their ability to reduce the tetrazolium salt (MTT) to bluish purple colored Formazan crystals, which can be solublized by acidified propanol and optical density measured at 540 nm. This assay proved to us that the SL mesostructures are not detrimental to the viability of eukaryotic cells even at a concentration of 50  $\mu\text{g/ml}$  (Figure 3.15A).

Hyperthermia experiment was also done using a Radio Frequency source. Magnetite loaded SL mesostructures (5 mg/ml  $\text{Fe}_3\text{O}_4$  nanoparticles) was used for this experiment. The data were collected at 0 min, 4 min, 10 min and 15 minutes for both the unirradiated SL sample and the magnetite-loaded SL mesostructures sample formed by laser irradiation. The data shown in Figure 3.15A clearly bring out that the biocompatible Sophorolipid mesostructures loaded with  $\text{Fe}_3\text{O}_4$  nanoparticles can serve as effective hyperthermia agents

### 3.6 Conclusions

Highly spherical mesoscale Sophorolipid molecular assemblies are synthesized using a simple one step method which involves irradiating a water solution of acidic sophorolipid with UV laser (Excimer, 248 nm) pulses. Remarkably, the laser assembled mesostructures exhibit strong green fluorescence, while the original sophorolipid molecules do not show any. Cyto-toxicity assay shows that these are non-toxic to living cells even at 50 $\mu\text{g/ml}$ . It is further shown that such mesostructures can be easily impregnated with super-paramagnetic iron oxide nanoparticles, and the corresponding synthesis protocol concurrently leads to a reduction in the assembly size down to 100 nm scales. Importantly, the fluorescence property is retained and the magnetite loaded assembly can be heated by RF excitation for hyperthermia application

### References

- 1 W. C. W. Chan, S. Nie, *Science*. 1998, **281**, 2016
- 2 J.F. Lovell, C.S. Jin, E. Huynh, H. Jin, C. Kim, J.L. Rubinstein, W.C.W. Chan, W. Cao, L.V. Wang, G. Zheng, *Nature Materials* 2011, **10**, 324
- 3 R. Weissleder, *Science* 2006, **312**, 1168.

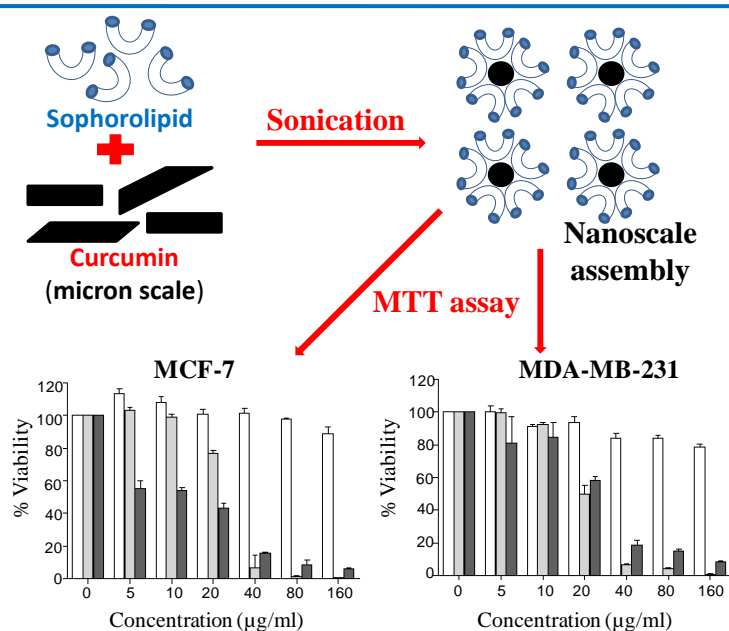
- 4 C.J. Murphy, T.K. Sau, A.M. Gole, C.J. Orendorff, J. Gao, L. Gou, S.E. Hunyadi, T. Li, *J. Phys. Chem. B.* 2005, **109**, 13857
- 5 M. Xu, L. V. Wang, *Rev. Sci. Instrum.* 2006, **77**, 041101-1.
- 6 R.G.M. Kolkman, P.J. Brands, W. Steenbergen, T.G van Leeuwen, *Journal of Biomedical Optic.* 2008, **13**, 050510-1
- 7 C. Kim, E.C. Cho, J. Chen, K.H. Song, L. Au, C. Favazza, Q. Zhang, C.M. Cobley, F. Gao, Y. Xia, L. V. Wang. *ACS Nano* 2010, **4**, 4559.
- 8 V. Biju, M. Ishikawa, A. Anas, A. Sujith M. Ishikawa, *Anal Bioanal Chem.* 2008, **391**, 2469.
- 9 O.T. Bruns, H. Ittrich, U. Beisiegel, K. Peldschus, M. G. Kaul, U. I. Tromsdorf, J. Lauterwasser, M. S. Nikolic, B. Mollwitz, M. Merkel, N. C. Bigall, S. Sapra, R. Reimer, H. Hohenberg, H. Weller, A. Eychmüller, G. Adam, U. Beisiegel, J. Heeren J. Heeren, *Nature Nanotechnology*, 2009, **4**, 193.
- 10 L. Rodrigues, I.M. Banat, J. Teixeira, R. Oliveira, *Journal of Antimicrobial Chemotherapy* 2006, **57**, 609.
- 11 P. Singh, S.S. Cameotra, *TRENDS in Biotechnology*, 2004, **22**, 142.
- 12 J.H. Fuhrhop, T. Wang, *Chem. Rev.* 2004, **104**, 2901.
- 13 I.N.A. Van Bogaert, K. Saerens, C. De Muynck, D. Develter, W. Soetaert, J.E.Vandamme, *Appl Microbiol Biotechnol.* 2007, **76**, 23.
- 14 A. Daverey, K. Pakshirajan, P. Sangeetha, *World Academy of Science, Engineering and Technology* 2009, **51**, 497.
- 15 N. Baccile, N. Nassif, L. Malfatti, *Green Chem.* 2010, **12**, 1564.
- 16 L. Zhang, P. Somasundaran, S.K. Singh, A.B. Felse, R. Gross, *Physicochem. Eng. Aspects* 2004, **240**, 75.
- 17 T.T. Nguyen, D.A. Sabatini, *Int. J. Mol. Sci.* 2011, **12**, 1232.
- 18 J. Chen, X. Song, H. Zhang, Y.B. Qu, J.Y. Miao, *Appl Microbiol Biotechnol.* 2006, **72**, 52.
- 19 A. Furstner, K. Radkowski, J. Grabowski, C. Wirtz, R. Mynott, *J. Org. Chem.* 2000, **65**, 8758.
- 20 M. Kasture, S. Singh, A. Prabhune, B.L.V. Prasad, *Langmuir* 2007, **23**, 11409.



- 21 M.B. Kasture, P. Patel, A. A. Prabhune, B. L. V. Prasad, *J. Chem. Sci.* 2008, **120**, 515.
- 22 S. Singh, A.A. Prabhune, B.L.V. Prasad, *New J. Chem.* 2008, **33**, 646.
- 23 S.L. Fu, S.R. Wallner, W.B. Bowne, M. D. Hagler, M.E. Zenilman, R. Gross, M.H. Bluth, *Journal of surgical research* 2008, **148**, 77.
- 24 V. Shah, G. F. Doncel, T. Seyoum, K. M. Eaton, I. Zalenskaya, R. Hagver, A. Azim, R. Gross *Antimicrobial agents and chemotherapy* 2005, **49**, 4093.
- 25 K. Joshi-Navare, A. Shiras, A. Prabhune, *Biotechnol J*, 2011, **6**, 509.
- 26 H. Isoda, H. Shinmoto, D. Kitamoto, M. Matsumura, T. Nakahara, *Lipids* 1997, **32**, 263.
- 27 D. Kitamoto, T. Morita, T. Fukuoka, M. Konishi, T. Imura, *Current Opinion in Colloid & Interface Science* 2009, **14**, 315.
- 28 S. Zhou, C. Xu, J. Wang, W. Gao, R. Akhverdiyeva, V. Shah, R. Gross, *Langmuir* 2004, **20**, 7926.
- 29 E. Zini, M. Gazzano, M. Scandola, *Macromolecules* 2008, **41**, 7463.
- 30 J. Penfold, M. Chen, R. K. Thomas, C Dong, T J. P. Smyth, A. Perfumo, R Marchant, I. M. Banat, P Stevenson,| A. Parry, I Tucker, I. Grillo, *Langmuir* 2011, **27**, 8867–8877
- 31 H. Huang, S. Delikanli, H. Zeng, D.M. Ferkey, A. Pralle, *Nature Nanotechnology* 2010, **5**, 602.
- 32 Y. Wang, N. Ma, Z. Wang, X. Zhang, *Angew. Chem. Int. Ed.* 2007, **46**, 2823.
- 33 M. Antonietti, S. Forster, *Advanced Material* 2003, **15**, 1323.
- 34 U Raul, R Heckmann, V Wray, S Lang, *Biotechnology Letters*, **21**, 973–977, 1999
- 35 C. P. Kurtzman<sup>1</sup>, N. P.J. Price, K J. Ray, T.M. Kuo<sup>2</sup>, *FEMS Microbiol Lett*, **311**, 2010, 140–146
- 36 X. Ma, H. Li, L. Shao, J. Shen, X. Song, *Appl Microbiol Biotechnol*, 2011, **91** 1623–1632
- 37 M. B. Avinash, T. Govindaraju, *Adv. Funct. Mater.* **2011**, 1–8.
- 38 Changming Cheng, Fangjie Xu, Hongchen Gu, *New J. Chem.*, 2011, **35**, 1072–1079.

## Chapter 4

# From Micron to Nano-Curcumin by sophorolipid co-processing: Highly enhanced bioavailability, fluorescence, and anti-cancer efficacy



Co-sonication of curcumin and acidic sophorolipid in aqueous solution is shown to lead to a dramatic enhancement of curcumin bioavailability through size reduction and encapsulation. The cytotoxicity effects of curcumin on breast cancer cell lines, MCF-7 and MDA-MB-231, are shown to be significantly enhanced by the formation of its complex with sophorolipid. The relative cytotoxicity of curcumin with its SL(A) complex is more due to the presence of glucose moiety. The results further suggest that sophorolipid based formulations, which solubilize and nano-encapsulate curcumin after lipid digestion, show great potential for curcumin cell entry.

## 4.1 Introduction

Curcumin is known to have antioxidant, anti-inflammatory, chemo-preventive and chemo-therapeutic properties.<sup>1</sup> The bioavailability<sup>2</sup> of curcumin is determined by the rate and concentration at which it enters the plasma and reaches the target sites. The oral bioavailability<sup>3</sup> of curcumin is low because a major portion of the compound remains unabsorbed due to a fairly low intestinal absorption capacity. Even a minor amount which is actually absorbed is rapidly metabolized in the liver and thrown out of the body by the gall bladder.<sup>4-6</sup> Several studies have verified that even a very high oral dose of curcumin (up to 1 g/kg<sup>-1</sup> of the body weight) is almost completely eliminated by the human metabolic system.

Curcumin (diferuloylmethane), a bright orange yellow pigment, is the main active ingredient of turmeric; an ancient spice known for its medicinal uses.<sup>7</sup> Curcumin exhibits tautomerism in its molecular structure and thus exists in the enol form in non-polar solvents, because of intra-molecular hydrogen bond formation. In polar solvents, however, it is observed in the diketo form.<sup>8</sup> The keto form of Curcumin acts as a proton donor in acidic and neutral media, whereas at pH values above 8.0, the enol form dominates and acts as an electron donor.

The existence of the phenolic, b-diketone, as well as the methoxy groups of Curcumin contribute to its free-radical scavenging property. This property imparts the anti-cancer nature to this compound.<sup>9-10</sup> However, as mentioned previously, these results have not been reflected well in clinical studies mainly due to the low oral bioavailability of Curcumin. Therefore several soft materials systems including liposomes,<sup>11-13</sup> microspheres,<sup>14</sup> dendrimres,<sup>15</sup> micelles,<sup>16</sup> hydrogels and solid lipid nanoscale particles<sup>17-20</sup> have been explored to design specific drug-delivery systems for Curcumin. These nano-assembly forming procedures designed to improve the bio-availability of curcumin are all inherently expensive and hence there is a strong urge to obtain cost-effective replacements for this system.

Biosurfactants<sup>21</sup> derived from microorganisms are an interesting category of bio-organic systems with potential applications in biomedical science. They can be produced from renewable feedstock or waste material<sup>22-23</sup> by natural fermentation. These amphiphilic compounds are known to easily form self-assemblies at different

pH conditions in aqueous environment. Sophorolipids are an eco-friendly and biocompatible class of amphiphilic biosurfactants which easily form emulsions in aqueous solution to reduce the surface tension and interfacial energies.<sup>24</sup> They possess unique structures that can be engineered to suit specific application domains.<sup>[25]</sup> Sophorolipid exists in two forms: acidic and lactonic. Acidic sophorolipids (SL(A)), are known to form micelles, which interact depending on the pH of the system.<sup>26-27</sup> SL(A), is composed of a sophorose unit attached to an oleic acid moiety through an ether bond on the C17 carbon atom of the fatty acid chain. This particular characteristic leaves the COOH group available and responsive to changes in pH of the solution giving rise to the possibility of a series of self-assembled structures.

## 4.2 Experimental

### 4.2.1 Synthesis of acidic sophorolipid (SL(A))

Crude sophorolipid mixture was synthesized by *Candida bombicola* processed by alkaline hydrolysis to convert it as acidic sophorolipid under heat treatment. In brief 20 gm. crude sophorolipid mixture was added in 50 mL 5M NaOH solution and reflux under stirred condition. Temperature of the solution was rises to 90 °C at constant rate 2°C/min, and then leaves the solution for 10 minutes and finally it was cool to room temperature. Color of the solution was yellow/pale yellow from the start point to the end. Temperature control is a crucial parameter because once it reaches beyond 90 °C, would reduce the final product due to the formation of oxidized species. Acidic sophorolipid was collected at pH 4 by adding 40 mL 18.5 wt% HCL solutions.

### 4.2.2 Synthesis procedure for the SL(A)+Cur assembly

SL(A) dissolved in 25 ml distilled water (1 mg/ml) was taken in a 50 ml beaker, and was kept for bath sonication for 30 minutes. 5 ml Curcumin solution (1mg/ml) in distilled water was mixed drop wise during sonication at the rate of 0.5 ml/min. The final volume was dried by rota-vapor and then 5 ml water was added for complete dispersion. The solution was filtered through a 0.22 µm filter paper to make sure that only the well-dispersed compound will go across the membrane.

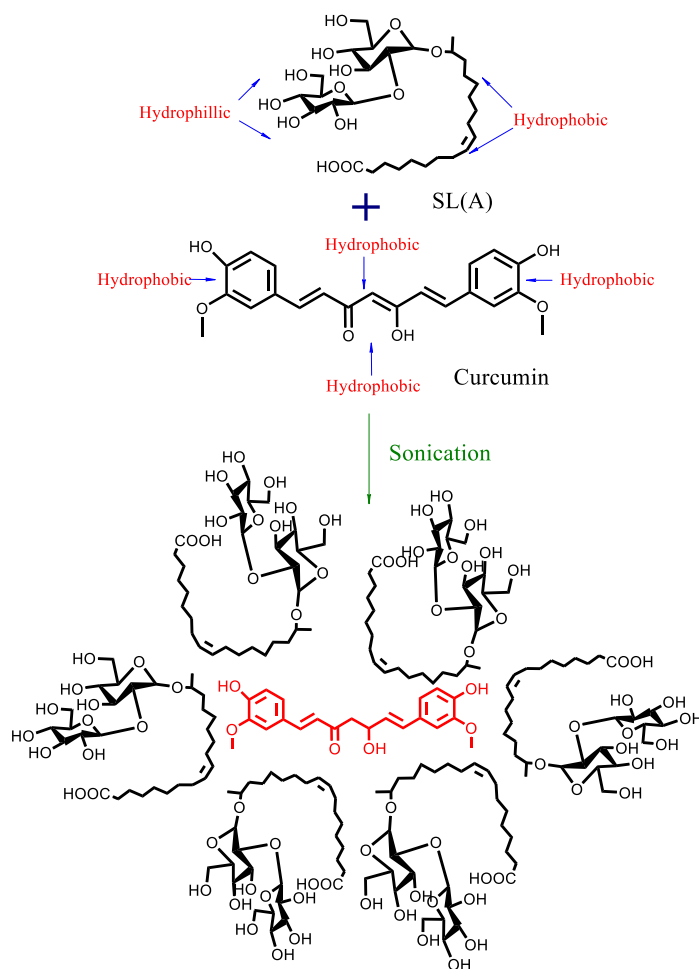


**Figure 4.1** Structure of SL(A)+Cur self-assembly. SL(A) is seen to completely encapsulate Curcumin through hydrophobic part because of its hydrophobic nature. The hydrophilic part of SL(A) makes this assembly soluble in aqueous environment and prevents it from degradation

### 4.3 Characterization

In this study, we have developed a novel formulation, namely a complex of acidic sphingolipid and curcumin ((SL(A)+Cur), to improve the water solubility, stability and bioavailability of curcumin in order to enhance its effectiveness in the context of anti-cancer activity. SL(A)+Cur complexes were prepared by sonication driven supramolecular self-assembly (Figure 4.1), and were characterized by using UV-Vis and photoluminescence (PL) spectroscopy, dynamic Light Scattering (DLS), Zeta potential, Fourier-transform infrared (FTIR), x-ray diffraction and scanning, Transmission electron microscopy (SEM and TEM, respectively). The as-synthesized

curcumin formulation showed significantly improved bioavailability in cancer cells compared to the curcumin in ethanol. The optimized curcumin formulation also exhibited more cytotoxicity in cancer cells. This study thus suggests a new cost-effective nanoscale self-assembly approach for improved curcumin delivery and therapeutic efficacy in cancer.

#### **4.3.1 UV-Vis and Photoluminescence studies**

UV-Vis absorption spectra were recorded on Varian CARY 100 Bio UV-Vis spectrophotometer, with 10 mm quartz cell at  $25\pm 0.1$  °C. For recording the spectra, 3 ml solutions of SL(A), Curcumin and SL(A)+Cur solution were prepared with concentration of 100 µg/ml. The solutions were mixed gently and subsequently the spectra were recorded.

#### **4.3.2 DLS measurements**

DLS measurements were carried out on Brookhaven Instrument model 90 Plus Particle Size Analyzer.

#### **4.3.3 Zeta Potential**

The surface charges of the SL(A), Curcumin and SL(A)+Cur were determined using a Zeta potential analyzer (Brookhaven Instruments Corporation, NY). The average Zeta potentials of the nano self-assembly dispersions were determined without any dilution.

#### **4.3.4 FTIR analysis**

FTIR spectra were recorded with KBr pellets in transmission mode using a Nicolet Magna IR-750 spectrophotometer at  $4\text{ cm}^{-1}$  resolution with 64 scans between 4000 and  $400\text{ cm}^{-1}$ . Two milligram of dried powder was mixed with 198 milligram KBr and analyzed.

#### **4.3.5 Scanning Electron Microscopy (SEM)**

Field emission scanning electron microscopy images were acquired on FEI QUANTA 200 microscope, equipped with a tungsten filament gun, operating at WD 10.6 mm and 20 kV. 10 µL aliquots of all three sample solution were placed on silicon wafer

and these were fixed on copper stubs with the help of carbon tape. The samples were dried at room temperature overnight and images were recorded without gold coating.

#### 4.3.6 Sample preparation for NMR

Chloroform was added in SL(A)+Cur aqueous solution to extract curcumin from nano-complex. The sample was rotator evaporator and vacuum dried for 60 min to remove chloroform. Curcumin crystals, as a control, were dissolved in chloroform and vacuum-dried as above the encapsulated curcumin. The obtained curcumin powders were dissolved in deuterated chloroform for <sup>1</sup>H NMR study.

#### 4.3.7 Cell lines and reagents

The human breast adenocarcinoma cell lines, MCF-7 and MDA-MB-231 used in the study were obtained from National Centre for Cell Science (NCCS), Pune, India. The cells were grown in DMEM containing 2 mM L-glutamine supplemented with 10% fetal bovine serum and 100 U/ml of penicillin-streptomycin. The cells were incubated in a humidified 5% CO<sub>2</sub> incubator at 37°C. Tissue culture plastic ware was purchased from BD Biosciences, CA, USA. Curcumin, Dulbecco's Modified Eagles Medium (DMEM), Fetal Bovine Serum (FBS) and 3-(4,5-dimethylthiazol-2-yl)-2,5-diphenylthiazolium bromide (MTT) were obtained from Sigma-Aldrich (St. Louis, MO). Penicillin/streptomycin and L-glutamine were obtained from Gibco BRL, CA, USA.

#### 4.3.8 MTT assay

The cell viability was determined by MTT dye uptake as described previously.<sup>32</sup> Briefly, the cells were seeded at a density of  $1 \times 10^5$  cells/ml density in 96-well plates. An untreated group was kept as a negative control. The cells were treated with different concentrations (0-160 µg/ml) of SL(A), Curcumin (dissolved in ethanol) and SL(A)+Cur. MTT solution (5 mg/ml) was added to each well and the cells were cultured for another 4 h at 37°C in 5% CO<sub>2</sub> incubator. The formazan crystals formed were dissolved by addition of 90 µl of SDS-DMF (20% SDS in 50% DMF). After 15 min, the amount of colored Formazan derivative was determined by measuring optical density (OD) using the ELISA micro plate reader (Biorad, Hercules, CA) at 570 nm (OD<sub>570-630</sub> nm). The percentage viability was calculated as:

$$\% \text{ Viability} = [\text{OD of treated cells}/\text{OD of control cells}] \times 100$$

### Statistical Analysis

All the experiments were performed in triplicates and repeated twice and the data are presented as mean  $\pm$  SD. Statistical analysis was conducted with the Graph Pad 4 prism program using one-way ANOVA. The  $p$ -values used for comparisons were  $<0.05$ . IC<sub>50</sub> values were calculated using Kyplot software.

## 4.4 Result and discussions

### 4.4.1 Optical properties

The optical properties of sophorolipid acidic SL(A), curcumin (Cur) and sophorolipid-curcumin (SL(A)+Cur) complex show distinct significant differences. SL(A) appears transparent, Curcumin solution looks turbid, whereas the SL(A)+Cur solution appears transparent yellow indicating curcumin solubilization. The photo-physical properties of curcumin are very sensitive to the medium. Curcumin has extensive absorption around 420 nm in organic solvent. However, its absorbance decreases in aqueous solution due to degradation of Curcumin in water by a reaction at the keto-enol group. Interestingly though, the sophorolipid shell imparts a hydrophobic surface to the curcumin core in the SL(A)+Cur complex and the outer hydrophilic portion of the sophorolipid assists in the solubility of the complex in water (Figure 4.2 A). This assembly in aqueous solution greatly assists in stabilization of the complex giving rise to the enhanced absorption at 420 nm in the aqueous medium.<sup>[8, 11]</sup>

Photoluminescence (PL) of the SL(A), Curcumin and SL(A)+Cur samples was recorded for comparison by excitation at the same wavelength of 420 nm in an aqueous solution. SL(A) sample exhibits no PL, while Curcumin exhibits weak excitonic emission at 550 nm due to low solubility.<sup>[28]</sup> However, on addition of SL(A) in Curcumin aqueous solution a strong emission is seen at 500 nm reflecting tremendous enhancement of the fluorescence intensity (Figure 4.2 B). The fluorescence maximum shifts from a broad unremarkable 550 nm band to a remarkable blue shifted band at 500 nm.<sup>11,29</sup> To confirm the improvement in PL, we performed some additional experiments.



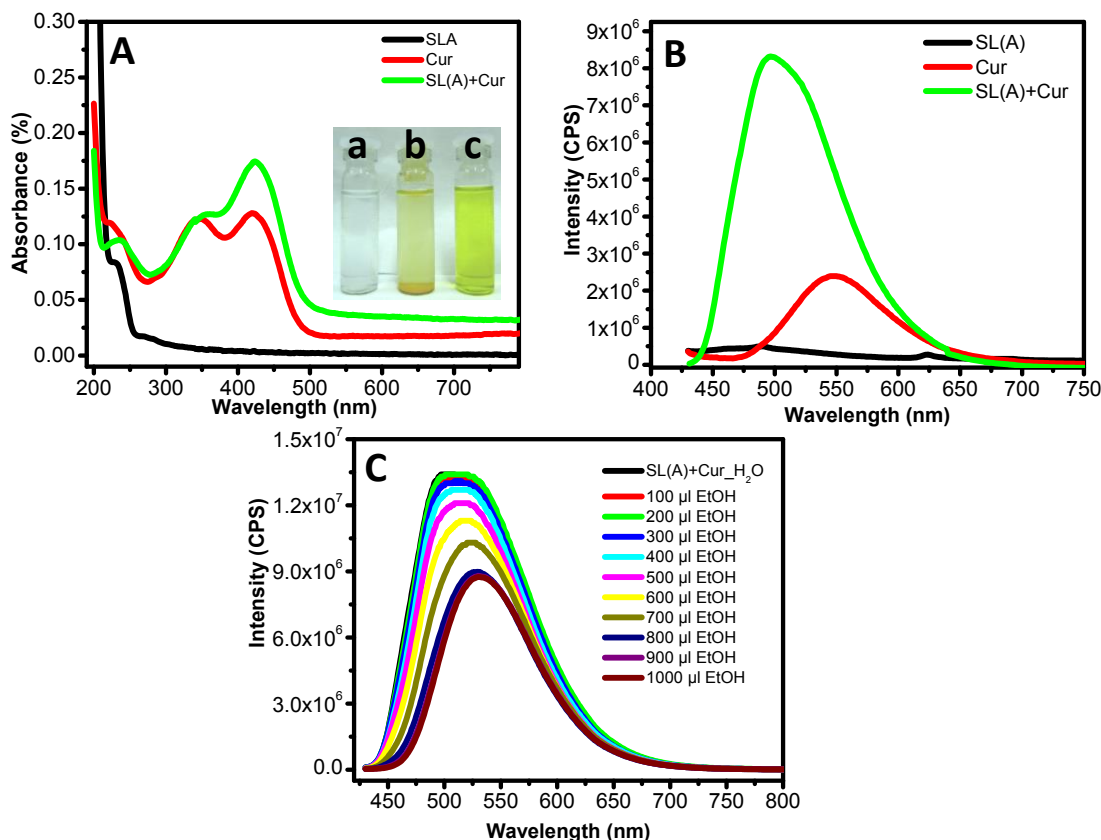


**Figure 4.2** (A) UV-Visible spectra of SL (A), Curcumin and SL(A)+ Cur solutions. SL(A) solution shows absorbance at  $\lambda=234$  nm and Curcumin solution at  $\lambda=344$  and 420 nm while SL(A) + Cur showing increase absorption at one peak at 420 nm; (B) Photoluminescence study of SL(A), Curcumin and SL(A)+ Cur solutions. SL(A) solution shows no PL, Curcumin solution shows PL at 550 nm while SL(A) + Cur showing very strong Photoluminescence at 500 nm; (C) Photoluminescence quenching and right shift of the PL of SL(A)+Cur self-assembly on gradually addition of ethanol solvent;

When we add ethanol gradually in this mixture, photoluminescence quenching is observed. This is probably due to disturbance of nonpolar region around Curcumin nanoparticles created by SL(A) self-assembly. Furthermore, a red shift is observed (from 500 nm to 550 nm) with the addition of ethanol to the SL(A)+Cur aqueous solution, clearly indicating a gradual degradation of the self-assembly yielding the original structure itself (Figure 4.2 C).

As described earlier, a large blue shift was observed when Curcumin was bound to the SL(A) micelles signifying that Curcumin in SL(A) micelles creates nonpolar

environment, possibly by binding to the hydrophobic regions of SL(A) micelles. Besides the shift in the fluorescence maximum, there was a remarkable improvement in the fluorescence intensity of Curcumin upon formation of the self-assembly with SL(A) (Figure 4.3). As seen from Figure 4.3 B a very feeble fluorescence is seen in the case of Curcumin particulates, while the well-dispersed and therefore well distributed SL(A)+Cur nanoparticulates exhibit enhanced fluorescence ( Figure 4.3D).

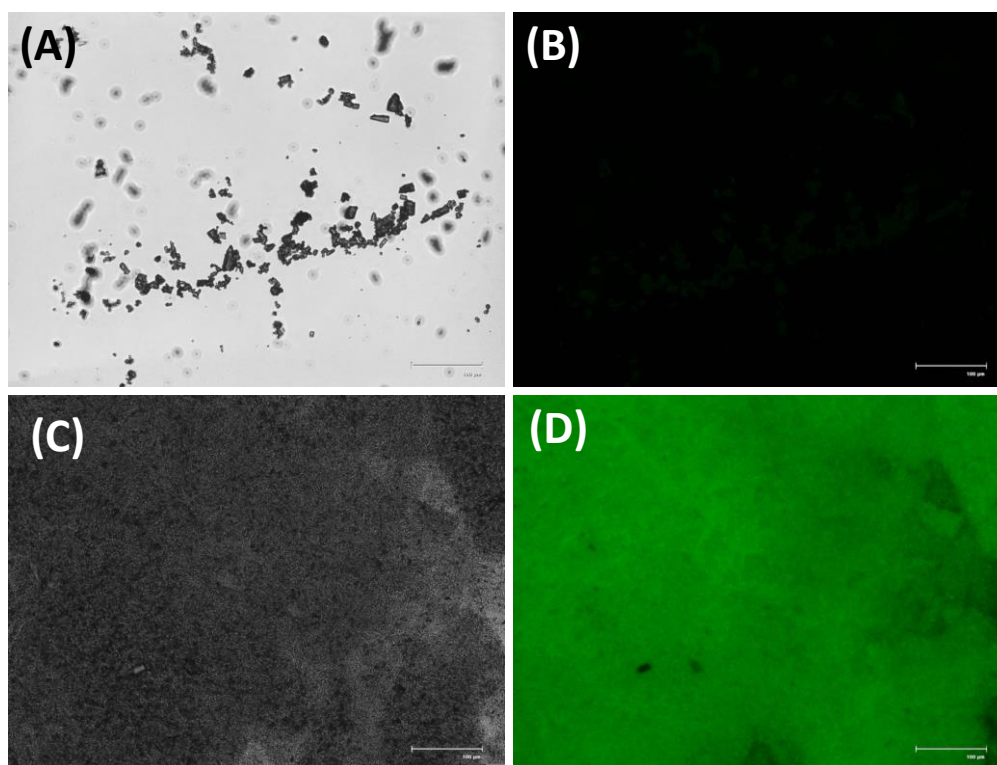


*Figure 4.3 (A and C) Optical Microscopy images of Curcumin and SL(A)+Cur self-assembly; (B) and (D) Fluorescence images of Curcumin and SL(A)+Cur self-assembly.(scale bar 100  $\mu$ m).*

#### 4.4.2 Particles Size Distribution and Zeta Potential

In this experiment, all solutions were analyzed at a constant shutter opening diameter in the DLS apparatus. DLS measurements for Curcumin, SL(A) and SL(A)+Cur (10 mg of each dissolved in 10 ml H<sub>2</sub>O) exhibit hydrodynamic radii of about 818 nm, 6.8.nm and 15.5 nm, respectively (Figure 4.4 A, C, E). This was also confirmed with the results obtained by SEM and TEM analysis. These data clearly show that the size of the SL(A)+Cur particles is ~6-7 nm indicating that there is a decreased agglomeration of Curcumin in aqueous solution due to its capping by SL(A) and there

is a definite increase in the size of SL(A)+Cur complex as compared to only SL(A) because of the additional encapsulation of Curcumin nanoparticles.

To understand the stability of SL(A)+Cur, Zeta potential measurements were done on all the three samples. The zeta potential values for the three sample were SL(A) = -17.30 mV, Curcumin = -15.14 mV, SL(A)+Cur= -24.38 mV (Fig. 4 B, D, F respectively). The increase in the zeta potential of SL(A)+Cur compared to individual SL(A) and Curcumin can be taken as an indication of an increased stability of the self-assembled complex.

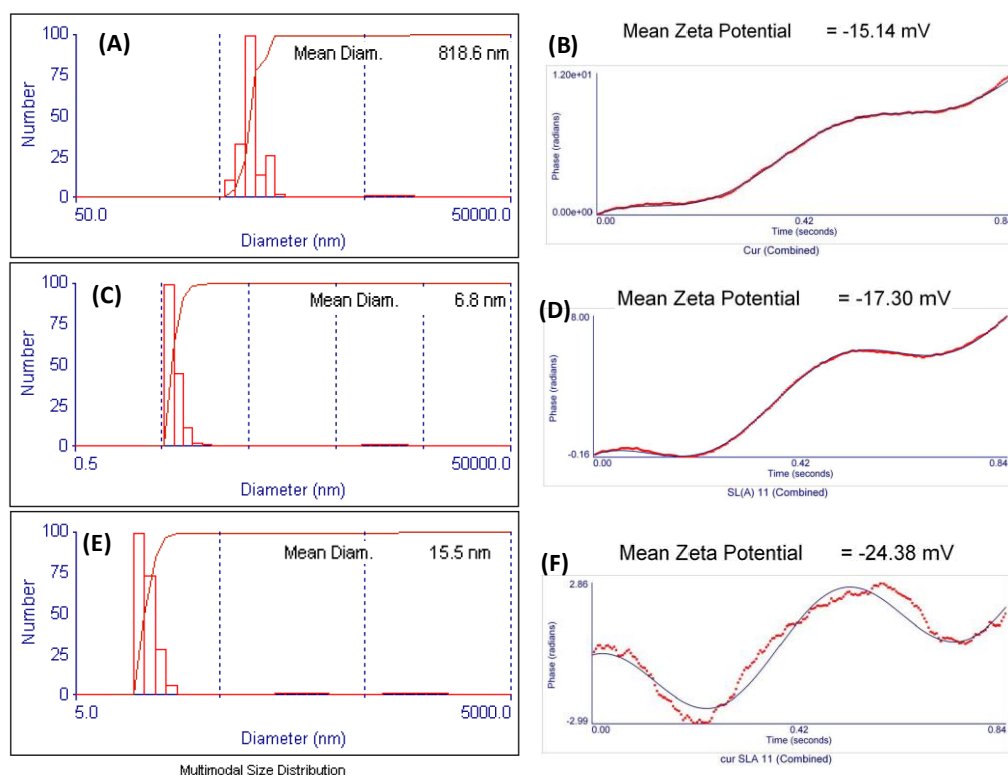


**Figure 4.4** DLS and Zeta Potential results for (A) Curcumin showing hydrodynamic radius of 818.6 nm and (B) corresponding Curcumin zeta potential; (C) SL(A) showing hydrodynamic radius of 6.8 nm and (D) corresponding SL(A) zeta potential; (E) SL(A)+Cur showing hydrodynamic radius 15.5 nm and (F) corresponding SL(A)+Cur zeta potential.

#### 4.4.3 Microscopy studies

SL(A), Curcumin and SL(A)+Curcumin samples were further examined by scanning electron microscopy (Figure 4.5 A, B and C). SL(A) exhibits a ribbon type

morphology (Figure 4.5 A) , Curcumin appears as large chunks forming undefined shape (Figure 4.5B), whereas SL(A)+Cur shows a fibrous morphology (Figure 4.5 C) which differs distinctly from that of SL(A). Remembering that these morphologies evolve in the solution drying process and do not represent the situation in the solution, it is clear that morphological organization of SL around Curcumin with hydrophilic groups

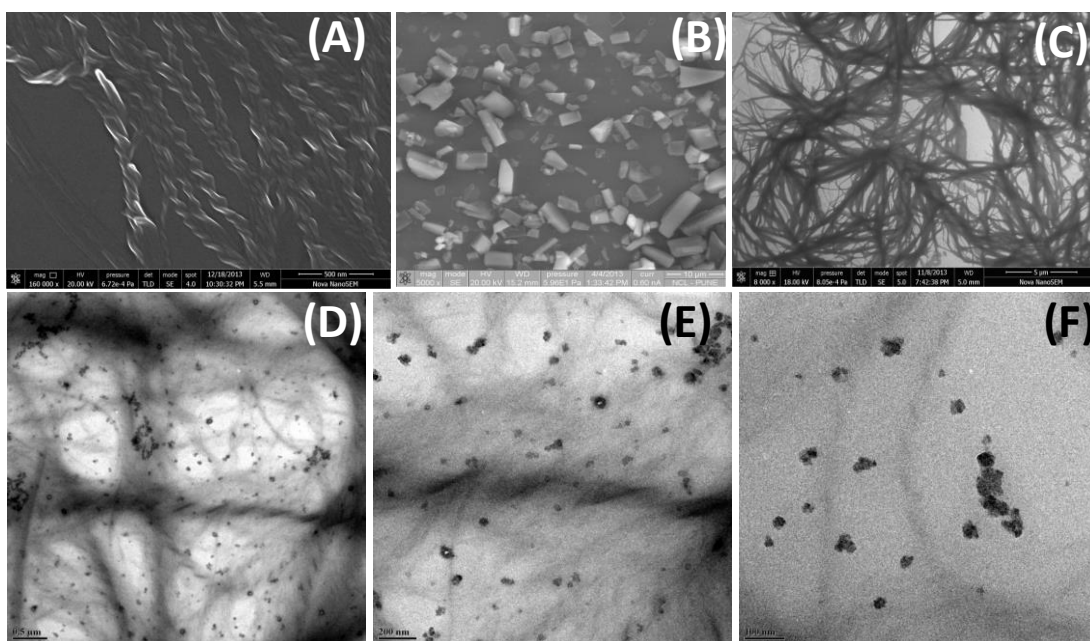


**Figure 4.5** (A) SEM of SL(A) showing ribbon structure; (B) SEM of Curcumin showing chunks of undefined structure; and (C) SEM of SL(A)+Curcumin exhibiting morphological change vis a vis SL (A); (D-F) High resolution TEM images of SL(A)+Cur (scale bar sizes for A, B, C, D, E, F are 0.5, 10, 5, 0.5, 0.2 and 0.1  $\mu\text{m}$  respectively).

protruding outside would change their organization and therefore the morphology during the drying process as compared to SL itself which does not have such preferential molecular organization in the solution. The TEM pictures at different levels of magnification (Figure 4.5 D-E-F) apparent in SEM (Figure 4.5 C) due to the corresponding limited resolution show tiny fairly uniformly dispersed Curcumin nanoparticles (< about 20 nm, some agglomerated on TEM grid) which were not apparent in SEM (Figure 4.5 C) due to the corresponding limited resolution.

#### 4.4.4 FTIR Analysis

Figure 4.6 shows the FTIR spectra for SL(A), Curcumin and SL(A)+Cur after sonication treatment for 30 minutes. The SL(A) reveals a broad band at  $3350\text{ cm}^{-1}$

corresponding to the O-H stretch frequency in the glucose moiety of the molecule. The asymmetrical and symmetrical stretch modes of methylene ( $\text{CH}_2$ ) groups occur at  $2928$  and  $2854\text{ cm}^{-1}$ , respectively. Sophorolipid has two strong absorption bands arising from C-O- and C-O stretching; the C-O absorption band at  $1744\text{ cm}^{-1}$  may include contributions from acid group.

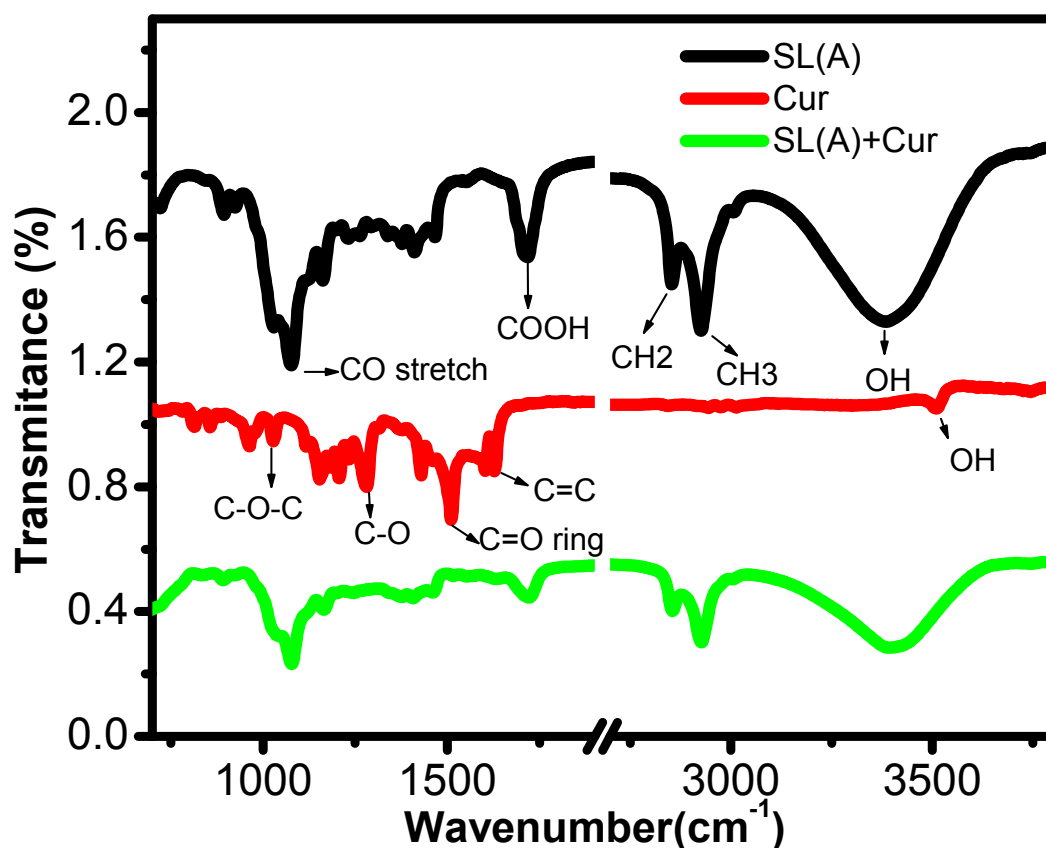


*Figure 4.6 FTIR analysis of SL(A), Curcumin and SL(A)+Cur.*

Moreover, sugar C-O- stretch of C-O-H groups is found at  $1048\text{ cm}^{-1}$  and the band at  $1452\text{ cm}^{-1}$  corresponds to the C-O-H in-plane bending of carboxylic acid ( $-\text{COOH}$ ) in the structure of the product. All these details are in conformity with the literature reports.<sup>29</sup> The FTIR spectrum of Curcumin shows a sharp one peak at  $3508\text{ cm}^{-1}$  indicating the presence of OH. The strong peak at  $1626\text{ cm}^{-1}$  has a predominantly mixed (C=C) and (C=O) character. Another strong band at  $1601\text{ cm}^{-1}$  is attributed to the symmetric aromatic ring stretching vibrations (C=C ring). The  $1508\text{ cm}^{-1}$  peak is assigned to the (C=O), while enol C-O peak was obtained at  $1272\text{ cm}^{-1}$ , C-O-C peak at  $1023\text{ cm}^{-1}$ , benzoate trans-CH vibration at  $959\text{ cm}^{-1}$  and cis CH vibration of aromatic ring at  $713\text{ cm}^{-1}$ .<sup>30</sup> The FTIR spectrum of SL(A)+Cur shows all the peaks

related to SL(A) and Curcumin peaks are seen to have been suppressed due to nano-encapsulation.

#### 4.4.5 X-ray diffraction (XRD) analysis

To examine the crystallinity of micelle-encapsulated SL(A)+Cur, XRD analysis was performed. XRD analysis of samples was done over broad angle range ( $2\theta = 10-80$  degrees). The powder X-ray diffractograms of SL(A), Curcumin and SL(A)+Cur dried powders are shown in Figure 4.7

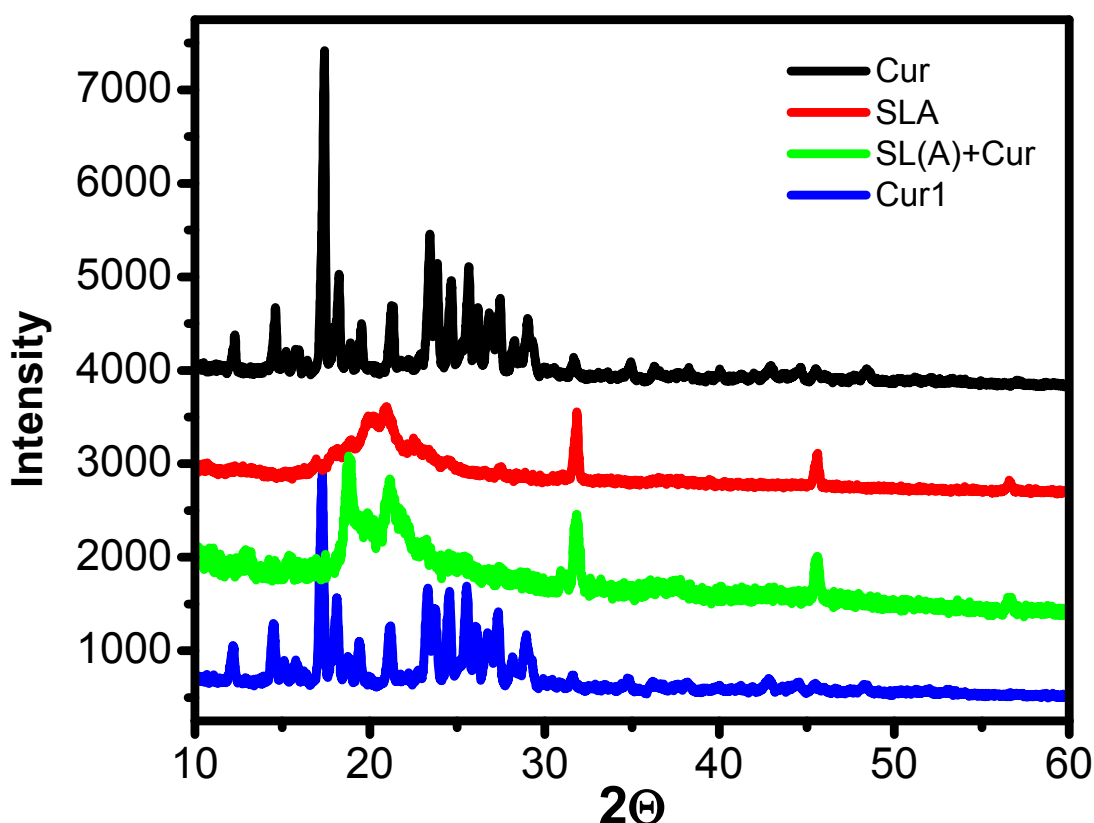


**Figure 4.7** XRD spectra of SL(A)+Cur self-assembly. Black line explain the Curcumin XRD pattern, red SL(A), green SL(A)+Cur while blue SL(A)+Cur after dissolve in chloroform solvent. Blue line showed unaffected nature of curcumin encapsulated in SL(A) self-assembly

The characteristic peaks of Curcumin appeared at diffraction angles of  $2\theta$  at 7.96, 8.90, 12.26, 14.54, 17.24°, etc. indicating that Curcumin is present as a crystalline form.<sup>31</sup> It is found that the characteristic diffraction peaks of the Curcumin are absent in the spectrum of the SL(A)+Cur nano-encapsulation, which suggests that Curcumin being nano-encapsulated its peaks are too broadened and the XRD pattern is dominated by the structure of sophorolipid component. Interestingly, the diffraction patterns of the material obtained after dissolution in chloroform showed a pattern



similar to that of pure Curcumin, indicating that the complex is broken down and the encapsulated Curcumin is released.

#### 4.4.6 Nuclear magnetic resonance analysis

We have confirmed the stability of curcumin after four month storage in refrigerator condition through NMR study of as synthesized and after four storage sample study.

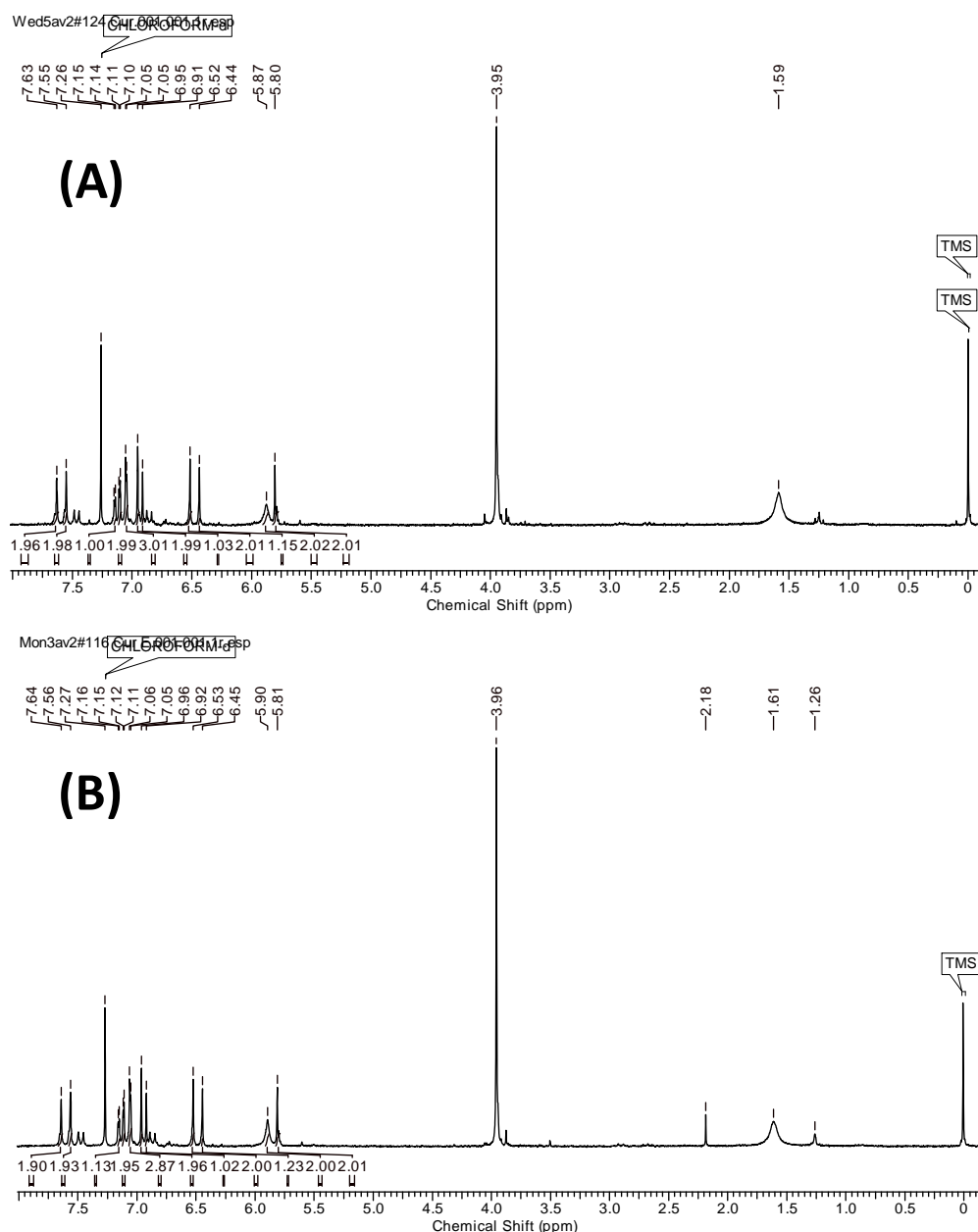


**Figure 4.8** (A) NMR spectra of curcumin in SL(A)+ Cur complex and (B) curcumin in SL(A)+ Cur complex after four month stability.

Sample preparation for the NMR study perform by addition of chloroform in

SL(A)+Cur self-assembled compound. Chloroform break the assembly and extract curcumin which was further dried in high vacuum condition. Figure 4.8 A illustrate the as synthesized curcumin (from SL(A)+Cur assembly) which match with reference NMR spectrum.  $^1\text{H}$  NMR spectrum of curcumin (200 MHz,  $\text{CDCl}_3$ ) was recognized by chemical shift ( $\delta$ ) of 3.96 (6H, s,  $\text{OCH}_3$ ), 6.53 (1H, s,  $\text{C}(\text{OH})=\text{CH}$ ), 6.92 (2H, d, 2,6-H), 6.96 (2H, d), 7.11 (2H, d), 7.56 (2H, s), 7.64 (2H, d, 1,7-H). Rather than a  $\beta$ -diketone,  $^1\text{H}$  NMR spectra of the curcumin denoted hydroxyl group, at  $\delta$  6.45 corresponding to enol-keto tautomer. Self-assembled structure of SL(L)+cur showed both SL(L) and curcumin identical peak without any contamination. Stability of SL(A)+Cur complex performed by four month old sample NMR spectra analysis (Figure 4.8 B), which shows identical peaks with as synthesized self-assembled complex.

#### 4.4.8 Cytotoxicity Assay

To evaluate whether SL(A) enhanced the bioavailability of curcumin in the cancer cells, cytotoxic potential of aqueous SL(A)+Cur was tested in breast cancer cell lines, MCF-7 and MDA-MB-231 and compared with that of aqueous SL(A), curcumin in water, and curcumin dissolved in ethanol, the latter being used as a positive control. Curcumin was administered to the cells at non-toxic doses of ethanol. After treatment with SL(A), both the breast cancer cell lines exhibited 80-100% viability upto the concentration of 160  $\mu\text{g}/\text{ml}$  showing that it was almost non-toxic to the cells. It can be observed that in SL(A)+Cur nano-complex, curcumin exhibited anticancer activity at extremely low doses starting from 6.66  $\mu\text{g}/\text{ml}$  compared to 40  $\mu\text{g}/\text{ml}$  concentration of curcumin dissolved in ethanol in MCF-7 cells (Figure 4.9 A).

As seen in the case of MCF-7 cells, curcumin dissolved in ethanol is more toxic than nano-complexes at moderate and low concentrations. In the low to moderate dose range (5-20  $\mu\text{g}/\text{ml}$ ), curcumin dissolved in ethanol has more concentration compared to the concentration of curcumin present in the SL(A)+Cur nano-complexes (0.83-3.33  $\mu\text{g}/\text{ml}$ ). Thus the nano-complexes do not show effective killing within this concentration. However, at higher dose range (40-160  $\mu\text{g}/\text{ml}$ ), the concentration of curcumin in SL(A)+Cur is also increasing (6.66 to 26.66  $\mu\text{g}/\text{ml}$ ) and thus we observe



the increase in cytotoxicity. Similarly, in MDAMB-231 cells (Figure 4.9 B), SL(A)+Cur exhibits cytotoxicity at 3.33  $\mu\text{g/ml}$  compared to 20  $\mu\text{g/ml}$  concentration of curcumin dissolved in ethanol. We have also added the data of curcumin (in water) that shows no cytotoxicity since curcumin does not go in water. These results clearly show that the bioavailability of curcumin is increased in the SL(A)+Curcumin complex as compared to the of curcumin dissolved in ethanol.

Interestingly, MCF-7 shows increased susceptibility to anticancer drugs at lower doses compared to MDAMB-231, the reason being the difference in estrogen and progesterone (ER/PR) receptor status in the cell lines. MCF-7 is ER/PR positive while MDAMB-231 is ER/PR negative, thereby being slightly insensitive to lower concentrations of anticancer drugs.

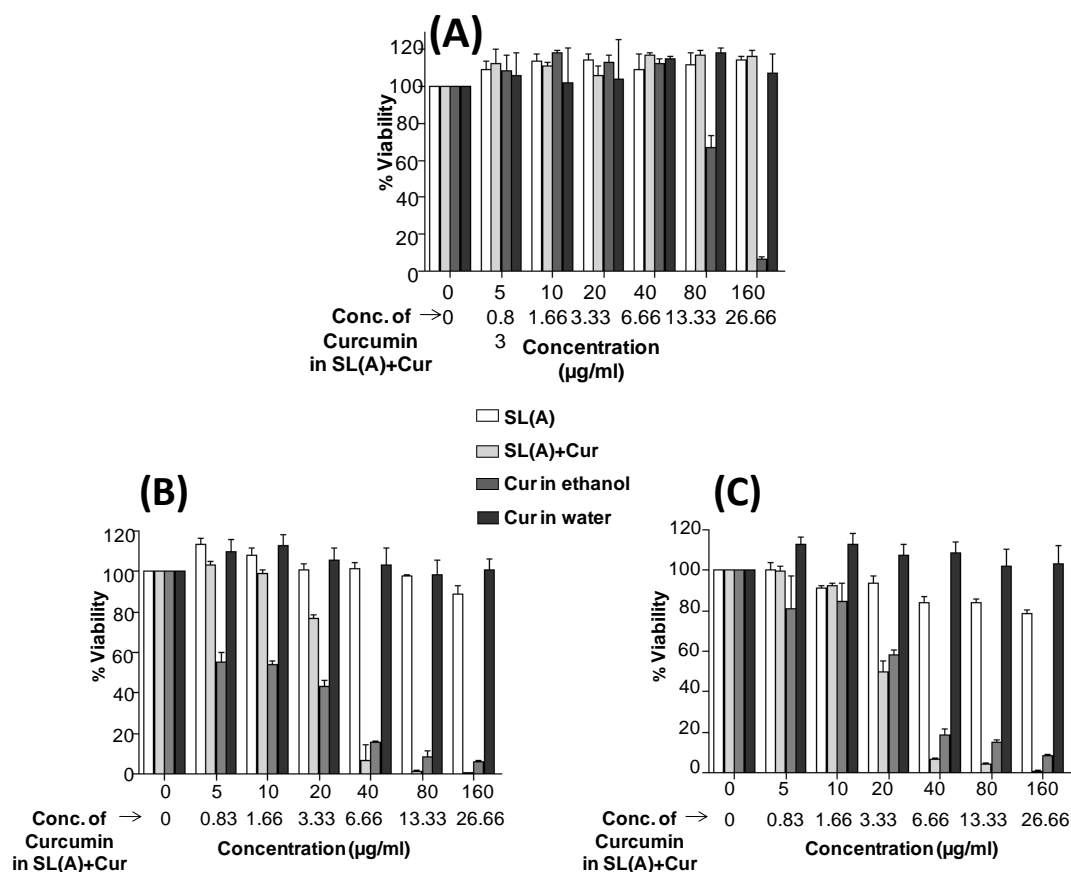


**Figure 4.9** Cytotoxicity analysis of SL(A), Curcumin and SL(A)+Curcumin by MTT assay in (A) HEK 293 cells (B) MCF-7 and (C) MDA-MB-231. All the data are presented as mean  $\pm$  SD of five independent experiments at  $p < 0.0001$ , indicating statistically significant differences compared to the control untreated group.

Moreover, SL(A) makes the curcumin present in the NPs more bio-available at lower

doses as compared to higher doses of curcumin dissolved in ethanol which explains the increased cytotoxicity of nano-complex.<sup>32-33</sup> This improved cytotoxicity of SL(A)+Cur complexes compared to curcumin in ethanol in cancer cell lines may be due to tautomeric molecular form of curcumin after SL(A) encapsulation.

We have compared the cytotoxicity of curcumin in water, curcumin in ethanol, SL(A) and SL(A)+Curcumin in non-cancerous cell line HEK 293 (Figure 4.9 C). Interestingly, except for Curcumin in ethanol (at higher doses), all others are non-toxic to the cells.<sup>34-40</sup>

## 4.5 Conclusions

Sophorolipid, an environmentally friendly, biocompatible and important class of biosurfactants is complexed with Curcumin to increase its solubility, stability, fluorescence and bioavailability. Particle size distribution, TEM and Zeta potential analyses suggest that the increase in cellular uptake could be attributed to the nano-encapsulation of Curcumin, its solubilization and stability in aqueous solution. It has been clearly established that the complex formation of Curcumin with SL(A) significantly reduced its therapeutic index, reflecting its increased bioavailability. This study emphasizes that solubilization by nano-encapsulation is an effective aspect of designing drug delivery systems.

## References

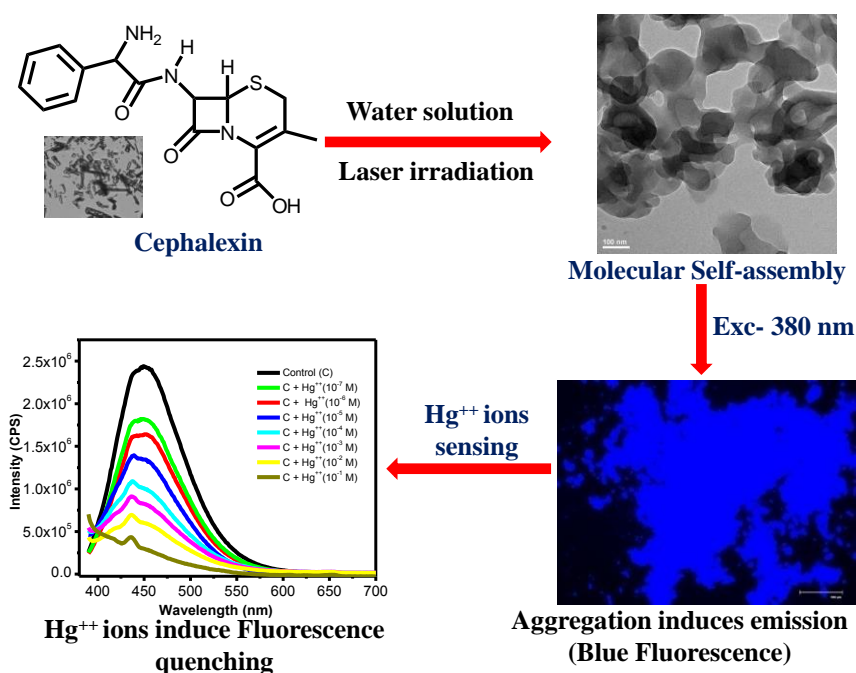
- 1 H. Yu, Q. Huang, *J. Agric. Food Chem.* 2012, **60**, 5373–5379
- 2 P. Anand, Ajaikumar B., B B. Aggarwal, *Molecular Pharmaceuticals*, 2007, **4**, 807–818
- 3 Kuo-Yi Yang, Lei-Chwen Lin, Ting-Yu Tseng, Shau-Chun Wang, Tung-Hu Tsai, *J. Chromatogr. B*, 2007, **853**, , 183–189
- 4 Reason W, Mysore S, M B Wang, Eri S Srivatsan, *Molecular Cancer*, 2007, **10**, 12
- 5 A. Shehzad, J. Lee, Y. S. Lee, *International Union of Biochemistry and Molecular Biology*. 2013, **26**, Pages 56–68
- 6 B. B. Aggarwal, K. B. Harikumar, *The International J of Biochemistry & Cell Biology*, 2009, **41**, 40–59

- 7 B. B. Aggarawal, A. Kumar, A. C. Bharti, *Anticancer Research*, 2003, **23**, 363-398
- 8 A. Barik, K. I. Priyadarsini, H. Mohan, *Photochemistry and Photobiology*, 2003, **77(6)**, 597–603
- 9 Albena T. Dinkova-Kostova, Paul Talalay<sup>1</sup>, *Carcinogenesis*, 1999, **20(5)**, 911–914
- 10 Y. M. Sun, H.Y. Zhang, D. Z. Chen, C. B. Liu, *Org. Lett.*, 2002, **4(17)**, 2909-2911
- 11 G. Began, E. Sudharshan, A. G. Appu Rao, *J. Agric. Food Chem.* 1999, **47**, 4992-4997
- 12 J. Barry, M. Fritz, A. Ramamoorthy, *J. Am. Chem. Soc.* 2009, **131**, 4490–4498
- 13 P. Basnet, H. Hussain, N Skalko-Basnet, *J of Pharmaceuticals Sciences*, 2012, **101**, 598-609
- 14 T. Ha Ho, T. P. T. Dao, M. C. Dang, *Adv. Nat. Sci.: Nanosci. Nanotechnol.*, 2013, **4**, 045008
- 15 P.R. Krishna Mohan, G. Sreelakshmi, Roy Joseph, *Vibrational Spectroscopy*, 2012, **62**, 77– 84
- 16 Z. Ma, A. Haddadi, O. Molavi, J. Samuel, *J of Biomedical Materials Research A*, 2007, 300-310
- 17 Bhawana, R. K. Basniwal, H. S. Buttar, N. Jain, *J. Agric. Food Chem.*, 2011, **59**, 2056–2061
- 18 B. B. Aggarwal, W. Yuan, S. Li, S. C. Gupta, *Mol. Nutr. Food Res.* 2013, **57**, 1529–1542
- 19 H. Hjorth Tønnesen, *Pharmazie*, 2006, **8**, 696-700
- 20 E. Gülçür M. Thaqi, F. Khaja, H. Önyüksel, *Drug Deliv. and Transl. Res.*, 2013
- 21 L. Rodrigues, I.M. Banat, J. Teixeira, R. Oliveira, *J of Antimicrobial Chemotherapy* 2006, **57**, 609.
- 22 A. Daverey, K. Pakshirajan, P. Sangeetha, *World Academy of Science, Engineering and Technology* 2009, **51**, 497.
- 23 I.N.A. Van Bogaert, K. Saerens, C. De Muynck, D. Develter, W. Soetaert, J.E. Vandamme, *App Microbiol Biotechnol.* 2007, **76**, 23.

- 24 L. Zhang, P. Somasundaran, S.K. Singh, A.B. Felse, R. Gross, *Physicochem. Eng. Aspects*, 2004, **240**, 75.
- 25 P. K. Singh, A. Prabhune, Satish Ogale, *Green Chem.*, 2013, **15**, 943–953
- 26 P. Singh, S.S. Cameotra, *TRENDS in Biotechnology*, 2004, **22**, 142.
- 27 S.L. Fu, S.R. Wallner, W.B. Bowne, M. D. Hagler, M.E. Zenilman, R. Gross, M.H. Bluth, *J of surgical research*, 2008, **148**, 77.
- 28 Achlesh Daverey, Kannan Pakshirajan, *Colloids and Surfaces B: Biointerfaces*, 2010, **79**, 246–53
- 29 D. Patra, E. E. Khoury, S. Darwish, R. M. Tafech, *Photochem and Photobio*, 2012, **88**, 319
- 30 T. T. T. Mai, Q. D. Le, X. P. Nguyen, J. S. Park, *Adv. Nat. Sci.: Nanosci. Nanotechnol.*, 2012, **3**, 025014
- 31 N. Kaewnopparat, S. Kaewnopparat, A. Jangwang, P. Panichayupakaranant, *World Academy of Science, Engineering and Technology*, 2009, **31**
- 32 K. J. Navare, Asmita Prabhune. *BioMed Research International* 2013(512495): 8
- 33 S. J. Koppikar, A. S. Choudhari, S. Suryavanshi, S. Kumari, S. Chattopadhyay, and R. Kaul-Ghanekar, *BMC Cancer*, 2010, **10**, 210
- 34 Rahmani AH, Al Zohairy MA, Aly SM, Khan MA, *Biomed Res Int*. 2014,761608
- 35 Gaurisankar Sa, Tanya Das, *Cell Division*, 2008, 3:14.
- 36 Y Kong, W Ma, X Liu, Y Zu, Y Fu, N Wu, L Liang, L Yao, T Efferth, *Molecules*, 2009, **14**, 5328-5338.
- 37 Jiang, M.-C., H.-F. Yang-Yen, J. J.-Y. Yen, and J.-K. Lin. *Nutr. Cancer*, 1996, **26**, 111–120.
- 38 Berrier, A. L., A. M. Mastrangelo, J. Downward, M. Ginsberg, and S. E. LaFlamme. *J. Cell Biol.* 2000, **151**, 1549–1560.
- 39 Jee, S. H., S. C. Shen, C. R. Tseng, H. C. Chui, and M. L. Kuo. *J. Invest. Dermatol* 1998, 111, 656–661
- 40 Park M-J, Kim E-H, Park I-C, *International Journal of Oncology*. 2002, **21(2)**, 379–383.

## Chapter 5

# Pulsed laser driven molecular self-assembly of Cephalexin: Aggregation induced fluorescence and its utility as mercury sensor



A fluorescent self-assembly of cephalexin was realized by pulsed laser irradiation process. An intense fluorescence emission was found in self-assembled form of the above process, due to occurrence of atypical aggregation-induced emission in cephalexin molecules. It was observed that fluorescence quenching of the self-assembled fluorescent nanostructures occurs in the presence of extremely low Hg<sup>++</sup> ions concentrations (10<sup>-7</sup> M) as compared to other heavy metal ions e.g. ferrous (Fe<sup>++</sup>) manganese (Mn<sup>++</sup>), Magnesium (Mg<sup>++</sup>) cobalt (Co<sup>++</sup>), nickel (Ni<sup>++</sup>), and zinc (Zn<sup>++</sup>) at the same concentration.

## 5.1 Introduction

Fluorescence is of the most powerful transduction mechanisms due to its high sensitivity and the number of different analytical parameters. These materials have generated much interest in the manufacture of optical, chemical and biosensing fields.<sup>1-2</sup> Bio-organic compounds are now being broadly used in fluorescent sensing over inorganic nanomaterials (Quantum dots and dyes) due to their biodegradability, biocompatibility and non-chemical synthesis.<sup>3-5</sup> These compounds have a wide range of applications due to their unique optical properties and non-toxic synthesis.<sup>6-8</sup> There is now a significant need for biologically synthesized materials with aggregation induced emission fluorescence designed for specific applications in materials science. Several efforts have been devoted for organic nano and micro particle synthesis of different sizes and shapes.<sup>9-12</sup> Aggregation induced quenching is the main setback for organic materials as it reduces fluorescence at high concentrations in solution. This reduced fluorescence intensity is usually due to induced non-radiative deactivation process in structural intermolecular vibronic interactions. Several strategies have been projected to surmount this aggregation induced quenching problem. To retain highly fluorescent property of materials in aggregated state, bulky substituents could be introduced to reduce intermolecular interaction and adverse aggregation.<sup>13-17</sup> Aggregation induced fluorescence presents opportunities for constructing various sensor probes. It is an array of self-assembled molecules which may represent homogeneous or heterogeneous assemblies via electrostatic forces (Columbic, van der Waals), hydrogen bonding as well as hydrophobic interactions. In the past decade several ordered molecular assemblies have gained interest for their formation of self-assemblies such as micelles, vesicles, and lamellar phases.<sup>18-23</sup> Different techniques have been introduced to build up these organic structures, such as Laser ablation, molecular beam deposition, physical vapour deposition, reprecipitation, electro spinning and self-organization.

Heavy metals and their compounds are naturally ubiquitous throughout the environment.<sup>24-27</sup> Heavy metal exposure results in adverse effects on human health including carcinogenicity, neurotoxicity and genotoxicity. Many biological systems can be affected at the cellular level by Mercury ( $\text{Hg}^{++}$ ) poisoning. In recent time  $\text{Hg}^{++}$  ions pollution has turned out to be a global concern. Thus, monitoring  $\text{Hg}^{++}$  ions in drinking water, food, and biological fluids is very crucial. There are several usual

detection procedures available for measurement of  $\text{Hg}^{++}$  ions such as inductively coupled plasma emission spectrometry,<sup>28-30</sup> inductively coupled plasma / mass spectrometry, atomic absorption spectroscopy,<sup>31-33</sup> and ultraviolet-visible spectroscopy. But these techniques require complex and expensive instruments, tedious groundwork, and certified professional despite being highly sensitive and selective. For on-site  $\text{Hg}^{++}$  ions measurement, fluorescent sensing has great advantage compared to the above techniques.<sup>34</sup> Fluorescence sensing for  $\text{Hg}^{++}$  ions is highly sensitive, but there is a scope for improving its photo stability and intensity. Although fluorescent sensors have high sensitivity and stability, there are some weaknesses for actual applicability, like cross-sensitivity toward other metal ions, lack of water solubility, short emission wavelengths and weak fluorescence enhancement factors. In the present work, we have developed an easily synthesized and very stable cephalalexin-assembly based fluorescent sensor for  $\text{Hg}^{++}$  metal ions.

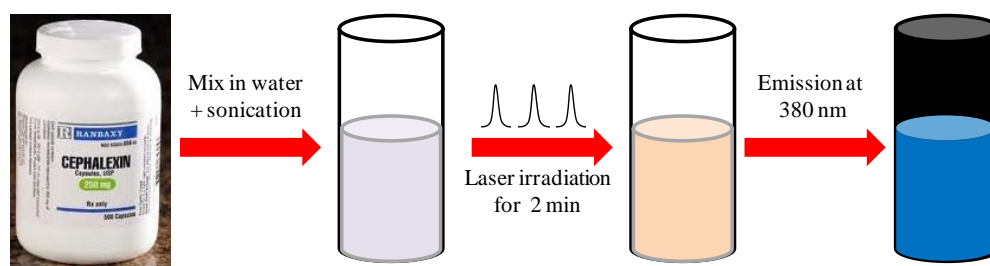


**Figure 5.1** Sketch Diagram of UV laser induced cephalalexin nanostructures synthesis procedure. Cephalalexin dissolves in water and sonication for 30 minutes then laser irradiation for 2 minutes. Laser induce cephalalexin self-assembly give blue fluorescence when excited at  $\lambda=380\text{ nm}$

Cephalalexin is a first generation cephalosporin antibiotic product, useful for the treatment of a number of bacterial infections.<sup>35</sup> Herein we introduce a process for the formation of novel self-assembled fluorescent nanostructures of cephalalexin with pulsed UV ( $\lambda=248\text{ nm}$ ) laser irradiation (Figure 5.1) without the addition of any stabilizing agent, or other organic or inorganic additives. Cephalalexin can be simply dissolved in water for preparing the sample for laser treatment process. Cephalalexin based nanostructures are highly fluorescent, in contrast to the feeble fluorescence property of the component molecules. In this process, no synthetic chemical steps were applied to generate fluorescent cephalalexin nanostructures. The nanostructures

created are entirely eco-friendly, and FDA approved cephalixin is used (allowable human intake = 500 mg/12 hours).

## 5.2 Experimental

### 5.2.1 Materials and Equipment's

High purity (GR grade) cephalixin was obtained from MD biomedical and was used as received. A 248 nm KrF excimer laser (Lambda Physik – Germany) with a maximum average power of 40 watts (pulse energy = 150 mJ) and a pulse-width of 20 ns was used in the irradiation process.

### 5.2.2 Experimental Process

The details of experiments performed and related procedures are given in a latter section. Briefly, in our experiments, cephalixin dispersed in water was laser treated with pulsed excimer laser ( $\lambda=248$  nm, pulse width 20 ns, energy density $\sim 120$  mJ/cm<sup>2</sup>). Microscopy studies and other physical characterizations were performed for the samples under different conditions. This process is very fast and does not involve any organic solvent, which is superior to existed synthesis procedures. The nominal size range of such cephalixin nanostructure was 0.2 - 0.4  $\mu\text{m}$  which could be reduced to average 100 nm by the optimizing process parameters such as laser irradiation time, energy and stirring solution. In 2 minutes of laser irradiation process only about 10 % sample is degraded which is easily separated out by centrifugation.

## 5.3 Characterization

The materials were characterized for their physical properties using various techniques as UV-Vis spectra of cephalixin nanostructures were monitored on a Jasco-V-570 uv/vis spectrophotometer operated at a resolution of 2 nm. The purified powders of cephalixin and cephalixin IR nanostructures were crushed with KBr, pelleted and the Fourier transform infra-red (FTIR) spectra were recorded on a Perkin-Elmer Spectrum-One instrument at a resolution of 4 cm<sup>-1</sup>. Ultraviolet wavelength  $\lambda =248$  nm KrF excimer laser (Lambda Physik – Germany) with a maximum average power of 40 watts (pulse energy = 120 mJ) and a pulse-width of 20



ns was used in the irradiation process. The repetition frequency was 10 Hz. Almost 80% of cephalexin was noted to get converted into the self-assembled nanostructures after 2 minutes laser treatment. Scanning electron microscopy (SEM) (FEI Quanta 200 3D) was used for the determination of morphology. Samples for transmission electron microscopy (TEM) were prepared by drop coating the isolated and re-suspended solution on carbon-coated copper grids. TEM measurements were performed on FEI Tecnai G<sup>2</sup> 200 KV instruments. Fluorescence microscopy was done on Zeiss AXIOPLAN 2.

### **5.3.1 UV-Vis and Photoluminescence studies**

UV-Vis absorption spectra were recorded on Varian CARY 100 Bio UV-Vis spectrophotometer, with 10 mm quartz cell at 25±0.1 °C. For UV spectra measurement, 100 µl solution of cephalexin and cephalexin IR (stock solution, 1mg/ml, 2.9 mM) were prepared by diluting it with 3 ml distilled water. Final solution was mixed gently and subsequently spectra were recorded.

### **5.3.2 Fluorescence Study**

This was carried out by observing the prepared samples under a fluorescence microscope (Fluor Cell Imaging station from molecular probe Life technologies) 10 micro-liter samples were taken on a clean glass slide and a cover-slip was put on it. The sample was excited at 380 nm (excitation optimized) and green colored fluorescence was observed.

### **5.3.3 FTIR analysis**

FTIR spectra were recorded with KBr pellets on FTIR spectroscopy in transmission mode using a Nicolet Magna IR-750 spectrophotometer at 4cm<sup>-1</sup> resolution with 64 scans between 4000 and 400 cm<sup>-1</sup>. Two milligram of dried powder was mixed with 198 milligram KBr and analyzed by the instrument.

### **5.3.4 Scanning Electron Microscopy (SEM)**

Field emission scanning electron microscopy images were acquired on FEI QUANTA 200 microscope, equipped with a tungsten filament gun, operating at WD 10.6 mm and 20 kV. A 10 µL aliquot of cephalexin and cephalexin IR nanoparticles solution was placed on silicon wafer and fixed on copper stubs with

help of carbon tape. The samples were dried at room temperature for overnight and images were recorded without gold coating.

### 5.3.5 NMR study

The samples were dissolved in deuterated heavy water ( $D_2O$ ) and the data were recorded on Bruker Avance instruments operating at 400 MHz ( $^1H$ ) frequencies. Chemical shifts are expressed in parts per million using tetra-methyl silane as the internal standard in the indicated solvent.

## 5.4 Results and Discussion

### 5.4.1 Optical microscopic properties

Optical microscopy study was used to explore for morphologies of cephalixin before (Cep) and after laser irradiation induced self-assembly formation (Cep IR). When Cephalixin was dissolved in water it yields a clear solution which creates a fine film (Figure 5.2 A) on glass slide while the powder form was crystalline in nature (inset Figure 5.2 A)

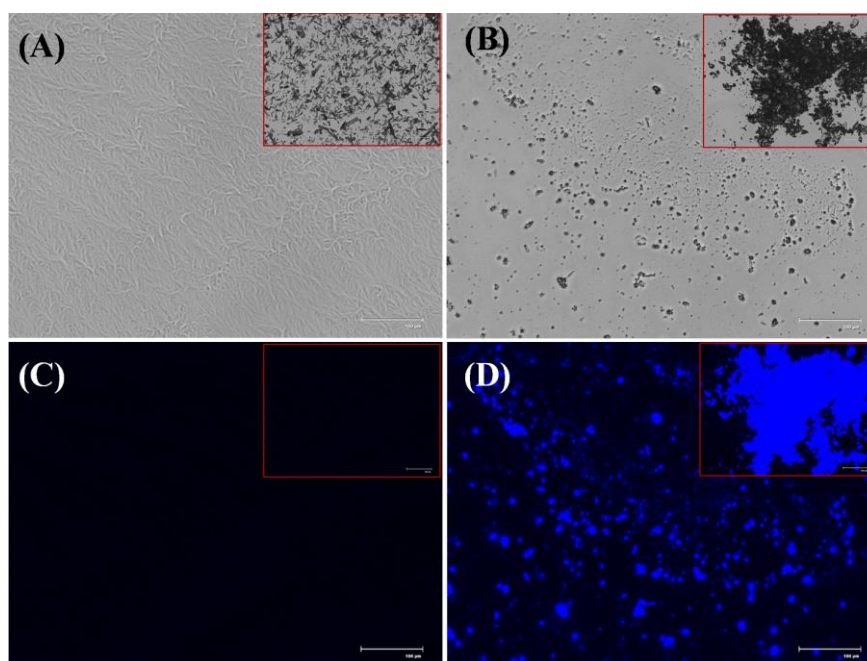


**Figure 5.2** Fluorescence study of laser induces cephalixin nanostructures. (A) cephalixin seen like film formation in while powder like crystal form (inset) (B) laser induce cephalixin form self-assemble morphology (C) Fluorescence image of untreated Cephalixin and (D) laser treated cephalixin. (Scale bar 100  $\mu m$ )

After 2 minutes of laser treatment self-assembled structures were form, as exhibited (Figure 5.2 B) and concentrate via rotary vapor as amorphous dry powder (inset Figure 5.2 B). Fluorescence study shows that cephalixin has very feeble fluorescence property which could not be clearly seen in Figure 5.2 C, while after laser treatment process, a strong and appealing blue colored fluorescence is seen to arise due to self-assembly induced fluorescence (Figure 5.2 D).<sup>36</sup> Since the optical microscope has resolution limitation, the morphological studies of laser processing of cephalixin nanostructures were performed by scanning electron microscopy. The laser irradiated cephalixin appeared as undefined flower like morphology which is illustrated in the SEM images Figure 5.3 A, B and elaborate morphological studies of these nanostructures could be illustrated by the TEM analysis. Laser irradiated cephalixin structures are clearly seen to be self-assembled morphological forms in the high resolution TEM images (Figure 5.3 C and D) which elucidate their size range of 200 - 400 nm.

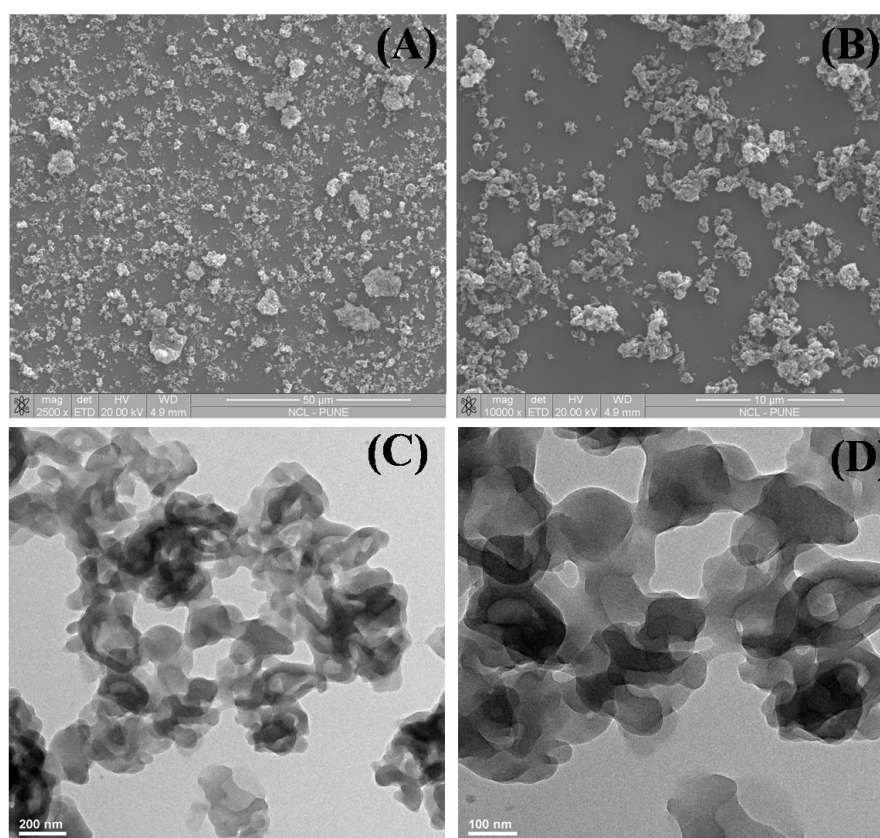


**Figure 5.3** SEM and TEM images of cephalixin nanostructures: (A) and (B) cephalixin as it appears without laser treatment after laser treatment (C-D) TEM images of cephalixin nanostructures: (Scale Bar A -50, B -10, C -0.2, D- 0.1μm)

### 5.4.2 Optical Properties

The optical properties of cephalixin and laser irradiated cephalixin show a significant difference in their appearance to the naked eye. Cephalixin solution in water appears transparent; while the laser treated one emerged little yellowish in color. Cephalixin solution showed UV absorption band with a peak at 260 nm which corresponds to the phenyl groups  $\pi-\pi^*$  transition, while after laser irradiation '(cephalixin IR) tailing with a peak arising at 370 nm probably because of  $n-\pi^*$  transition after self-assembly of cephalixin, as clearly seen in Figure 5.4 A.<sup>37</sup>

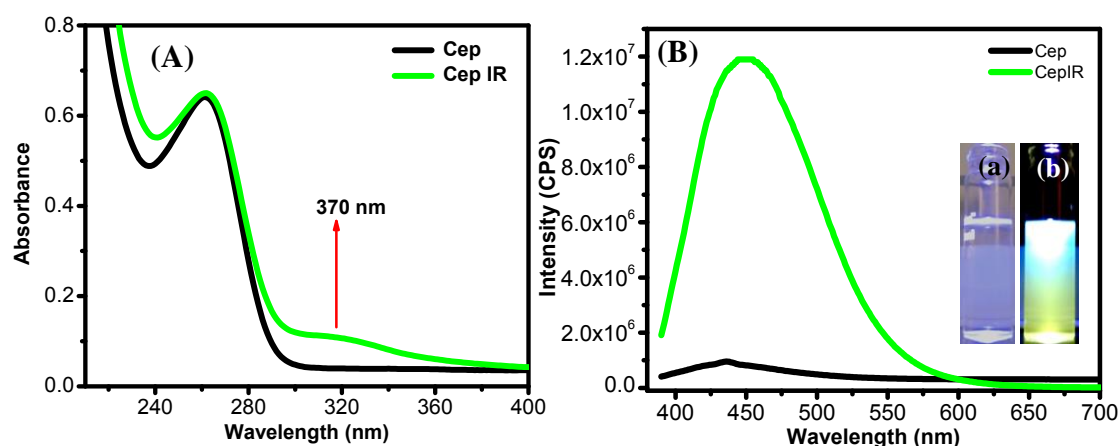


**Figure 5.4 (A)** UV–Visible spectra measurement of untreated and laser treated cephalixin solution. Untreated cephalixin solution shows absorbance at  $\lambda=260$  nm while laser treated shifts absorption shows similar absorption pattern tailing toward visible region  $\lambda=370$  nm which is probably due to  $n-\pi^*$  transition. **(B)** PL study of laser treated cephalixin microstructures. Untreated cephalixin has feeble PL while laser treated Cephalixin shows remarkably strong blue PL at 460 nm at Exc-380 nm.

Photoluminescence analyses of cephalixin and cephalixin IR samples were performed with identical 380 nm excitation wavelength. In cephalixin sample, very feeble excitonic emission is observed, whereas in laser irradiated sample (Cep IR), strong emission appears in the visible spectral region at 460 nm (Figure 5.4 B). Appearance of fluorescence was further studied by fluorescence microscopy analysis, which also confirmed the appearance of strong blue fluorescence in cephalixin IR while feeble fluorescence was observed in cephalixin (Figure 5.4 B). Based on the literature survey, in our case formation of microscopic structures may be due to the non-thermal photochemical process.<sup>38</sup> There is no ambient heating of the solution

during the UV laser irradiation treatment process for such short duration. For further study we recorded FTIR spectra (Figure 5.5) which show the results for cephalixin before and after laser irradiation for 2 minutes. Un-irradiated cephalixin sample shows a broad band at  $3420\text{ cm}^{-1}$  corresponding to the O–H stretch frequency in the molecule. Two strong absorption bands of cephalixin arising from carboxy (COOH,  $1750$ ), amide ( $\text{NH}_2$ ,  $1684$ ) as well as the C–C stretching at  $1590$  are also noted.

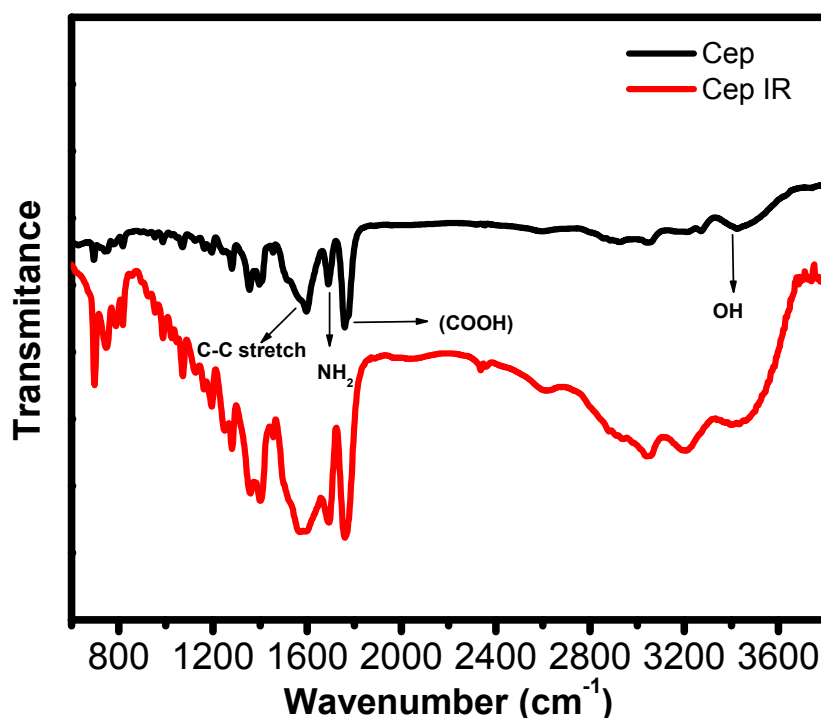


*Figure 5.5 FTIR data of unirradiated and laser irradiated cephalixin (Cep IR).*

For the un-irradiated case (cephalixin) the molecular bands are in agreement with the literature reports.<sup>39</sup> FTIR peaks that occur in the sample after laser irradiation are identical to the un-irradiated sample but with broadening. A similar peak structure before and after laser irradiation treatment implies that the basic molecular structure of the cephalixin is intact after the UV laser treatment. Thus the self-assembled structures appear to originate through excited state interactions amongst cephalixin molecules.

#### 5.4.3 Nuclear Magnetic Resonance analysis

To understand the molecular process of cephalixin molecule self-assembly we have performed nuclear magnetic resonance (NMR) spectroscopic analysis of both, the before and after laser treatment samples.  $^1\text{H}$  NMR spectra were collected in  $\text{D}_2\text{O}$

solvent at 200 MHz. The cephalexin NMR spectrum (Figure 5.6 A) shows signatures at  $\delta$  1.80 (s, 3H), 3.03 (d, 1H,  $J = 17.95$  Hz), 3.47 (d, 1H,  $J = 17.86$  Hz), 5.00 (d, 1H,  $J = 4.29$  Hz), 5.16 (s, 1H), 5.61 (d, 1H,  $J = 4.29$  Hz), 7.48 (m, 5H).<sup>40-42</sup> Based on NMR evidence we can speculate that cephalexin used is pure, without any organic impurity.

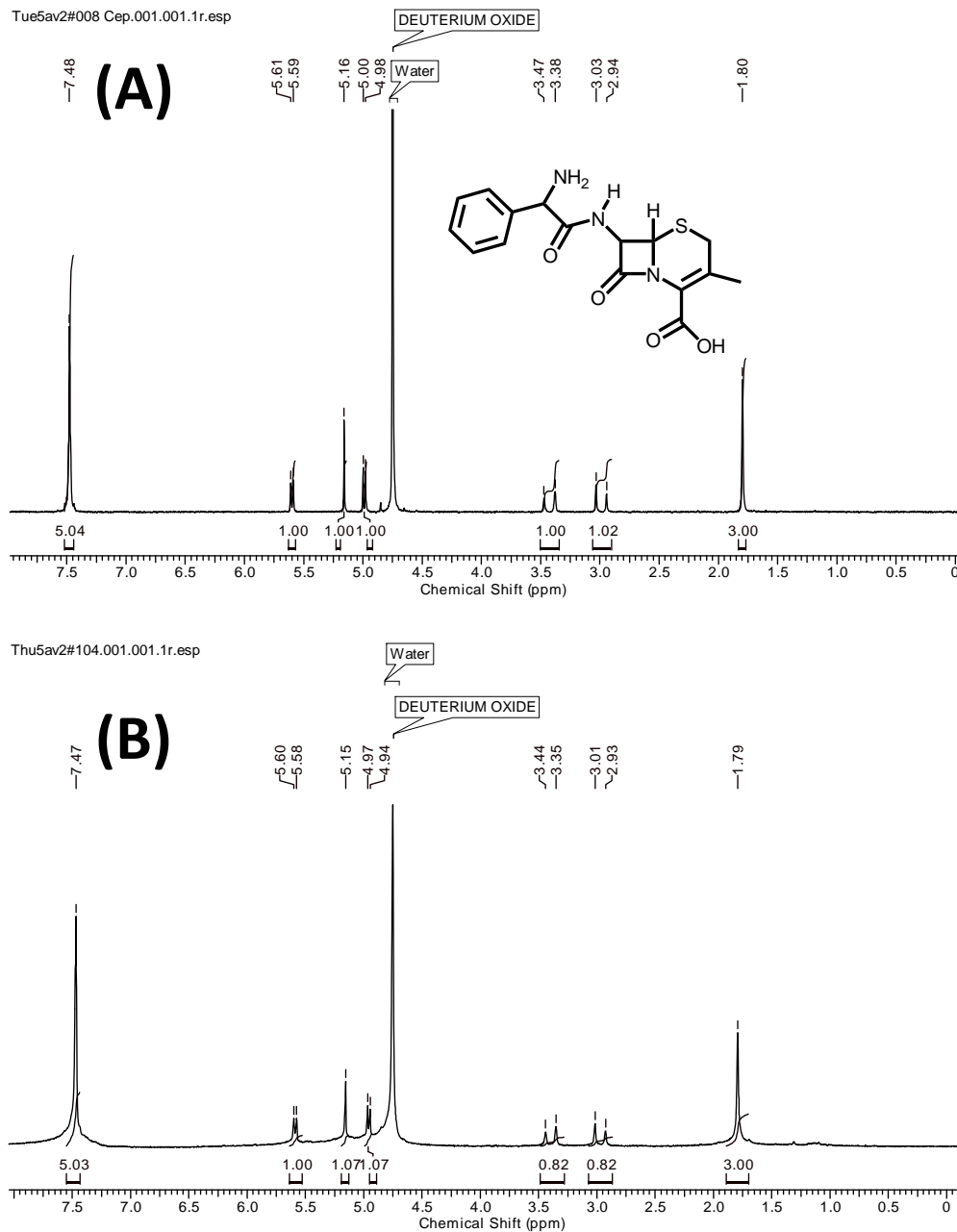


**Figure 5.6** Nuclear magnetic resonance spectra of cephalexin and laser irradiated cephalexin. Before laser irradiation (A) and after case (B) were depicted the identical NMR spectra with some broad peak area which is probably due to the self-assembly formation.

In Figure 5.6 B, we have shown <sup>1</sup>H NMR spectra of the sample after laser treatment which presents identical peaks as before irradiation case;  $\delta$  1.79 (s, 3H), 3.03 (d, 1H,  $J$

= 17.95 Hz), 3.46 (d, 1H,  $J = 17.86$  Hz), 4.99 (d, 1H,  $J = 4.29$  Hz), 5.16 (s, 1H), 5.60 (d, 1H,  $J = 4.29$  Hz), 7.47 (m, 5H). Some NMR peaks (at  $\delta$  1.86 (s, 3H), 5.05 (d, 1H,  $J = 4.29$  Hz), and 7.54 (m, 5H)) of laser irradiated cephalixin case appear with broadening which is a characteristic property<sup>43-45</sup> of molecular self-assembly.

Bearing in mind that  $\text{Hg}^{++}$  ion has specific affinity towards anionic sulfide (sulphur ligand); we checked its detectability with the cephalixin fluorescent nano-structure assembly. Based on sulfur ligand affinity to  $\text{Hg}^{++}$  ions, we found a notable application of this fluorescent cephalixin self-assembled nanostructure for  $\text{Hg}^{++}$  ion sensing in its aqueous solution. Our experiments show  $\text{Hg}^{++}$  ions concentration dependent fluorescence quenching of molecular assembly.

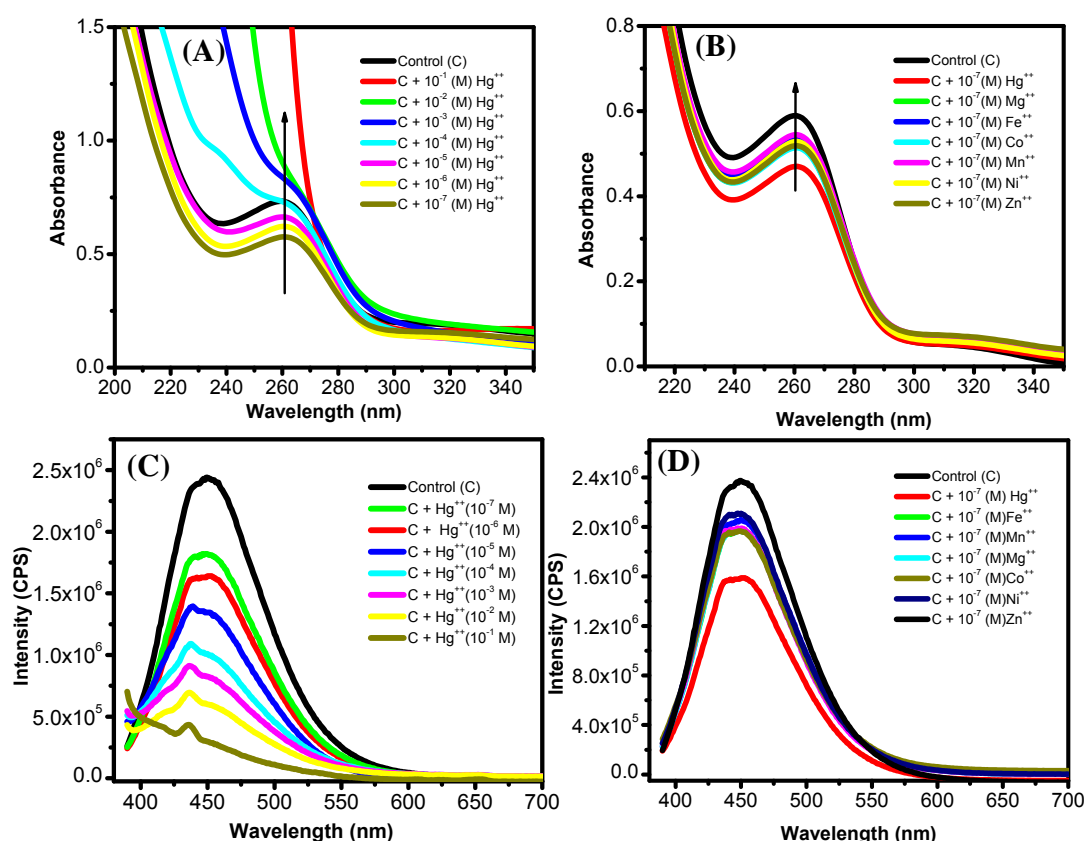


**Figure 5.7** (A) UV spectra of Cep IR assembly concentration with increase  $\text{Hg}^{++}$  concentration and (B) is represent other heavy metal with identical conc. (C, D) is the PL spectra of A and B samples with identical Cep IR and  $\text{Hg}^{++}$  concentration respectively.

Fluorescence sensing of these nanostructures due to high affinity of  $\text{Hg}^{++}$  ions for bonding towards negative sulfur molecule binding site in Cep IR assembly. Figure



5.7A shows the change in the cephalixin IR UV spectra with increasing concentration  $\text{Hg}^{++}$  ions. Change in UV spectra of Cep IR is due to the weak electrostatic interaction of  $\text{Hg}^{++}$  ions with negative sulfur group. Other heavy metals like  $\text{Mg}^{++}$ ,  $\text{Fe}^{++}$ ,  $\text{Co}^{++}$ ,  $\text{Zn}^{++}$ ,  $\text{Mn}^{++}$ ,  $\text{Ni}^{++}$  do not show significant UV spectral changes (Figure 5.7 B).<sup>46</sup>

Figure 5.7 C illustrates the gradual decrease in photoluminescence intensity of the Cep IR nanostructure with increasing  $\text{Hg}^{++}$  ion concentration. As we can observe that the photoluminescence intensity of the Cep IR solution (Figure 5.7 D) toward the other metal ions presence such as  $\text{Mg}^{++}$ ,  $\text{Fe}^{++}$ ,  $\text{Co}^{++}$ ,  $\text{Zn}^{++}$ ,  $\text{Mn}^{++}$ ,  $\text{Ni}^{++}$  also decreases. But one can observe that reduction in photoluminescence intensity in the presence of other metals ions is much smaller compared to  $\text{Hg}^{++}$ .

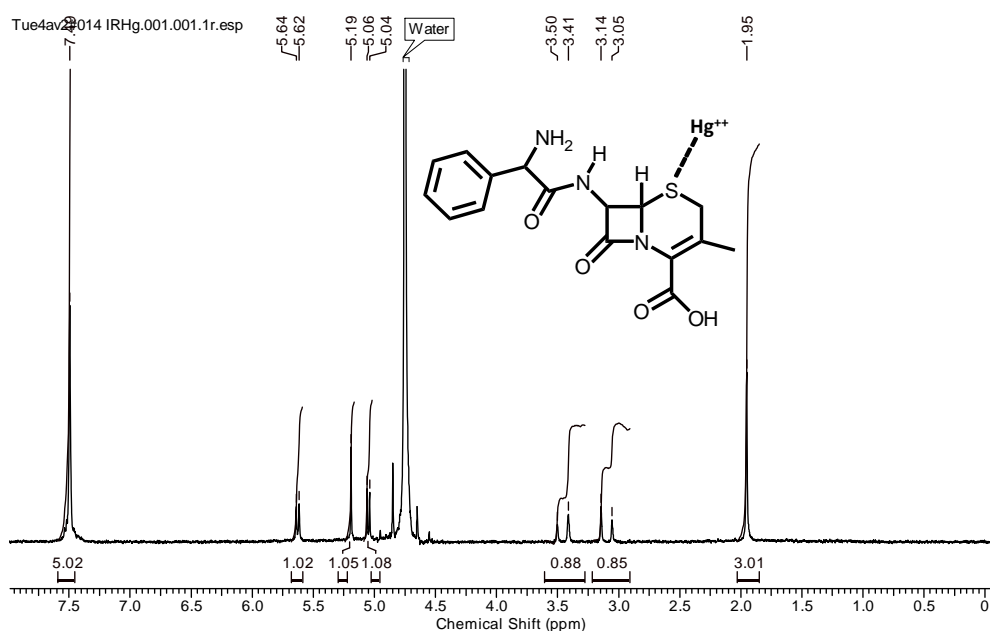


**Figure 5.8** Nuclear magnetic resonance spectra of laser irradiated cephalixin after  $\text{Hg}^{++}$  metal sensing. Laser irradiated cephalixin NMR spectra shows deshielding effect in peak position due to the Sulfur group interaction with  $\text{Hg}^{++}$  ions in solution medium.

This small decrease in PL intensity for other ions as compared to  $\text{Hg}^{++}$  ions is due to external heavy atom induced quenching. Quenching behavior of self-assembled cephalixin structures is the decrease in fluorescence intensity with increase in the  $\text{Hg}^{++}$  ions concentration due to the complex formation of  $\text{Hg}^{++}$  and Sulfur. The <sup>1</sup>H NMR spectrum (Figure 5.8) of laser irradiated sample of cephalixin shows a small shift (towards deshielded region 3.14 (d, 1H,  $J = 17.95$  Hz), 3.51 (d, 1H,  $J = 17.86$



Hz), 5.06 (d, 1H,  $J = 4.29$  Hz), 5.19 (s, 1H), 5.64 (d, 1H,  $J = 4.29$  Hz), 7.49 (m, 5H)) in the delta value of 1H peaks after addition of  $\text{Hg}^{2+}$  ions. It shows the interaction of  $\text{Hg}^{++}$  with heteroatom (S) of the cephalixin self-assembly.<sup>46-48</sup> The electrostatic interaction between Cep IR and  $\text{Hg}^{++}$  ion results in formation of metal-ligand complex which induces quenching of the photoluminescence.

## 5.5 Conclusions

Cephalixin molecular assembly was prepared by a simple one step process which involved laser treatment of cephalixin water solution with UV laser (Excimer, 248 nm) pulses for a short duration. The laser induced assembly exhibits a strong and appealing aggregation induced blue fluorescence, whereas the mother cephalixin molecules show only a very feeble fluorescence. The fluorescent assembly is shown to detect extremely low concentration of  $\text{Hg}^{++}$  ions in aqueous solution due to the presence of negative sulfur molecule binding site.

## References

1. Z Chang, Y Jiang, H Qiu, Ben Zhong Tang, Chem. Commun., 2013, **49**, 594
- 2 H Shi, J Dai, Li-wen Shi, Mei-hua, Chuan Dong, Chem. Commun., 2012, **48**, 8586–8588
- 3 B An, S Kwon, S Jung, S Y Park, J. AM. CHEM. SOC. 2002, 124, 14410-14415
- 4 Han Yu and Limin Qi, Langmuir 2009, **25(12)**, 6781–6786
- 5 X Zhang, X Lu, Y Zhen, Jie Liu, W Hu, J. Mater. Chem. C, 2014, **2**,5083
- 6 M Kirkus, S Knippenberg, D Beljonne, S C. J. Meskers, J. Phys. Chem. A 2013, 117, 2782–2789
- 7 S Li, S M. Langenegger, R Ha'ner. Chem. Commun., 2013,**49**, 5835
- 8 G Wang, R Zhang, C Xu, Xiaowei Zhan, ACS Appl. Mater. Interfaces 2014, **6**, 11136–11141.
- 9 Quansong Li , Llu ´s Blancafort. Chem. Commun., 2013, **49**, 5966
- 10 W Liu, Y Wang, M Sun, D Zhang, Wenjun Yang, Chem. Commun., 2013, **49**, 6042

- 11 G Kwak, H Kim, I K Kang, S H Kim, *Macromolecules*, Vol. 42, No. 5, 2009
- 12 Y S Zhao, A Peng, H Fu, Y Ma, J Yao, *Adv. Mater.* 2008, 20, 1661–1665
- 13 Z Zhao, S Chen, J W. Y. Lam, B Z Tang, *J. Mater. Chem.*, 2011, 21, 7210–7216
- 14 R Wei, P Song, A Tong, *J. Phys. Chem. C* 2013, **117**, 3467–3474
- 15 L Gao, Q Song, X Huang, J Huang, *J of Colloid and Interface Sci.* 323, 2008, 420–425
- 16 D K. Scrafton, J E. Taylor, T D. James, *J. Org. Chem.* 2008, **73**, 2871–2874
- 17 K E. Achyuthan, D G. Whitten, *Photochem. Photobiol. Sci.*, 2006, **5**, 931–937
- 18 J Wakita, H Sekino, Y Urano, S Ando, *J. Phys. Chem. B*, Vol. 113, No. 46, 2009
- 19 Y Chen, Y Lv, F Zhang, Z Bo, C-Y Liu, *Langmuir* 2009, 25(**15**), 8548–8555.
- 20 M Kumar, S J. George, *Nanoscale*, 2011, **3**, 2130–2133
- 21 P. K. Singh, A. Prabhune, Satish Ogale, *Green Chem.*, 2013, **15**, 943–953
- 22 T Hiroseab, K Matsuda, *Chem. Commun.*, 2009, 5832–5834
- 23 M R. Ams, D Ajami, J R Jr. *Beilstein Journal of Organic Chemistry* 2009, 5, 79
- 24 Y J Huang, Y-B Jiang, S D. Bull, Tony D. James, *Chem. Commun.*, 2010, **46**, 8180–8182
- 25 M Kastantin, B Lin, J Ressler, M Tirrell, *Macromol. Biosci.* 2007, **7**, 189–194
- 26 A C. Coleman, J M. Beierle, J T. Mika, B L. Feringa, *NAT NANO | VOL 6 | SEPTEMBER 2011*
- 27 T Noguchi, T Shiraki, A Dawn, Seiji Shinkai, *Chem. Commun.*, 2012,**48**, 8090-8092
- 28 W Chen, S A. Elfeky, Yse´ Nonne, John S. Fossey, *Chem. Commun.*, 2011, **47**, 253–255
- 29 L Gao, L Zhao, X Huang, J Huang, *J of Colloid and Interface Sci*, 2011, **354**, 256–260
- 30 S A. Elfeky, Lora Poncel, W Chen, John S. Fossey, *New J. Chem.*, 2009, **33**, 1466–1469
- 31 T Nishimura, T Cho, A M. Kelley, K Sakurai. *Bull. Chem. Soc. Jpn.* 2010, **83**, 9
- 32 H E. Hamm, S M. Meier, A M. Preininger, *PROTEIN SCI.* 2009, **18**, 2326—2335.

- 33 X Zheng, D Wang, Z Shuai, X Zhang, *J. Phys. Chem. B* 2012, **116**, 823–832
- 34 P Koley, A Pramanik, *Soft Matter*, 2012, **8**, 5364–5374
- 35 Sijian Hou, Ka Yan Kitty Man, and Wai Kin Chan, *Langmuir*, 19, **6**, 2003
- 36 A. D. Deshpande, K. G. Bahet, N. R. Chatterjee, *CURRENT SCI.*, 87, **25**, 2004
- 37 N. GIACOMINO, M. CERRA, E. BARONI, E. FORMENTINI, *Revue Méd. Vét.*, 2012, **163**, 431-440
- 38 M Fanun, V Papadimitriou, A Xenakis, *J of Colloid and Interface Sci.*, 2011, **361**, 115–121
- 39 Vijay J, Sahadevan JT1, Mehra Gilhotra R, *J of Young Pharmacists Vol 4 / No 1*
- 40 C Bahamondes, L Wilson, A Illanes, *Biotech and Biopro Engi.*, 2012, **17**, 711-721
- 41 Joseph W. Ndieyira, N Kappeler, R A. Gabriel Aepli, *NAT. NANO. VOL 9, MARCH 2014*
- 42 R Jagannathan, P Poddar, A Prabhune, *J. Phys. Chem. C*, Vol. 111, No. 19, 2007
- 43 Vivekanandan K.E, K. Gokul Raj, M. Pandib, *INT J CURR SCI* 2012, **4**, 1-7
- 44 Y Hu, H Cheng, *Environ. Sci. Technol.* 2013, **47**, 3752–3760
- 45 Y Hung, T-M Hsiung, Yu-Fen Huang, C-C Huang, *J. Phys. Chem. C*, 2010, **39**, 114
- 46 S Wang, E S. Forzani, N Tao, *Analytical Chemistry*, 2007, **12**, 79
- 47 E S. Pilkington, L J. Warren, *Environmental Science & Technology*, 1979, **13**, 3
- 48 G Aragay, A Puig-Font, M Cadevall, A Merkoç, *J. Phys. Chem. C*, 2010, **114**, 19

## Chapter 6

---

# Research Summary and Future Scope

---

**In this chapter some of the salient features of our work have highlighted and an attempt to summarize the entire PhD research has been made. In addition to this a broad vision for future research work has also been provided.**

## 6.1 Thesis Summary

The objective of this thesis was to develop novel routes towards the synthesis of fluorescence nanostructures for different biomedical applications like bioimaging and drug delivery.

Traditionally fluorescent materials have been synthesized by chemical method that includes dyes and heavy metals, many of which were toxic by nature. All these materials either involve toxic organic solvent or highly toxic precursors for the processing. In our research, a new UV laser irradiation route towards the synthesis of fluorescent mesostructures materials has been explored. This process involves a completely bio derived compound, sophorolipid for the synthesis of fluorescence materials. The process can take place at room temperature and ambient conditions. We demonstrate that this process can be used to make a range of fluorescent nanoparticles. It is also revealed that this UV laser irradiation process presents new avenues and promises of forming new fluorescent nanostructures and molecular self-assemblies which have remained largely unexplored. Furthermore, in the PhD research, the use of sophorolipid has been explored to encapsulate hydrophobic drug curcumin for stability and increased bioavailability in aqueous medium. This curcumin encapsulation through sophorolipid molecules enhances its cyto-toxicity towards human cancer cell line while remaining non-toxic to normal cells. Finally in another work, UV laser irradiation has been used for aggregation induced fluorescence in cephalixin molecule. This fluorescent cephalixin molecule was found to be an excellent material for mercury sensing in aqueous environment.

Specific results that we obtained have been summarized herein:

1. Pulsed UV laser irradiation process is introduced to engineer fluorescent mesostructures from bio-derived sophorolipid by laser treatment at room temperature and ambient conditions. Highly spherical mesoscale sophorolipid molecular assemblies are synthesized using a simple one step process which involves irradiating water solution of acidic sophorolipid with UV laser (Excimer, 248 nm) pulses. Surprisingly, the laser assembled mesostructures exhibit strong green fluorescence, while the original sophorolipid molecules do not show any. Inherent fluorescence in

the sophorolipid molecule appeared due to the unsaturation in oleic acid moiety of the molecule. Cyto-toxicity assay shows that these fluorescence mesostructures are non-toxic to human cells even at 50 $\mu$ g/ml. It is further shown that such mesostructures can be easily impregnated with super-paramagnetic iron oxide nanoparticles, and the corresponding synthesis protocol concurrently leads to a reduction in the assembly size down to  $\sim$ 100 nm scales. Importantly, the fluorescence property is retained and the magnetite loaded assembly can be heated by RF excitation for hyperthermia application

2. Sophorolipid, an environmental friendly biosurfactants and amphiphilic nature had been applied to increase solubility, stability and bioavailability of curcumin. Co-sonication of curcumin and acidic sophorolipid in aqueous solution is shown to lead to a dramatic enhancement of curcumin bioavailability through size reduction and encapsulation. The interaction between the two is studied and discussed based on optical absorption, photoluminescence, dynamic light scattering, Zeta potential, microscopy, Infrared spectroscopy and X-ray diffraction measurements. The cytotoxicity effects of curcumin on human breast cancer cell lines, MCF-7 and MDA-MB-231, are shown to be significantly enhanced by the formation of its complex with sophorolipid while normal cell were ineffective. The probable region for the increase cyto-toxicity of curcumin with its SL(A) complex is because of the presence of glucose moiety. The results further suggest that sophorolipid based formulations, could increase solubility and enhance bioavailability of nano-encapsulate curcumin after lipid co-processing, show great potential for curcumin cell entry.

3. Enormous effort has been devoted to the synthesis of organic nano and micro particles of different sizes and shapes. We revealed the UV laser derived aggregation induces fluorescence in cephalixin molecules, which shows specific applications toward the fluorescence sensing of mercury metal ions in aqueous medium. Antibiotics are most important products of biotechnology, synthesized by microbial process, out of these  $\beta$ -lactam antibiotics being the most admirable. Herein we report pulsed UV laser induced formation of novel self-assembled

fluorescent nanostructures of cephalixin without addition of any stabilizing agent or other organic or inorganic additives. This fluorescent property of aggregated cephalixin is suitable for the selective detection of trace amounts mercury ( $\text{Hg}^{++}$ ) ions. It has been observed that  $\text{Hg}^{++}$  ions can quench the fluorescence intensity of aggregated cephalixin at extremely low concentrations compared to other heavy metal ions e.g. ferrous ( $\text{Fe}^{++}$ ) manganese ( $\text{Mn}^{++}$ ), Magnesium ( $\text{Mg}^{++}$ ) cobalt ( $\text{Co}^{++}$ ), nickel ( $\text{Ni}^{++}$ ), and zinc ( $\text{Zn}^{++}$ ).

## 6.2 Future work

### 1. Synthesis of fluorescent nanomaterials from bio-derived compounds

With an ever increasing of side effects of inorganic heavy metals in bio-imaging field, conventional bio-compatible resources have gained prime importance. Due to the risks involved in current cancer identification processes, the need for alternative bio-derived fluorescence materials has gained momentum in recent years. Microbially synthesized compounds have great potential to compete with established inorganic nanomaterials and these can also reduce health related problems. Biocompatible polymer and antibody have been used to make inorganic nanomaterials non-toxic as well as specific targeting for cell environment. Though, antibody gives very good outcome in specific cell receptor recognition, these are expensive technique for large scale applications. There are also several other issues such as drug loading for inorganic nanomaterials which limit their widespread usage. In light of these drawbacks, the uses of bio-derived materials and biosurfactants in biomedical devices have been tried in last decade with promising results. Biosurfactant is an important material since it offers inexpensive synthetic routes (synthesis from cheap or waste materials etc.) in addition to a very stable chemical nature.

### 2. Application of Sophorolipid for increase hydrophobic drug encapsulation

Most of the drugs used in different disease treatment are hydrophobic in nature. One of the major obstacles to the large scale deployment of hydrophobic compound for various disease treatments is their non-solubility in aqueous environment.

Commercially available polymer based systems are used as capping for these drugs to make soluble in aqueous medium, but it requires additional expensive material for its cellular entry. Hence several alternative systems like biosurfactants have been studied. Based on our results on curcumin effectiveness with sophorolipid encapsulation it would be the very exciting material for increase solubility of highly value medicinal hydrophobic compound.

With the use of novel biosurfactant, sophorolipid molecules and other precursors like antibiotics, I would be interested in the synthesis of such bio-derived based systems for application in biomedical field. Different cell membrane component and phospholipids structures can be incorporated for the same purpose.



# List of Publications

---

- **Pradeep Kumar Singh**, Ruchira Mukherji, Kasturi Joshi-Navare, Abhik Banerjee, Rohan Gokhale, Satyawar Nagane, Asmita Prabhune and Satishchandra Ogale. “Fluorescent sophorolipid molecular assembly and its magnetic nanoparticle loading: a pulsed laser process” **Green Chem**, 2013,15, 943-953
- **Pradeep Kumar Singh**, Kirtee Wani, Ruchika Kaul-Ghanekar, Asmita Prabhune and Satishchandra Ogale. “From Micron to Nano-Curcumin by sophorolipid co-processing: Highly enhanced bioavailability, fluorescence, and anti-cancer efficacy” **RSC Adv.**, 2014, 4, 60334–60341
- Mandakini Biswal, Kirti Bhardwaj, **Pradeep K. Singh**, Pooja Singh, Prasad Yadav, Asmita Prabhune, Chandrashekhar Rode and Satishchandra Ogale. “Nanoparticle-loaded multifunctional natural seed gel-bits for efficient water purification” **RSC Advances**, 2013, 3, 2288–2295
- Kasturi Joshi-Navare, **Pradeep Kumar Singh**, Asmita A. Prabhune. “New yeast isolate *Pichia caribbica* synthesizes xylolipid biosurfactant with enhanced Functionality” **Eur. J. Lipid Sci. Technol.** 2014, 116, 1070–1079
- **Pradeep Kumar Singh**, Kirti Bhardwaj, Asmita Prabhune. “Green synthesis of controlled size silver nanoparticles using *Lantana camara* leaf extract & their antibacterial properties” communicate to **RSC Advances**
- **Pradeep Kumar Singh**, Asmita Prabhune and Satishchandra Ogale. “Pulse laser (UV) drive molecular self-assembly of Cephalexin: Aggregation induce fluorescence and its utility as mercury sensor” Manuscript under preparation
- **Pradeep Kumar Singh**, Asmita Prabhune and Satishchandra Ogale. Green synthesis of fluorescent cholesterol nanostructures. Manuscript under preparation

## Patents

- Fluorescent, spherical sophorolipid mesostructures for imaging and therapeutic applications. **Pradeep Kumar Singh**, Asmita Prabhune and Satishchandra B Ogale. Publication number- WO2013164758 A1
- From Micron to Nano-Curcumin by sophorolipid co-processing: Highly enhanced bioavailability, fluorescence, and anti-cancer efficacy. **Pradeep Kumar Singh**, Asmita Prabhune and Satishchandra B Ogale. Patent number- 20130034491